Wet Biomass Treatment

Energy and Sanitation System Concepts

Recalde Moreno Del Rocio, M.D.R.

DOI
10.4233/uuid:e508869c-25b6-41b1-b8f0-1b51a4180717

Publication date
2024

Document Version
Final published version

Citation (APA)
Recalde Moreno Del Rocio, M. D. R. (2024). *Wet Biomass Treatment: Energy and Sanitation System Concepts*. [Dissertation (TU Delft), Delft University of Technology]. https://doi.org/10.4233/uuid:e508869c-25b6-41b1-b8f0-1b51a4180717

Important note
To cite this publication, please use the final published version (if applicable).
Please check the document version above.

Wet Biomass Treatment

Energy and Sanitation System Concepts

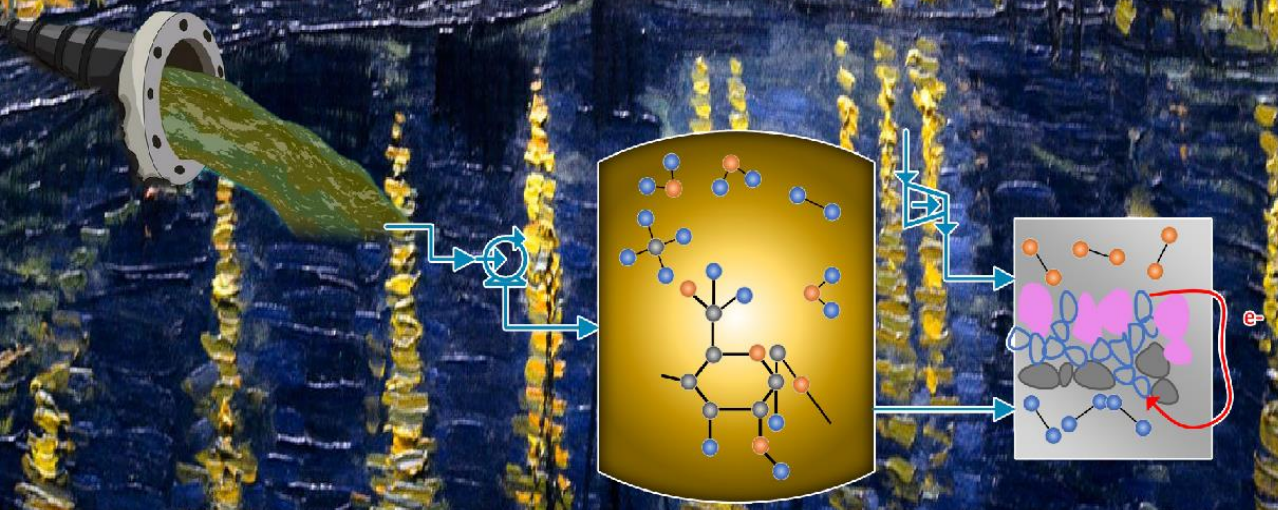

Mayra Recalde

Cover Background
Vincent Van Gogh: Starry Night Over the Rhone

Wet Biomass Treatment

Energy and Sanitation System Concepts

Proefschrift

ter verkrijging van de graad van doctor
aan de Technische Universitieit Delft,
op gezag van de Rector Magnificus prof.dr.ir. T.H.J.J. van der Hagen,
voorzitter van het College voor Promoties,
in het openbaar te verdedigen op
dinsdag 5 maart 2024 om 10:00 uur

door

Mayra del Rocío RECALDE MORENO

Master of Science in Mechanical Engineering

Technische Universiteit Delft, Nederland,

geboren te Riobamba, Ecuador

Dit proefschrift is goedgekeurd door de promotoren:

Samenstelling promotiecommissie:

Rector Magnificus	voorzitter
Prof.dr. A. Purushothaman Vellayani	Technische Universiteit Delft, promotor
Prof.dr.ir. B.J. Boersma	Technische Universiteit Delft, promotor
Onafhankelijke leden:	
Prof.dr. A.J.M. van Wijk	Technische Universiteit Delft
Prof.dr.ir. J.B. van Lier	Technische Universiteit Delft
Prof.dr.ir. M.A. van den Broek	University of Groningen
Prof.dr. E.E. Silva Lora	Universidade Federal fe Itajub (Brazil)
Dr.ir. R.E.F. Lindeboom	Technische Universiteit Delft

Keywords: Solid oxide cell, exergy destruction, exergy efficiency, wet biomass, energy efficiency, exergy destruction.
Printed by: Ipskamp printing
Cover by: Mayra Recalde

ISBN: 978-94-6473-422-5

To Amaru

Content

Summary

The global market for the wastewater treatment industry has been compelled to devise new concepts due to several factors. Currently, approximately 80% of untreated wastewater is discharged worldwide. The conventional technology for municipal solid waste treatment, which has been in use for over a century, is only partially effective in terms of effluent quality and energy balance. The highly flammable CH_4 gas emitted from municipal solid waste landfills impacts the chemical composition of the atmosphere, potentially affecting the Earth. Thus, new concepts for wastewater treatment should address multiple social challenges related to energy and sanitation technologies. A well–implemented wastewater treatment system not only contributes to mankind wellbeing, which results in more effective population planning, but also ensures the optimal utilization of environmental resources.

The conceptual basis presented in this work is a combination of gasification and solid oxide cell (SOC) technologies for producing sustainable energy (fuel and electricity) from wastewater. Two gasification methods were investigated, namely dry and supercritical water gasification (SCWG). Gasification should address certain technical challenges, such as achieving almost complete conversion of organics into a gas product, high–yield syngas, a high lower heating value (LHV), an optimum water content for efficient operation, a strategy to efficient heat recovery, and an high energy efficiency, for seamless integration with SOCs.

Consequently, a highly efficient wastewater dry gasifier–solid oxide fuel cell (SOFC) power plant was developed (Section 2). This system reaches high efficiency because the configuration contributes to the increment of the H_2 yield in the gasifier. And part of the external energy required by the dryer and gasifier was replaced by process heat and electrical energy. The aforementioned technical challenges of gasification can be addressed by integrating an energy–efficient self–heating fluidized bed dryer and an indirectly heated multistage gasifier. The gasifier is heated by a microwave plasma torch and process heat. The system generates a net power of 6.2 kW. This configuration provides favourable process conditions, enabling a high energy conversion efficiency (electricity production) of 65% when using biomass with a water content of 75 wt.% that is dried to 30 wt.% before being fed to the gasifier. The energy efficiency of the 90 wt.% biomass moisture is approximately 59%. The highest energy efficiency reported in the literature was 61% at a biomass moisture content (MC) of 50 wt.%. Optimal operating conditions of the gasifier and SOFC can be combined to generate

sufficient power and process heat for air and fuel preheating. The most significant exergy destruction is observed during heat transfer in the preheating process, with considerable exergy destruction also generated by the post–stack combustor (PSC).

A parametric analysis of the SCWG–SOFC (Section 3) system estimates the energy and exergy performances of the system under diverse operating conditions for the SCWG and SOFC. The SCWG temperature and dry biomass concentration are critical for the complete conversion of biomass into a gas product. Under the most challenging conditions selected from the available experimental data from literature, a carbon conversion efficiency of 40%, and a biomass MC of 85 wt.%, the system generates a net power of 3.6 kW, reaching an energy efficiency of 40% at an SOFC fuel utilisation of 0.95. Contrarily, the system achieved an efficiency of 44% when operated at a temperature of 500°C and a dry–biomass concentration of 5 wt.%. This operation ensured almost complete biomass conversion, indicating that the SCWG product gas had a sufficiently high thermomechanical exergy suitable for integration with downstream cycles to increase system efficiency. The operating costs can be reduced by increasing the system capacity for syngas production [1]. The highest irreversibility was observed in air and fuel processing during heat transfer. Operation at high fuel utilisation reduces exergy destruction during heat transfer because it minimises stream temperature difference.

A combined wastewater SCWG–reversible solid oxide cell (rSOC) system (Section 4) is a new fuel, power generation, and energy storage configuration. The new layout significantly increases the system capacity for hydrogen production and improves thermodynamic efficiency by reducing exergy destruction by the recovery of the heat of water evaporation in the SCWG–rSOC in the electrolyser (EL) mode. This concept leverages the fact that SCWG, operating at the highest biomass moisture, ensures an almost complete conversion of dry biomass into syngas. The SCWG–rSOC–EL mode, powered by low–cost renewable electricity, generates 122 kW of syngas exergy, whereas the SCWG alone generates 9.5 kW of syngas exergy. During fuel cell operation, the rSOC generates a power of approximately 98 kW compared with the 8 kW generated in the SCWG–SOFC system. The system efficiency of the SCWG–rSOC–EL mode was directly proportional to biomass moisture. With 95–wt% biomass moisture, the system reaches energy and exergy efficiencies of 91 and 73%, respectively. The highest exergy efficiency reported in the literature for power and syngas production in an SCWG–Rankine cycle combined system was approximately 20% at dry–biomass concentration < 10 wt.% [2].

The variation in the operating conditions of the rSOC determines the thermal behaviour of the system (endothermic and exothermic operations). An exothermic operation can achieve the highest efficiency in the SCWG–rSOC–EL mode. Operation at high pressure, with a temperature between 600–700°C, and rSOC high fuel utilisation renders the SCWG–rSOC–electrolyser mode highly exothermic. The process heat product of the exothermic operation is used for fuel and air preheating, which significantly reduces the demand for external heat and improves system efficiency. However, the maximum exergy destruction was observed in preheating rSOC reactacts owing to the considerable temperature difference between the streams in the heat exchangers.

The results indicate that a gasification–SOC plant is a potential method for highly efficient energy recovery from wastewater, renewable electrical energy storage, and sanitation. However, the proposed socially implementable technology requires further research and development. New system configurations that use efficient heat transfer techniques are required. The most critical exergy destruction affecting system efficiency occurs during air and fuel preheating. The complete conversion of biomass into a product gas should be experimentally demonstrated by applying the proposed concepts under variable operating conditions.

In the future, society should look at alternative energy generation systems based on wastewater treatment at medium or large scales. Humans need to develop new methods to provide sustainable energy and sanitation services to improve the quality of life and reduce environmental degradation.

Samenvatting

Onmiddelijke verbeteringen zijn nodig om op verschillende gebieden duurzame menselijke ontwikkeling na te streven. Energieopwekking op basis van de verbranding van fossiele brandstoffen resulteert in de uitstoot van broeikasgassen, met als gevolg opwarming van de aarde. De wereldwijde lacune in de afvalwaterzuivering, die afkomstig is van menselijke nederzettingen en industriële en landbouwactiviteiten, veroorzaakt ernstige aantasting van het milieu.

Het doel van dit onderzoek was om nieuwe maatschappelijk uitvoerbare concepten te vinden voor duurzame energieproductie (brandstof en stroom) en afvalwaterzuivering. De conceptuele basis was een combinatie van vergassing en solid oxide cell (SOC)–technologieën, die biomassa gebruiken met een vochtgehalte van meer dan 80% op gewichtsbasis. Dit soort systemen werken bij een hoge temperatuur en zowel atmosferische als hoge druk. Een thermodynamische evaluatie werd gebruikt om de effectiviteit van de voorgestelde systeemconfiguratie te beschrijven.

Vergassing is een veelgebruikte methode om uit biomassa een gasvormig product te maken, maar de prestaties zijn van cruciaal belang bij het werken met afvalwater. Er zijn aanzienlijke uitdagingen voor de vergassing van afvalwater: (1) Het hoge vochtgehalte van de biomassa heeft grote invloed op de energiebalans van het systeem. (2) Vrijwel volledige omzetting van biomassa in een gasvormig product is technisch nog niet haalbaar. (3) De vergasser vereist aanzienlijke hoeveelheden energie voor de endotherme vergassingsreacties. (4) Het is moeilijk om te voldoen aan de eisen voor efficiënte gasreinigingstechnologie.

De vergassingsprestaties kunnen worden verbeterd door de opwekking van elektriciteit en warmte te integreren. SOC's zijn zeer efficiënte elektrochemische apparaten voor zowel brandstofproductie als stroomopwekking, doordat de werking omkeerbaar is. Een SOC kan het door vergassing geproduceerde gas omzetten in brandstof of stroom. Vergassings– en SOC–technologieën werken beide bij hoge temperaturen, en de uitlaatgassen van de brandstof– en zuurstofelektroden van de SOC zijn potentiële vergassers en warmtebronnen voor het endotherme vergassingsproces. Dit werk onderzocht twee vergassingsmethoden, plasmavergassing en superkritische watervergassing (SCWG), gecombineerd met SOC–technologie. De energie die nodig is om biomassa met een hoog watergehalte te verwerken door vergassing kan worden

geminimaliseerd door de thermofysische eigenschappen van het water te variëren middels druk en temperatuur, welke de verdampingswarmte beïnvloeden.

Als resultaat werd een hoogefficiënte afvalwaterzuiveringsinstallatie voor thermochemische vergassing en vaste oxidebrandstofcel (SOFC) ontwikkeld (hoofdstuk 2). Dit systeem omvat een energiezuinige zelfverwarmende wervelbeddroger en een indirect verwarmde meertrapsvergasser die wordt verwarmd door een microgolfplasmatoorts en proceswarmte. De droger maakt gebruik van de latente warmte van stoom onder druk, waardoor het energieverbruik van het drogen aanzienlijk wordt verminderd. De indirect verwarmde tweetrapsvergasser zorgt voor de volledige omzetting van biomassa in syngas door scheiding van pyrolyse en vergassing. De indirect verwarmde vergasser en optimale verhouding vergassingsmiddel garanderen de productie van syngas met een hoge verbrandingswaarde: Het syngas is rijk aan H2 en CO en laag in CO2. Deze configuratie biedt gunstige procescondities om een hoge energieomzetting (elektriciteitsproductie) efficiëntie van 65% te bereiken bij gebruik van biomassa met een watergehalte van 75% (op gewichtsbasis), gedroogd tot een watergehalte van 30% voordat het naar de vergasser wordt gevoerd. Een gasreinigingsunit scheidt de onzuiverheden. Dankzij een tweetraps SOFC kan het systeem een groter deel van de brandstof benutten.

Een SCWG–SOFC gecombineerd systeem (Hoofdstuk 3) is een eenvoudige methode voor het verwerken van natte biomassa. Een droger is niet nodig omdat het water het vergassingsmiddel is en het geproduceerde syngas relatief schoon is. Het superkritische water bevordert de afbraak van organisch materiaal in gasproducten en de scheiding van anorganische materialen. De SCWG–omzetting van biomassa in gas hangt af van de effectiviteit van de katalysator en de bedrijfsomstandigheden van de vergasser. Het gebruik van een combinatie van een hoge temperatuur en een hoog vochtgehalte van de biomassa bevordert de volledige omzetting van biomassa, maar het rendement van de vergasser neemt drastisch af en de technische beperkingen van bouwmaterialen worden belangrijk. Daarentegen belemmert het werken met de SCWG bij een lagere temperatuur en een lager vochtgehalte van de biomassa de volledige omzetting van biomassa, waardoor de toepassing van een actieve katalysator nodig is. Deze omstandigheden beïnvloeden de efficiëntie van het SCWG–SOFC–systeem en hebben de introductie van SCWG–technologie in industriële toepassingen vertraagd. In deze studie is een parametrische analyse uit van het SCWG–SOFC–systeem uitgevoerd om de energie– en exergieprestaties van het systeem onder verschillende bedrijfsomstandigheden voor de SCWG en SOFC te schatten. De gegevens waren nuttig voor het ontwerpen van een nieuwe

systeemconfiguratie met een betere efficiëntie en minder technische beperkingen. Als resultaat bereikte het systeem een efficiëntie van 44% bij gebruik bij hoge temperatuur (500°C), een vochtgehalte van >90% op gewichtsbasis en een hoge brandstofbenutting in de SOFC. Deze operatie zorgde voor een bijna volledige omzetting van biomassa, wat ervoor zorgde dat het SCWG–productgas een voldoende hoge thermochemische exergie had die geschikt was voor integratie met stroomafwaartse cycli om de systeemefficiëntie te verhogen.

Een omkeerbaar gecombineerd SCWG–SOC (rSOC)–systeem (hoofdstuk 4) is een nieuwe configuratie die wordt gebruikt voor brandstof– en stroomopwekking en energieopslag. Deze methode biedt een mogelijke oplossing om de bedrijfskosten te verlagen en de thermodynamische efficiëntie van het SCWG–systeem te verbeteren. De nieuwe configuratie heeft tot doel de capaciteit van het systeem voor waterstofproductie aanzienlijk te vergroten en de thermodynamische efficiëntie te verbeteren door de vernietiging van exergie te verminderen. De SCWG–rSOC–systeemconfiguratie gebruikt minder proceseenheden en de vernietiging van warmteoverdracht exergie wordt verminderd door een lager temperatuurverschil tussen stromen. Het concept maakt gebruik van het feit dat SCWG, werkend bij het meest verhoogde biomassavocht, zorgt voor een bijna volledige omzetting van de droge biomassa in syngas. De lage oplosbaarheid van anorganische stoffen in superkritisch water garandeert een gemakkelijke verwijdering. Het relatief schone productgas van SCWG, rijk aan H2O, is dus een potentiële brandstof voor een rSOC die in de elektrolysemodus werkt. Het systeem, aangedreven door goedkope hernieuwbare elektriciteit, elektrolyseert het gasproduct om een aanzienlijke hoeveelheid syngas te genereren. Bij het stroomafwaartse koelproces komt voelbare warmte vrij die wordt gebruikt voor de brandstof– en luchtvoorverwarming. Het water dat in een gasopwaardeereenheid wordt afgescheiden is minimaal. Het syngas wordt opgeslagen voor verdere stroomopwekking. Tijdens de werking van de brandstofcel wordt de rSOC gevoed door het SCWG–syngas en opgeslagen syngas dat wordt gegenereerd in de rSOC–elektrolysermodus. De systeemefficiëntie van de SCWG–rSOC in de elektrolysermodus is recht evenredig met het biomassavocht. Met een vochtgehalte van 95 gew.% biomassa bereikt het systeem een exergie–efficiëntie van 73%. De hoogste exergie–efficiëntie die in de literatuur wordt gerapporteerd bij het toepassen van verschillende configuraties, is ongeveer 20%. De systeemcapaciteit voor de productie van waterstof of stroom wordt meer dan tien keer zo groot.

De verkregen resultaten geven aan dat een vergassings–SOC–installatie mogelijkheden biedt voor zeer efficiënte energieterugwinning en –opslag, naast

sanitaire doeleinden. De maatschappelijke toepassing van de voorgestelde technologieën vereist echter meer onderzoek en ontwikkeling. Er zijn nieuwe systeemconfiguraties nodig die verschillende technieken voor warmteoverdracht gebruiken. De meer kritische exergievernietiging, die de systeemefficiëntie beïnvloedt, vindt plaats bij de voorverwarming van lucht en brandstof. Het is noodzakelijk om de volledige omzetting van biomassa in een gasvormig product experimenteel aan te tonen door de voorgestelde concepten onder variabele bedrijfsomstandigheden toe te passen. In het geval van onvolledige omzetting van biomassa in de vergasser, is het noodzakelijk om het gedrag van de rSOC in de elektrolysemodus te begrijpen wanneer brandstof met een mengsel van H2O en hogere koolwaterstoffen wordt gebruikt.

In de toekomst zou de samenleving kunnen kijken naar alternatieve energieopwekkingssystemen op basis van afvalwaterzuivering op middelgrote of grote schaal. De mensheid moet nieuwe methoden ontwikkelen om duurzame energie en sanitaire voorzieningen te leveren om de levenskwaliteit te verbeteren en de aantasting van het milieu te verminderen.

1

Introduction

Mayra Recalde: The Forgotten Lake

Wastewater treatment is vital for social and technological development.

1.1 Overview

Sustainable development requires new technologies that efficiently address multiple social challenges, such as sanitation and clean electrical energy. These technologies must be efficient in producing zero emissions (microbial, organic and inorganic water contaminants, and greenhouse gases), ensuring better global energy distribution, and providing an equitable and sustainable infrastructure for serving the increasing global population.

Over the past decades, there has been a significant increase in the total fuel consumption of non–industrialised countries, such as China, as well as in marine and aviation bunkers. Meanwhile, the fuel consumption of the top–emitting countries has remained relatively constant. According to the Energy Transition Outlook (ETO), net zero emissions should be achieved by 2050 [3] [137].

However, a strong relationship exists between energy and water resources in all sectors. Demand, distribution, and infrastructure are parallel but highly independent. For example, industries use energy and freshwater to produce products. Human settlements, as well as industrial and agricultural activities, are the primary sources of water pollution [3]. Approximately 80% of the global wastewater is discharged untreated [4]. Consequently, the global population may be affected by the absence of wastewater treatment systems [5]. In addition, the lack of opportunities and appropriate technology to prevent environmental degradation in human settlements has resulted in numerous refugee movements [6]. The United Nations recognizes the pressing need for humanity to enhance its capacity and willingness for more efficient resource consumption and production while simultaneously achieving economic growth without causing environmental damage [7]. In this regard, promoting fair and equitable utilisation of environmental resources is highly desirable.

The sustainable treatment of wet biomass, such as human waste, manure, and food residues, is essential for public health and the energy sector. Ensuring the elimination of faecal bacteria and viruses from soil and water is vital for maintaining a healthy community. Additionally, it contributes to the production of clean electrical energy, aligning with the transition towards a sustainable energy system.

Sanitation–related diseases cause approximately 2.2 million deaths per year, primarily affecting children younger than five [186] [78]. Furthermore,

more than one billion people still practice open defaecation. Sanitation refers to the collection, storage, transportation, and transformation of human excreta and wastewater [76]. It has multiple benefits for health and the ecosystem, as well as food security, business growth, and energy. Sanitation is a crucial element in sustainable development [77]. However, there is currently a global disparity in terms of sanitation. The Sustainable Development Goals for 2030 aim to ensure universal access to adequate and equitable sanitation and hygiene, thereby eliminating open defaecation. Nonetheless, these goals can be effectively achieved through radical innovations in sanitation, which should incorporate the safe recovery and reuse of water, nutrients, organic matter, energy, and minerals [79].

Therefore, there is a strong emphasis on promoting innovative sanitation technologies. Some programs have funded sanitation technologies that are affordable, resource–recovery oriented, off–grid capable, and economically viable [80]. Thermochemical, electrochemical, and biological processes have been extensively studied through various initiatives to harness energy from human sludge. As with any new technology, a thorough understanding of the underlying physics and chemical reactions involved in these processes is crucial. Such technologies can process organic matter to produce several types of biofuels, such as syngas, biochar, and bio–oil. The quality obtained for the syngas produced depends on the specific conversion process employed and the chemical composition of the biomass being treated.

Some sewage demonstration plants produce hydrochar via hydrothermal carbonisation, and this method appropriately treats biomass with a high MC. However, engineering limitations require a solution to improve conversion efficiencies [83]. A human waste electrolysis cell, coupled with molecular hydrogen (H_2), was developed by Kangwoo et al. [84]. Its energy efficiency is extremely low compared with those of ideal electrolysis units. The direct pyrolysis of faecal sludge has been utilised to produce biochar [80], which is a promising method for thermal management [85]. However, information on the physical properties of biochar obtained from faecal sludge for further use as a carbon (C)–neutral fuel is unavailable.

Biological technologies, such as conventional activated sludge (CAS), have been widely used in the last century. However CAS is a highly energy–intensive process that is relatively ineffective in treating toxic substances. Moreover, it produces waste–activated sludge whose disposal is becoming

increasingly expensive and complicated [8] [9]. The wastewater industry requires new innovations to reduce the adverse impact of water usage on society and environment. This can be achieved by harnessing the material resources available in wastewater, including recovered water/energy, nutrients, and valuable inorganics, which are essential for social prosperity [8]. Anaerobic digestion (AD) is a biological technology that stabilises the waste solids produced during municipal wastewater treatment and generates biogas with efficiencies ranging from approximately 20 to 70% [10]. A multigeneration system concept integrated with biogas produced from the AD process of sewage sludge, can generate power, freshwater, heat, and H_2. The overall energy and exergy efficiencies of such a system were found to be 63.6 and 40%, respectively, while the digestion energy and exergy efficiencies were 78.1 and 57.2%, respectively [11]. However, the AD method requires new combinations of techniques to enhance biogas production for technological adaptation, commercialisation, and environmental considerations [12] [13]. The energy balance of an integrated CAS–AD system must account for the energy utilised in CAS wastewater treatment, as it can affect the overall efficiency of wastewater treatment.

Among thermochemical processes, pyrolysis and gasification have the primary advantage that feedstock can be converted into fuel within seconds or hours, unlike biological treatment, which requires days or months. In terms of gas emissions, gasification and pyrolysis are more environmentally–friendly than combustion and incineration [82]. The high temperatures involved in these processes help destroy pathogens, and their continuous process can be facilitated via compact reactors [17].

Biomass gasification is a widely accepted conversion method that has attracted considerable research attention. It can directly transform faecal matter into a safe product, free from pathogens, while also recovering syngas [14]. Furthermore, it is possible to integrate gasification with existing biological treatment processes [9]. The investigation of biomass gasification–based polygeneration plants is underway to explore their technical and environmental benefits [15] [13].

1.2 Wastewater composition

Table 1.1 lists the proximate analysis and energy content of different fuels and wastewater from various sectors. Sewage is a solution that contains organic and inorganic materials, along with a high concentration of water. The energy

content of sewage depends on the organic content. Petroleum wastewater, sewage sludge, and coal have similar energy values of approximately 23 MJ kg^{-1}. The high MC of sewage may be advantageous or disadvantageous depending on the treatment procedure. Apart from energy, the recovery of valuable solids from wastewater is also crucial. The extraction of valuable elements from sewage sludge can have monetary value [19]. Sewage sludge contains useful elements such as metals (silver (Ag) and copper (Cu)) and nutrients, while the phosphorous concentration in wastewater can range from 4 and 16 mg L^{-1}. Petroleum wastewater sludge is characterised by high levels of heavy metals [18]. Faecal matter (FM) has a heating value of 25 MJ/kg when dried and charred [138].

Table 1.1. Feedstock properties relevant to thermal conversion process

Feedstock	Coal [16]	Wood [17]	Manure [17]	AVG HF [81]	Primary sewage sludge [17]	Petroleum wastewater sludge [18]
Proximate analysis						
Fixed carbon (%)	38.6			7.3		10.51
Volatile fraction (%, db)	40	70–90	57–70	4	60–80	5.52
Ash (%, db)	15.7	0.1–8	19–31	11.7	25	5.06
MC (%, fresh weight)	5.7	35–60	21–99.7	77	90–95	78.91
Energy content (db) (MJ/kg)	24.3	19–22	13–20	20.45	23–29	23.60

db–dry basis, AVGHF–average composition of all human faeces samples

1.3 Gasification; a method for biofuel and mineral recovery

Gasification is currently implemented at the industrial level. However, the resulting gas is of low quality and contains high amounts of impurities (such as tar, particles, hydrochloric acid (HCl), and hydrogen sulphide (H_2S)). The design of a proper gasifier enhances tar reduction, thereby improving conversion efficiency. For energy recovery, undesirable substances may be eliminated from the produced gas. Furthermore, gasification requires a considerable amount of energy due to the endothermic nature of the reactions and the dewatering of high–moisture feedstocks. Heat can be supplied through the combustion of a portion of the gas produced using oxygen (O_2) from air or an external source of heat (allothermal gasification) [86]. Therefore, the thermal efficiency and design of a

gasifier are dependent on energy consumption during the gasification and drying processes, which represents the primary limitation of this technology.

Gasification involves thermochemical and hydrothermal reactions. The process operates at high temperatures (between 400 and 1400°C) and ambient or high pressures (up to 34 bar). Consequently, organic matter decomposes into gaseous products, separating some inorganic matter. Various parameters define the efficiency of a gasification process, such as the product gas composition, energy content, cold gas efficiency (CGE), carbon conversion efficiency (CCE), and tar char content [20].

The complete conversion of organics into gaseous products and the separation of inorganics depend primarily on operating conditions such as temperature, gasification agent (H_2O, O_2, H_2O/O_2, supercritical water (SCW)), pressure, residence time, use of catalyst, and gasifier design [21][22] [23][24]. Syngas is the primary product of biomass gasification. The incomplete conversion of biomass into gaseous products generates char and tar, which is a mixture of aromatic hydrocarbons. The production of tar is a potential challenge in biomass gasification, as it can lead to blockages in downstream equipment [25] and reduce syngas production, consequently affecting the system efficiency. The average tar yield from dry gasifiers has a minimum of approximately 0.4 g Nm^3 and a maximum of 50 g Nm^3. Fuel cells have a minimum tar tolerance of less than 1 g Nm^3 [26]. Tar content below 0.05 g/Nm3 is required for the producer gas to be suitable for downstream processes [20].

Fuel conversion in dry gasification can be optimised by applying different strategies. Staged gasification promotes a high conversion of tar and char within a gasifier by creating various thermal levels [27][28].

Table 1.2. Conversion of dry sewage sludge gasification

Biomass feedstock	Gasification method	Temperature °C	Tar content g/Nm^3	Gasifier agent	CCE %	Ref.
Sewage sludge	Bench–scale fluidized bed	850	29.4	oxygen		[46]
Sewage sludge + limestone	FBG	850	20.21	Steam–oxygen		[47]
Sewage sludge	FBG	850	15	Steam–oxygen		[30]
Sewage sludge + limestone	FBG	850	27	Steam–oxygen		[48]
Sewage Sludge	Two–stage	802 first stage 798 second stage	2.19	Air–steam	91.9	[49]
Sewage Sludge + AC	Three–stage	709 first stage 802 second stage 798 third stage	0.22	Air–steam	93.15	[50]
Sewage Sludge + Fe–impregnated AC	Three–stage	650 first stage 815 second stage 815 third stage	0.041	Air–steam	75.79	[51]
Sewage sludge	SCWG continuous	600		Supercritical water	73	[52]
Chicken manure	SCWG FBG continuous	620		Supercritical water	99.2	[43]

AC: activated carbon, CCE: carbon conversion efficiency, FBG: fluidized bed gasifier

According to Kargbo et al. [29], two–stage gasification systems are 25% more economical than single–stage reactors. Materazzi et al. [29] proposed a two–stage fluidised bed plasma–gasifier converter process in which the levels of tar are almost negligible after plasma treatment. Table 1.2 lists the CCE of dry sewage sludge converted into syngas using single and staged gasification methods. The three–stage dry gasifier favoured almost complete fuel conversion, which was substantially reduced in the two–stage gasifiers. High gasification temperature > 800°C significantly reduces char and tar, promoting tar cracking and reforming reactions [30], whereas the MC of biomass influences the thermal balance and chemistry of the gas product. Biomass with MC lower than 35 wt.% ensures adequate gasification performance [31]. Drying is a pretreatment process that usually removes excess water from biomass. The application of a dryer to sludge requires a considerable amount of heat, leading to high costs. Some authors have reported that dry gasification is inefficient for feedstocks with high MC [13].

SCWG is a process for treating feedstocks, such as municipal sludge, with high MC to produce syngas [32]. SCWG operates at pressure and temperature exceeding the critical point of water pressure > 25 MPa but relatively lower temperature (400–600°C) than dry gasification (800–1200°C) [33]. This process avoids water drying because supercritical water is the reaction medium and reactant, in addition to biomass [34]. Complete gasification and product distribution depend primarily on pressure, temperature, dry matter content, residence time, and the catalyst [35] [36]. The gaseous products are H_2, CO_2, and methane (CH_4) [37]. One of the advantages is that the solubility of inorganic salts in supercritical water is low, which is key to separating and recovering phosphorus from sewage sludge [38] [20]. Thus, the costs of processing and purification units in SCWG are low [39].

SCWG technology has the potential for large–scale applications [53]. The average H_2 production cost with SCWG technology is US$ 0.111 N m^3 at the laboratory scale [39] and is lower than that of dry biomass gasification [1] but higher than that of fossil fuel–based H_2. Considering the relatively high prices, SCWG should not be regarded as a single process but in combination with other processes, such as power generation [33]. The H_2 production cost can be reduced by increasing the system capacity [1]. This reduction can be achieved by using a combination of operating parameters [32]. However, several challenges need to be solved, such as severe corrosion of the reactor in a high–temperature

environment [45]. This requires complete gasification at low temperatures and the preparation and screening of catalysts with high activity and long life. In addition, SCWG systems must be optimised for energy efficiency [1]. The development of commercial biomass SCWG requires the resolution of these issues before implementing biomass SCWG at the industrial wastewater level.

Syngas produced by gasification has an advantage over solid or liquid fuels produced by diverse methods such as pyrolysis and fermentation. They can be directly processed in the fuel electrode (anode) of an SOC, generating power or fuel (H_2, CO, or CH_4) with high efficiency. Fortunately, SOC technology fed by natural gas or H_2O is employed at the industrial level, whereas SOCs for direct liquid and solid fuel processing are still in the research and development stage.

1.4 Power and fuel generation in solid oxide cells

Among power production technologies, solid oxide fuel cell (SOFC) are the most efficient for converting chemical energy from fuel into electrical energy. SOFCs are devices with no noise or moving parts, with their exhaust gases free of NO_x. A SOC is a high–temperature electrochemical technology that utilises fuel electrodes, oxidant electrodes, and solid electrolytes, as illustrated in Figure 1.1. The chemical potential difference between the fuel and oxidant electrodes generated an open–circuit voltage. At the circulating current, charge transfer occurs in the oxidant electrode via the electrochemical reduction of O_2 [110][111]. Hence, oxygen ions (O^{2-}) were transported through the electrolyte. The O^{2-} transports current, and another charge transfer occurs at the interface of the gas, electrolyte, and fuel electrode. This produces different electrochemical reactions, such as the electrochemical oxidation of combustible fuels (H_2 and CO), where electrons are released to generate power. When an external source supplies electricity to the SOC, H_2O and CO_2 are reduced, with the O_2 of the compounds reacting with electrons, producing H_2, CO, and O_2. Similar to other electrochemical systems, an SOC performs reversible operations. In other words, an electrical energy supply drives H_2 or CO production via redox chemical reactions (an electrolysis (EL) mode), and the SOC generates electrical energy when the same reactions are reversed (a fuel cell (FC) mode) [54]. The production of CO and O_2 via CO_2 redox chemical reactions is a potential method for C capture.

An essential advantage of a SOFC system is the relatively direct recovery of CO_2 from the anode exhaust, which is rich in H_2O and CO_2, with some

remaining H_2 and CO. The combustion of the residual combustible gas produces highly concentrated CO_2, which is relatively easy to separate and can be used in multiple applications. The SOFCOM proof–of–concept is a fuel–cell–based polygeneration plant that can produce electricity, heat, and clean water. The recovered CO_2 is converted into a fast–growing biomass (microalgae) in a photobioreactor [115].

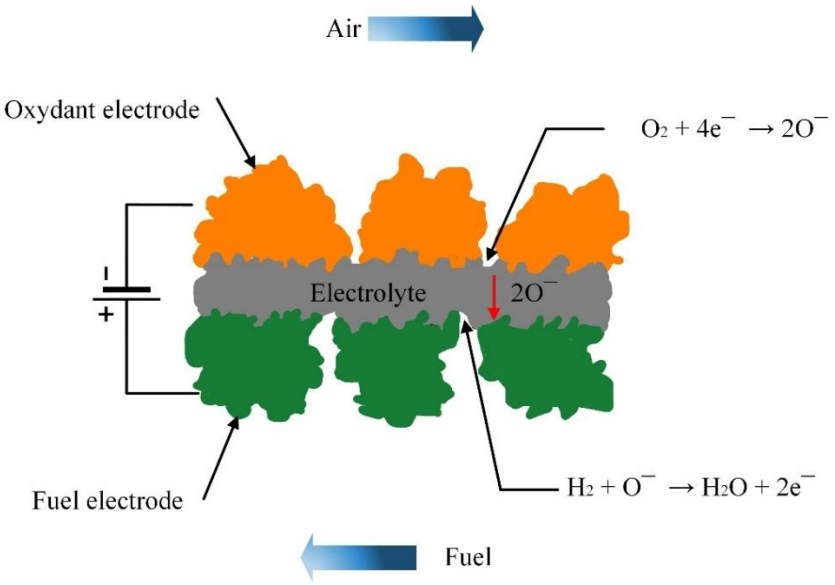

Figure 1.1. SOFC technology

The fuel electrode of the SOC electrochemically oxidises or reduces gases, such as H_2 or H_2O, and also promotes heterogeneous reactions and direct electrochemical oxidation of the fuel [55]. If external power is applied, fuel can be generated from C1 molecules [56], depending on the fuel electrode design. These features render SOCs flexible fuel devices. The optimal performance of an SOC depends on the SOC design, balance of the plant of the SOC system, and operating conditions, such as pressure, temperature, fuel utilisation, and current density. Variations in the operating conditions influence chemical and electrochemical reactions, which in turn control the generation of fuel, power, exhaust gases, and process heat because of the endothermic and exothermic behaviours of these reactions [57]. The primary design parameters of SOFCs, operating temperature, and fuel utilisation significantly influence thermodynamics and system efficiency. High fuel utilisation implies high power and heat generation in SOFCs, requiring cathode air to cool the SOFC stack [58].

Anode re–oxidation determines the range of operation of an SOFC stack. Lower fuel utilisation can extend the lifetime of a stack without degrading the anode [59].

Furthermore, internal reforming of hydrocarbon fuels is possible in nickel–based anodes when carefully optimised and operated [112]. The operating parameters of an SOFC stack during internal reforming are critical to avoid C deposition and thermal stress. The system cost, complexity, and realisation of high–efficiency SOFC performance for long–term operation depend on the operating parameters of SOFCs. Numerical simulations of direct internal reforming of CH_4 show that partial recycling of the anode exhaust reduces the risk of coking but does not eliminate it because it depends on the SOFC stack temperatures and molar H/C/O ratios [113]. The temperature distribution and fuel composition of an SOFC stack depend on the kinetics of fuel reforming and shift reactions [112].

The primary challenge with SOC technology is achieving stable operation using fuels containing impurities and hydrocarbons, such as CH_4 or higher hydrocarbons, such as benzene or toluene. The primary difficulties are C deposition on the fuel electrode, deactivating the SOC, and heat distribution due to CH_4 reactions with endothermic or exothermic behaviour [60] [61]. The chemical and electrochemical reactions in the SOC anode when the system contains impurities and hydrocarbons require sufficient understanding because of the complex structure of SOCs and the complex mechanisms involved in the thermochemical or electrochemical decomposition of hydrocarbons and impurities in the fuel electrode [62][63][64]. A gasifier design with almost cero higher hydrocarbon generation will reduce the mentioned SOC challenge.

1.5 Energy production from SOC gasification–combined system

Several factors have rendered SOC technology attractive for integration with gasification processes. SOC is a highly efficient exothermic and endothermic energy conversion method. The high operating temperature of SOFCs (600–1000°C) is advantageous for utilising produced heat in a bottoming cycle or gasifier. Thermodynamic calculations of the gasification–SOFC–gas turbine integrated system indicate that the system can achieve a high electrical efficiency of 74% [93] as a result of SOFCs. To maximise the performance of SOFC systems, SOFC hybrid systems, such as SOFC–GT and SOFC–GT–organic Rankine cycle, have been developed. Recently, a combination SOFC–

engine hybrid system has been presented by Kang et al. [114]. This method enhanced the electrical efficiency of the system in comparison to SOFC–micro gas turbines.

By coupling SOCs with gasification, high chemical and thermal efficiencies in the gasifier–SOC combined system can be achieved [65]. SOCs and gasification processes operate at high temperatures and generate exhaust gas streams containing CO_2, H_2O, and O_2 at elevated temperatures. The chemical components of these streams can serve as fuel sources for the fuel electrode of SOCs and as gasifying agents. The combination of SOCs with biomass gasification can increase the value and yield of syngas. This approach shows promise as a highly efficient method for fuel and power generation [66]. However, it must address the resistance of SOCs to C from different gasification products, such as CO, CH_4, tar, and sulpur (S)–containing compounds in flue gas [61]. Obtaining by the gasification process complete solid fuel conversion into a gas product with negligible tar concentrations is critical for developing SOFC technology and the implementation of an inexpensive gas–cleaning process. According to the literature, thermodynamic equilibrium models assume the complete conversion of solid fuel into syngas owing to simplifying assumptions. Some models enhance thermodynamic model accuracy using modification methods, such as those employing tar and char, by modifying coefficients [20].

In terms of experimental and thermodynamic simulations of biomass gasification, different research groups have investigated combined SOFC systems. The use of SOFCs in waste–to–energy systems has been demonstrated at TUDelft [67] on a laboratory scale for power generation by integrating a plasma gasifier (PG)–SOFC system with a wastewater–ammonia SOFC system. Recently, experimental demonstrations have presented a combination of a two–stage biomass gasifier, SOFC system, C filter, and desulphurise unit at 90°C to clean the gas. The system efficiency reached 39.6% with 69% fuel utilisation [68]. The integration of gasifier–SOFC systems and SCWG–SOFC has been extensively investigated in recent years. However, there are only a few dry gasifier–SOFC combined systems fuelled with sewage at the pilot and simulation stages. Some methods have reported moderate efficiencies lower than 10%, with biomass moisture of 85 wt.% [69] [70]. SCWG–SOFC thermodynamic efficiencies of approximately 50% have been reported, assuming complete biomass conversion with biomass moisture of 85 wt.% [71].

Integrating steam electrolysis and gasification to produce syngas offers a solution for managing intermittent energy sources, such as wind and solar. The concept is to store electricity by producing syngas [72]. By including the reversible characteristics of electrochemical processes, syngas consumption for electricity production is possible. The fuel efficiency of an electrolysis plant in a syngas mode reaches approximately 70% [73].

No experimental results have been obtained regarding the continuous operation of SOFCs fuelled with gases containing high amounts of hydrocarbons originating from incomplete gasification [63]. Designing a highly efficient sewage system for energy generation requires an understanding of the conversion of sewage in a gasifier and the conversion of the gas produced in an SOC fuel electrode. However, several aspects need to be defined in an SOC fuelled with the gas produced by wastewater gasification. These aspects include the SOC reversible power, fuel production characteristics, fuel flexibility, and heat production. The complete conversion of sewage into gaseous products depends on the operating conditions and reactor design. The influences of these factors on system performance have received little attention. Hence, a gasification–SOC system configuration for high–efficiency energy generation from wastewater has not been realized.

A thermodynamic simulation of energy conversion systems based on minimisation of Gibbs energy using flow sheets such as Cycle–Tempo and Aspen Plus™ is a practical approach to investigate the performance of wastewater gasification–SOC combined systems for fuel and power production [48]. This simulation contributes to calculating the first– and second–law efficiencies. It conducts sensitivity analysis and optimises the new innovations. The basis of this simulation is applying the chemical, physical, and electrochemical principles previously analysed for each process to obtain a technically and economically feasible and efficient novel system concept for wastewater treatment. In addition, the analysis considers the engineering limitations caused by the operating parameters of the system.

The thermodynamic analysis of a wastewater gasification–SOC system determines the energy and exergy efficiencies and the contributions to irreversibilities caused by the components of the system. The expected results represent an alternative to the currently applied conventional activated sludge – anaerobic digestion (CAS–AD) methods for wastewater treatment. This novel system can represent a sustainable energy and sanitation service infrastructure for

the increasing global population. It also aids in the reduction of CH_4 (an extremely flammable gas) emissions from municipal solid waste landfills, which can influence the ambient atmospheric composition [74], [38]. Furthermore, introducing a superior alternative to CAS–AD methods could greatly accelerate the adoption of these technologies.

1.6 Research objectives and scope

This dissertation examines the technical parameters necessary for the successful integration of a gasifier–SOC as an efficient wastewater treatment process. The performances of two gasification methods, dry gasification and SCWG, were investigated. Gasification needs to address some barriers to effective integration with SOC technology. These barriers include achieving almost complete conversion of the fuel into syngas within a gasifier of approximately 100% CCE to reduce the cost of the gas–cleaning process. The gasifier requires an optimal water content for efficient operation. The gasifier–SOC system integration requires a thermal strategy to recover process heat and exhaust gas distribution. The new system was tested at a dry biomass flow rate of 0.56 g s^{-1}.

Main research question: Previous studies have identified research directions for biomass gasification (SOCs), mainly considering dry biomass (moisture content < 40 wt.%,), using an intensive gas–cleaning unit to remove impurities (including tar) and a gasifier at thermodynamic equilibrium, and their implication on energy efficiency. Thus far, the literature has not reported attempts for power generation efficiency > 50% from biomass with MC higher than 85 wt.% [75] with gasifier desing to reach almost full carbon conversion (almost cero tar production). The main research question is how to develop the wastewater gasifier-SOC technologies for the same.

This dissertation addresses three concerns that identify some criteria for the technical feasibility of a wastewater gasification SOC process:

(i) the extent to which a dry gasifier–SOFC wastewater system is technically feasible for electricity generation

(ii) the influence of the operating parameters of a wastewater SCWG–SOFC system on its technical feasibility and energy efficiency

(iii) the best SCWG–SOC system configuration for enhancing the productivity of syngas from SCWG

Chapter 2 presents a novel integrated system concept for wastewater dry gasification integrated with an SOFC to achieve high efficiency and determines its technical feasibility. The basis of the system design is process heat integration. Gasifier and drying technologies have been experimentally demonstrated in literature reports or thermodynamically shown as attractive for achieving almost complete conversion of the fuel into syngas and being energetically efficient. The system processes biomass with an MC > 75 wt.%, different from the system configuration proposed in the literature. A gasifier–SOFC system model in the Cycle Tempo (CT) flowsheet program was used to design, analyse, and optimise the thermodynamics of the system. The effects of the dryer, gasifier, and SOFC operating conditions on these processes were considered and discussed.

Chapter 3 presents the background associated with the influence of operating conditions on the design of an SCWG in experimental and modelling research, with the combination of operational parameters determining the technical feasibility of the SCWG. In this study, a wastewater SCWG–SOFC system model was built to perform a thermodynamic analysis of the system using the Aspen Plus™ flowsheet program. The SCWG–SOFC system model is sensitive to operating parameters, such as SOFC fuel utilisation, SCWG temperature, and wastewater MC. The system model **is used** to identify potential process flows that can be integrated into subsequent cycles to improve system performance.

Chapter 4 develops a conceptual design of a wastewater SCWG–reversible SOC (rSOC) system to demonstrate high efficiency and a significant increase in the system capacity for H_2 production when the system operates in an EL, and an increase in power generation when the system operates in an FC. The results were compared with syngas production from a stand–alone SCWG unit and the power generated from a conventional SCWG–SOFC. The proposed system is a new approach to combat the high operating costs and engineering challenges of SCWG, facilitating their commercialisation.

We developed a thermodynamic analysis of the wastewater SCWG–rSOC system using a system model in the Aspen Plus™ flowsheet program. The system simulates the SCWG–rSOC–EL mode and in an FC mode and the results are compared with the SCWG–SOFC conventional system. The efficiencies and

exergy losses were calculated under different operating conditions. The thermodynamic analysis includes a sensitivity analysis of important operating parameters, including biomass MC, rSOC stack temperature and pressure, and current density. An rSOC mathematical model was developed using Fortran code in Aspen Plus™ to simulate the thermal behaviour of the rSOC stack. The rSOC model was validated using data from simulations reported in the literature. The model calculated the endothermic and exothermic behaviours of the rSOC stack under different operating conditions.

The conclusion and recommendations are presented, and future studies are proposed in Section 5.

2

Sewage gasification–solid oxide fuel cell power plant

Johannes Vermeer: Girl with a Pearl Earring

Women worldwide need to work hard to obtain pure water, which is essential for the care of the family.

Introduction

2.1.1 Gasification as energy recovery technology

To achieve the highest energy efficiency, biomass gasification plants generally operate to produce electricity in combined heat and power (CHP) configurations. In Europe, biomass gasification plants in these configurations have capacities lower than 1 MWe. In addition, allothermal gasification avoids the combustion of gaseous products, thereby maintaining the heating value of syngas and producing syngas without N_2 dilution [87]. Table 2.1 compares the operating conditions and efficiencies of several biomass thermal power plants. The lower heating value (LHV) of biomass was calculated from the elemental composition using a method proposed in [87].

Thermodynamic calculations for a human–sludge plasma–gasification–SOFC power plant indicate that the ηel of the system is negatively influenced by the high MC of feedstocks and high electricity demand of PGs. In the system model of Liu et al. [69], the ηel barely reached 5.4%, whereas in Mountouris et al. [70], the ηel had a value of 10%. According to experimental investigations, the ηel is high when relatively dry wood is used as the feedstock. The integration of plasma gasification with a steam turbine by Rutberg et al. [88] yielded an ηel of 33%. Panopoulos et al. [89] produced an ηel of 35.5% by combining allothermal steam gasification and a SOFC. Bang et al. [90] investigated the configuration of a two–stage autothermal gasification–SOFC micro–gas turbine power plant. This system achieved an ηel of 48%. The gasifier–SOFC configuration may contribute to increasing efficiency.

Toonssen et al. [91] reported that wet–biomass supercritical water gasification (SCWG)–GT systems achieve efficiencies up to 50%, and Facchinetti et al. [92] reported that the system SCWG–fuel processing turbines, GTs, and Rankine cycle reach an efficiency of 63%. However, these gasifiers have limitations in terms of catalysis and the development of high–pressure systems carrying combustible and toxic gases.

Dry biomass gasifier–SOFC–GT power plants operating at a pressure of 9 bar can reach a high electrical efficiency of 74% based on the thermodynamic calculations performed by Santhanam et al. [93]. In this combined system, heat is transferred from the SOFC stack to the gasifier via heat pipes, with the exhaust gas from the anode used as the gasifying agent. Nevertheless, high tar production and engineering limitations are expected in this combined system.

The gasifier comprised a char combustor and steam gasifier. The combustor is the primary heat source for the gasifier. This system is highly efficient because part of the exhaust gas from the SOFC anode is used as a source of steam and heat for the steam gasifier. The depleted air from the SOFC cathode is utilised as a source of O_2 and heat in the char combustor, and the process heat provides energy to the process streams. Nevertheless, owing to the relatively low operating temperature, the gas also has a high tar content, mostly exceeding 10 gNm^{-3} [86][95]. In addition, the oxidation of part of the fuel in the char combustor reduces the heating value of the produced syngas.

Using a similar gasifier configuration, Herrmann et al. [75] presented a gasifier–SOFC–steam turbine power plant fed with wood chips at an MC of 50%. Dolomite– and nickel–based catalysts can catalytically crack tar. The condensation heat of the exhaust steam from the steam turbine was used to dry the wet wood chips. This system achieved a high ηel of 61.2%. However, when biomass with a high inorganic content feeds this power plant, catalyst deactivation is possible. Furthermore, the heat production of district heating applications reduces steam turbine power generation.

The performance of a biomass gasification SOFC power plant can be significantly improved by recirculating SOFC exhaust gases to the gasifier, particularly from the anode side, and transporting heat into the gasifier via heat pipes from the post–combustion of anode and cathode exhaust gases.

Incorporating a dewatering unit before the feed enters the gasifier is required for all these systems. Evaporative and non–evaporative drying technologies commonly used for low–rank coals have been summarised by Rao et al. [96]. Such technologies can also be applied to dry faecal sludge. In particular, the excellent performance of a self–heating recuperation–based fluidised–bed dryer, which considerably reduces energy consumption during drying, has been reported [97]. Liu Y. et al. [98] investigated the above–mentioned wet biomass superheated steam dryer via experiments and simulation, reducing the energy consumption by 5% compared to the original drying system.

A multistage gasifier that separates pyrolysis and gasification into single controlled stages achieves high process efficiencies and produces syngas with low tar concentrations and high char conversion rates [99] [100]. The gasification of sewage sludge with activated C in two– and three–stage gasifiers produced H_2–rich and tar–free syngas [101]. Using plasma as a postprocessing stage for tar decomposition in a two–stage gasifier results in a tar–free gas product [102].

Table 2.1. Performance of different gasification-based combined system power plants.

	Liu et al. [69]	Mount-ouris et al. [70]	Rutberg et al. [88]	Pano-poulos et al. [89]	Bang et al. [90]	Facchinetti et al. [92]	Santha-nam et al. [93]	Sadhu-khan et al. [94]	Her-mann et al. [75]
Gasification process	Plasma	Plasma	Plasma	Allother.	Hybrid-Allother. two stage	SCWG	Allother.	Two FBG	Alloth er.
Results base on	Model	Exper.	Exper.	Exper.	Exper.	Model	Model	Model	Model
Biomass	Faecal matter	Sewage sludge	Wood	Wood	Wood	Wood	Casuarina	Straw slurry	Wood
Moisture content wt. (%)	80	68	20	10	32.2	80	15	8.5	50
Feed (kg/s)	0.0008	2.89	1	0.025	0.043	NA	2.2	0,064	0.41
Feed LHV (kJ/kg)	16841	15351	18437	19301	18183	18600	15500	14600	19301
Reactor temperature (°C)	>800	1000	900-1200	790-890	>800	400	800	950	850
Reactor pressure (bar)	Atm.	Atm.	Atm.	Atm.	Atm.	300	9	Atm.	Atm.
System net electrical efficiency LHV (%)	6.4	10	33	35.4	48	63	73.6	64	61
System net electrical efficiency HHV (%)	5.94	5,95	23	27	30	NA	70	62	57
Electricity generator	SOFC	Gas engine	Brayton and steam cycle	SOFC	SOFC	SOFC-Rankine cycle-GT-Fuel processing	SOFC-GT	SOFC	SOFC-Steam turbine

Plasma is an ionised gas resulting from an electrical discharge that provides sufficient energy to convert gas into plasma [103]. Owing to the resistance of the plasma, the gas reaches extremely high temperatures (ranging from 3000 to 7000°C) [104]. Hot gas is then used as a heat source for applications such as gasification [105]. The production of reactive species, such as atomic O and H_2 or hydroxyl radicals, is an additional advantage of using plasma. These species significantly enhance tar decomposition compared with conventional processes [106]. The reaction mechanism of plasma gasification is similar to that of conventional gasification [107]. However, unlike traditional gasification methods, partial fuel oxidation does not occur, resulting in a synthetic gas with a high calorific value [108]. The microwave–driven plasma biomass gasification concept has been experimentally demonstrated using cellulose as a model compound. The results are promising for the further development of small–scale gasification systems [109].

This study investigated a microwave plasma gasification power plant for processing faecal sludge. This method is most suitable for power production using SOFCs. However, the primary limitations of biomass gasification restrict the ηel of the system. These limitations include the impurities produced and the high energy demand for the gasification and dewatering of faecal sludge. Gasification is a mature technology, but the process has not been sufficiently understood, with numerous methods to improve this technology proposed in the last few years. Therefore, this study designed a moist faecal–sludge–gasification SOFC power plant configured to achieve an high ηel.

We proposed a new method for increasing the calorific value of syngas, thereby achieving high system efficiency. This system comprised an energy–efficient self–heating fluidised–bed dryer, an indirectly heated multistage PG, a microwave plasma torch, and an SOFC. Unlike the system configurations proposed in the literature, either from our group or other groups, in the present study, biomass at ≥75 wt.% MC was analysed, char combustion was avoided or reduced to the minimum as a heat source for the gasifier, and hydrocarbons, including tar, were entirely reformed in the PG. In addition to the microwave plasma torch, the system can use process heat to meet the energy demands of gasification and drying processes. Finally, a bottoming cycle such as a micro–steam turbine (MST) is used to generate additional power.

The present study developed steady–state thermodynamic modelling using the CT program [116], which contains several models for components and

processes that are combined to establish the desired system. The model results were compared with numerical and experimental data reported in the existing literature.

The effects of varying the operating conditions of the dryer, gasifier, SOFC, and MST on the processes in the system were considered and discussed. The sensitivity of the ηel of the system to these operating conditions was also investigated. The optimal operating conditions were determined from the perspective of electrical efficiency. Energy and exergy analyses were used to define the optimal heat integration network.

2.2 Methodogy

2.2.1 Plant design

Figure 2.1 shows the plant design. Dried faecal sludge was fed into a two–stage gasification process with a pyrolysis zone reactor (PZR) and PG to produce syngas. Several available energy sources provide gasification heat: SOFC waste heat, the combustion of depleted fuel from a SOFC, coupling with heat pipes, and electricity for a microwave–assisted plasma torch [109]. The recirculation of part of the anode exhaust from SOFC–2 to the PZR is another source of heat. This heat integration limits the power of the plasma torch used in the PG. This reduces the partial oxidation of fuel produced because none or only a small amount of O_2 is necessary, consequently maintaining a high heating value of the gas produced.

The high temperature and gas composition in the plasma torch favour the complete reforming of tar [106], improving the gas quality. The waste heat from the SOFC and heat required for the PZR were comparable. The intercooler between two SOFC stacks connected in series enabled heat integration between the two units. A two–stage SOFC improves SOFC power generation efficiency and combined cycle efficiency. This configuration increases the voltage of SOFC–1 and reduces the power of the air blower in the SOFC system. Araki et al. [117]. numerically demonstrated an improvement of 5% of the SOFC efficiency using two–stage SOFCs. The SOFC stack requires excess fuel supply during fuel–cell operation to avoid anode oxidation. However, the amount of fuel required must be optimised. High fuel utilisation implies high heat production per unit of fuel, which increases the SOFC temperature and, consequently, the air blower power for SOFC cooling purposes. Two stacks in series achieved a slightly higher power than one stack. Intercooling between stacks reduces the amount of air used for cooling. Santhanam et al. [93] and Aravind et al. [118] demonstrated the relevance of two–stage SOFCs in a gasifier–SOFC system

context in which high efficiencies were achieved. Furthermore, the two–stage SOFC prevents the use of recirculation blowers [119]. This configuration prevents the use of the catalytic partial oxidation unit presented by Liu et al. [69], where syngas is combusted to control the H/C/O ratios and preheat fuel. Further details are presented in the Results and Discussion sections.

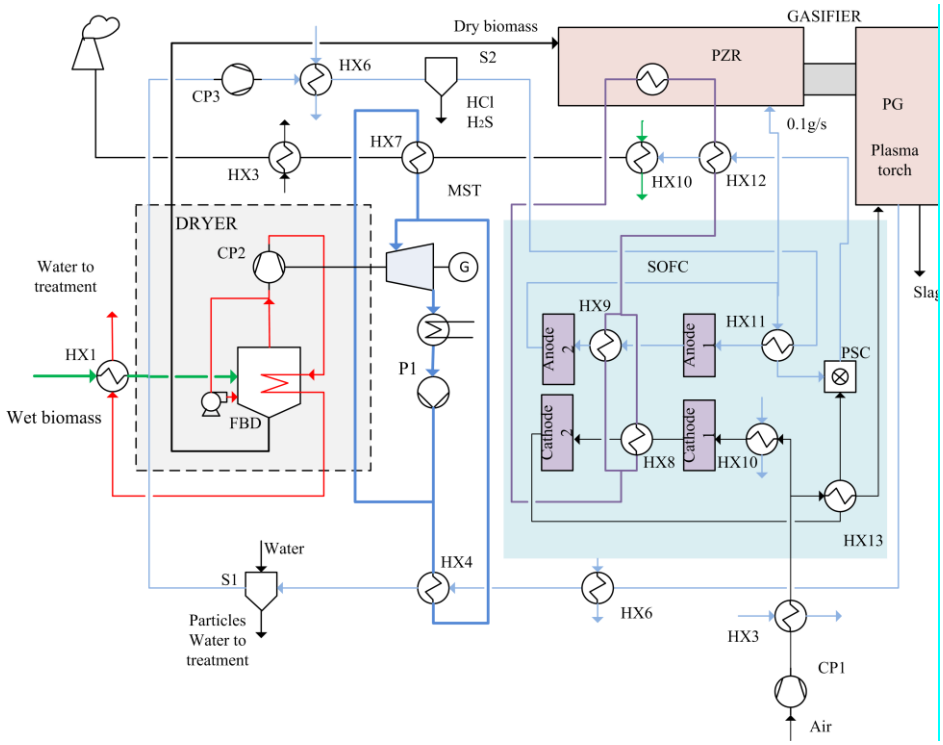

Figure 2.1. Process flow of the gasifier–SOFCMST system

As the MC of faecal biomass exceeds 90%, it cannot be gasified efficiently without removing a substantial amount of water. Therefore, most of the moisture is evaporated in a dryer in the most energetically efficient manner until an optimal MC is reached. The chemical reactions in the gasifier determine the optimal MC. The dryer unit operates on recycled sensible heat and recovered latent heat by compressing exhausted steam [98]. Compared with thermal drying, superheated steam drying does not require syngas combustion but uses power for steam compression. In addition, the system offers the possibility of using an MST in combination with a dryer, gasifier, and SOFC to enhance electric power output and overall plant efficiency.

2.2.2 Plant operation

In the system shown in Figure 2.1, faecal sludge containing 60–92% water was preheated in the heat exchanger HE1 to < 100 ºC at 1 atm and then fed into a fluidized bed dryer (FBD) to evaporate free water. The latent heat from the recycled steam compressed by compressor CP2 was used in the heat exchanger of the FBD for water evaporation in the bed. Then, after heating wet biomass in HE1, the condensate was transferred to a water treatment plant. Steam recirculated in the FBD was used as the drying medium.

After drying, the dry biomass enters an indirectly heated gasifier, which consists of two primary reactors: PZR and PG. First, the PZR, which operates at 700°C and 1 atm, decomposes the dry biomass. It is thermally coupled with heat pipes and fed with SOC–depleted fuel at a feed rate of 0.1 g s^{-1}. In this step, the steam is superheated and the biomass is converted into a mixture of gases and solids. Then, these products enter the PG to produce syngas using steam as the gasifying medium. The hot product gas leaving the PG at 950°C is used to evaporate water in HE4 and preheat the atmospheric air in HE3.

After passing through the heat exchangers, HE6 and HE4, the syngas at 120°C is cleaned to remove particles and water in a scrubber (S1). The partially clean syngas is heated in HE6 to 300°C, and S compounds and HCl are removed in a gas cleaning unit (S2). The clean syngas is heated in HE11 to 800°C and fed to anode–1 of the SOFC. Air is heated to 650°C in HE10 and fed to cathode–1 of the SOFC. Syngas is oxidised to produce electricity and heat in the SOFC–1 stack. The heat from the fuel and air from SOFC–1 are transferred to the PZR via heat pipes represented by HE8 and HE9. Then, the two streams are fed to the anode and cathode of SOFC–2, respectively, and the fuel is further oxidised to produce electricity and heat. Exhausted fuel from SOFC–2, at a rate of 0.1 gs^{-1}, is fed to the PZR, and the remaining part passes through heat exchanger HE11 to preheat the incoming fuel for the SOFC–1 anode. The exhaust gas, namely air with reduced O_2 concentration (16 mol%), from the SOFC–2 cathode preheats the air fed to the PG in HE13 to 800°C. The two streams are utilised in a PSC. Further details of the PSC are provided in the following sections.

Flue gases provide heat to the PZR via HE12 and pass through a heat exchanger (HE10) to transfer heat to the cathode air to obtain the required SOFC cathode inlet temperature. Next, the air in HE3 is preheated (shown in the two parts of Figure 2.1). The vapours produced in HE4 and HE7 are at 300°C and 30 bar. They are expanded in the steam cycle to be converted into electricity and

power for compressor CP2. Following the expansion, the vapour is condensed and pressurised in pump P1. Low condenser pressure is assumed based on a cooling water temperature of 15°C.

2.2.3 Plant model developed using CT

Plant model and assumptions: The feedstock used for this analysis was faecal sludge, and its ultimate composition is presented in Table 2.2. The gasifier and SOFC were the most important components of the combined system.

Table 2.2. Faecal biomass composition.

Ultimate Composition (wt.%–dry basis)	
H	6.3
C	42.96
N	2.36
S	0.10
O (by difference)	35.78
Ash	12.50
Moisture (% wet basis)	60–92
Energy content LHV (dry), (MJ/kg)	16.84

Gasifier model: The operating conditions of the gasifier were 1100°C and 1.013 bar. The syngas composition was determined by the gasifier design, gasifying medium, and gasifier operating conditions such as temperature, steam–to–biomass ratio (SBR), and air–to–fuel ratio. This two–stage gasifier produced an almost tar–free gas (200 μgm^{-3}) [106] suitable for SOFC applications, and the highest H_2 yield is achieved by steam gasification [120].

For this analysis, the PZR products were char, unpyrolysed biomass, tar, and syngas, and the PG products were a mixture of H_2O, N_2, H_2, CO_2, CH_4, CO, HCl, and H_2S, assuming that the char consisted of solid C. A mechanical system transports solid compounds generated in the PZR to the PG [121][122]. In this study, the gasifier was simulated based on chemical equilibrium considerations and Gibbs free energy minimisation. Assuming that the gasifier provides adequate residence time to reach equilibrium at the operating temperature and pressure, the electricity conversion to microwave energy is 95% [123].

Generally, a gasifier may include the following reactions drying, pyrolysis (2.1) and (2.2), combustion, reduction, and reforming reactions (2.3)–(2.9).

$H_2O_{(l)} \rightarrow H_2O_{(g)}$ $\Delta H = 43.99$ kJ/mol (2.1)

$C_6H_{12}O_5 \rightarrow C_{3.75}H_{2.25}O_{0.5} + 0.5CO_2 + 0.25CO + 2.88H_2O + C_{1.5}H_2O_{0.38}$ (2.2)

$C + O_2 \rightarrow CO_2$ $\Delta H = -394$ kJ/mol (2.3)

$C + 0.5O_2 \rightarrow CO$ $\Delta H = -111$ kJ/mol (2.4)

$H_2 + 0.5O_2 \rightarrow H_2O$ $\Delta H = -242$ kJ/mol (2.5)

$C_{(s)} + 2H_{2(g)} \rightarrow CH_{4(g)}$ $\Delta H = -74.8$ kJ/mol (2.6)

$C_{(s)} + CO_{2(g)} \rightarrow 2CO_{(g)}$ $\Delta H = 172$ kJ/mol (2.7)

$CH_{4(g)} + H_2O_{(g)} \rightarrow CO_{(g)} + 3H_{2(g)}$ $\Delta H = 206$ kJ/mol (2.8)

$CO_{(g)} + H_2O_{(g)} \rightarrow CO_{2(g)} + H_{2(g)}$ $\Delta H = -41$ kJ/mol (2.9)

Gasification involves the reaction of C with a gasifying agent (steam, CO_2, or a mixture of these gases (2.7) and (2.8)). These reactions are endothermic; therefore, gasification requires heat to maintain the reaction temperature. This heat is supplied by the combustion of part of the gas produced with O_2 (2.3)–(2.5) or by an external source of heat [86].

The gas composition was controlled by the steam–to–biomass ratio (2.8). However, a considerable amount of steam reduces the gasifier temperature, and additional heat is required to heat the steam. The highest LHV for syngas was obtained with a biomass MC of 0% [124], which cannot easily be achieved. Furthermore, a higher temperature contributes to a higher production of H_2 and an increased gas yield. However, it lowers the gas heating value [125]. A high reactor temperature is favourable for the thermal cracking and steam reforming of tar as the concentration of higher hydrocarbons decreases and those of syngas, H_2, and CO increase [126][127]. Moreover, the smallest feedstock particle size of < 0.3 mm provides the maximum yield of gas products, whereas the feedstock particle size in the range of 0.3–0.5 mm obtains the optimum gas composition and highest LHV of gas products [128][129].

In this study, the steam for gasification was produced from moisture in the biomass entering the PZR (30 wt.%). Then, it is heated and converted into steam for gasification. Moreover, 0.1 gs^{-1} of steam–rich depleted fuel is fed into the reaction biomass flow, as shown in Figure 2.1. The ratio of steam to dried biomass in the PZR is

$$SBR_{PZR} = \frac{\dot{m}_{steam}}{\dot{m}_{(dry\ biomass)}} \quad (2.10)$$

The ratio of available steam to pyrolysis gas in the PG is given by Equation 2.11 (steam is added to the PG in addition to that generated in and fed to the PZR):

$$\mathrm{SBR_{PG}} = \frac{\dot{m}_{\text{added steam}}}{\dot{m}_{(\text{pyrolysis gas})}} \quad (2.11)$$

SOFC model: The SOFC model calculates the output power, composition, and flow rate of the exhaust gases. These values depend on the operating conditions of the SOFC, including the temperature, pressure, syngas composition, fuel utilisation, and current density, as presented in Table 2.3. The fuel utilisation in SOFC–1 and SOFC–2 was varied to satisfy the heat requirements of the system. The resistance of the cell used in the calculation was estimated from the work of Jiang et al. [130] using anode–supported SOFCs (type 1) with a Ni+ yttria–stabilised zirconia (YSZ) anode and a YSZ–samaria–doped ceria (SDC) electrolyte. For comparison, the resistances of a commercially available Ni–YSZ anode, LSM–YSZ cathode, and YSZ electrolyte reversible solid oxide cell (type 2) are presented [131].

The stable operation of the stack may be disturbed by C deposition on the electrodes. The stable operating region was determined via equilibrium calculations using a C–H–O ternary diagram [132]. The steam–C ratio of the produced gas was controlled at S/C = 2 to prevent the deposition of C on the electrodes. A C–H–O ternary diagram prepared using the software package Fact Sage™ indicated that this value was in the C–free region and safe for SOFC operation.

Table 2.3. SOFC Stack: Assumed Parameters and Operating Conditions

Parameters and Operating Conditions	
SOFC–1 stack layers of cells	230
SOFC–2 stack layers of cells	120
Fuel Utilization SOFC–1 (%)	45–55
Fuel Utilization SOFC–2 (%)	50–60[a]
Current density SOFCs (Am^{-2})	1200
Cell Resistance (Ωm^2) (800°C) type 1	2.5e–5 [130]
Cell Resistance (Ωm^2) (900°C) type 2	5.0e–5 [131] [b]
Operating Temperature (°C)	900
Operating Pressure (bar)	1.013

a leading total fuel utilization of ~ 84% for the complete SOFC system.

b Comparison (different cell types).

Furthermore, C deposition might occur in pipelines and cause blockages, which may result in unfavourable consequences during system operations. According to Aravind et al. [133], biosyngas heating or cooling influences the

syngas composition, thus affecting the deposition of solid C, particularly in cleaning units and heat exchangers. However, several conditions, such as the kinetics of the reactions at low temperatures, short residence time of the gas, catalytic activity on the surface of the slag, and operating conditions of the gas cleaning unit, may influence C deposition. Therefore, although thermodynamic equilibrium conditions can prevent C deposition, they may still occur. Currently, C deposition in pipelines does not occur in biomass coal power plants that use hot syngas for steam generation [134]. However, this field needs further exploration and will therefore constitute the scope for future investigation.

Dryer unit model: In the dryer unit presented in Figure 2.1, wet biomass is dried from 60 to 92 wt.% to the optimum MC, which is determined by the gasification process, in a self–heated recuperation FBD using steam as the drying medium, as experimental conducted by Yuping et al. [98]. In the FBD, free water evaporates.

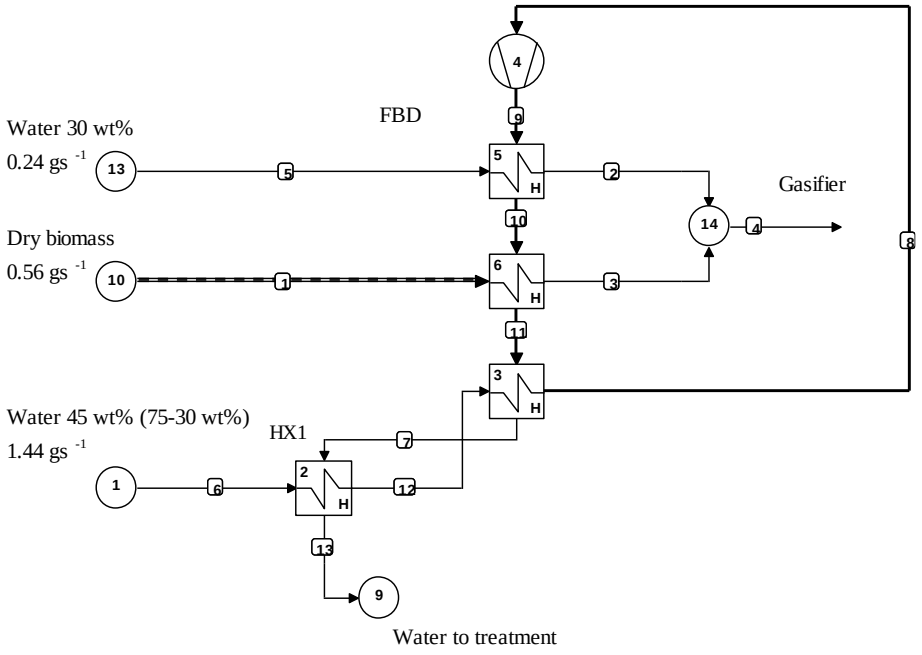

Figure 2.2. Layout of the superheated steam dryer modelled in CT.

The produced water vapour is pressurised to 2 bar, and then, latent heat is exchanged with the biomass in the bed, as shown in Figure 2.15. The MST drove the compressor. As shown in Figure 2.2, to simulate the FBD in the CT, three separate streams were assumed as follows: stream water with 45 wt.% is the flow rate of the free water that will be evaporated from the biomass from 75 to 30

wt.%; stream dry biomass is the flow rate of the dry biomass (25 wt.% of the total flow); stream water 30 wt.% is the flow rate of the final MC in the biomass. HE3 simulates the HE in the FBD (see Figure 2.1), where water is evaporated, and HE2 simulates HE1 (see Figure 2.1), where water is preheated. HE5 and HE6 simulated the temperature increase in the flows of dry biomass and the final MC in the biomass. The pressure of the compressor is adjusted to achieve a reasonable temperature difference in HE2, HE3, HE5, and HE6 and maintain the HE2 outlet temperature lower than that of the saturated water; therefore T < 100°C. Fluidising steam, which is the drying agent, was recirculated, and the model considered the energy consumption of the blower.

Table 2.4. MST: Assumed Parameters and Operating Conditions.

MST input	
Isentropic efficiency of expander	70% [136]
Isentropic efficiency of compressors	75%
Mechanical efficiency of compressors	95%
Turbine inlet temperature	300°C
Turbine inlet pressure	30 bar
Generator efficiency	95%

PSC: Exhaust gas combustion from the SOFC–2 anode and cathode occurs in the PSC. The air factor (λ) is the cathode–anode exhaust gas ratio divided by the stoichiometric ratio of these flows.

Energy and exergy model: The ηel of the SOFC–MST gasifier was calculated using Eq. 2.12, where $P_{el,\ out}$ is the electricity generated by the SOFC stack and MST (kW); $P_{el,\ in}$ is the electricity consumed by the plasma torch (kW); and $P_{el,\ aux}$ is the total power consumption of auxiliary components, including compressors and pumps (kW), $\dot{m}_{biomass}$ is the mass flow rate of the dry biomass fed to the system (kg s^{-1}); and the LHV biomass is the lower heating value of the dry biomass (kJkg^{-1}).

$$\eta_{el} = \frac{P_{el\_out} - P_{el\_in} - P_{el\_aux}}{\dot{m}_{biomass} \times LHV_{biomass}} \quad (2.12)$$

The net exergy efficiency (ηEx,el) of the gasifier–SOFC–MST is expressed using Eq. 2.13 as the ratio of the exergy of the products to that of the fuel input.

$$\eta_{Ex,el} = \frac{P_{el\_out} - P_{el\_in} - P_{el\_aux}}{\dot{m}_{biomass} \times E_{x,biomass}} \quad (2.13)$$

CGE, which is an indicator of the efficiency of the gasification process, is expressed using Eq. 2.14, where $\dot{m}_{syngas}$ is the mass flow rate of syngas (kg s^{-1}), LHVsyngas is the lower heating value of syngas (kJkg^{-1}), and E_h is the external heat (kW).

$$CGE = \frac{\dot{m}_{syngas} \times LHV_{syngas}}{\dot{m}_{biomass} \times LHV_{biomass} + E_h} \quad (2.14)$$

2.3 Results and Discussion

2.3.1 Gasifier gas composition

A

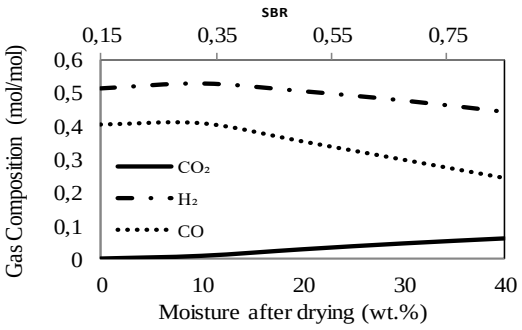

B

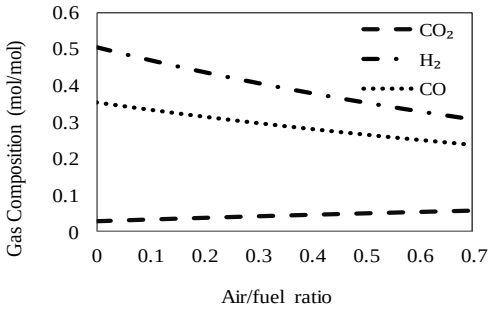

Figure 2.3. (A) Effect of the SBRPG on gas composition with air/fuel ratio = 0. (B) Effect of the air/fuel ratio on PG gas composition at 30 wt.% moisture; T = 1100°C.

Figures. 2.3A and 2.3B show the equilibrium gas composition at the PG as a function of the gasifying agent, and Equations. (2.3)–(2.9) govern the variation. The amount of CO_2 increases, whereas H_2 and CO decrease with increasing air–to–fuel ratios, as indicated by Equations. (2.3)–(2.5) (see Figure 2.3B). The amounts of H_2 and CO increase, as indicated by Eq. (2.8), reaching an optimal value at an SBRPG within the range of 0.35–0.4, whereas CO_2 is almost constant. At a higher SBRPG, CO_2 increases but CO and H_2 decrease significantly, as indicated by Eq. (2.9), because H_2O dilutes the gas (see Figure 2.3A).

Table 2.5 presents the operating conditions and gas composition of the experimental data compared with the results from the equilibrium calculations (Models I and II) at a specific SBR and air/fuel ratio in the PG. The equilibrium gas composition of the PG utilising steam as a gasifying agent, Model I, was also observed in the experimental results of plasma gasification obtained by Yoon et al.[107]. The results of Model II, utilising air and steam, are consistent with the experimental results of Rutberg et al. [88].

Table 2.5. Gasifier syngas composition: effect of the gasifier agents, steam and air, on the syngas composition; comparison between the present models and reported data.

Syngas composition (mol%)	Present Model I[a]	Yoon et al. [107]	Present Model II[b]	Rutberg et al. [88]
N_2	1.0	–	14.76	38.4
CO_2	3.16	6.00	5.37	9.3
H_2	56.36	57.00	44.38	28.1
CH_4	0.00	2.00	0.00	–
CO	39.47	35.00	32.95	23.7
Biomass	Excreta[c]	Glycerol[c]	Excreta	Wood
Gasification temperature (°C)	1100	NA	1100	900–1200
Fed MC (wt.%)	30 AD[d]	0	30 AD[d]	20
Gasifying agent	steam	steam	air/steam	air/steam
Air/fuel ratio	0	0	0.4	1.5
Steam to biomass ratio (SBR)	0.6[e]	0.8	0.6	NA
Cold gas efficiency (%)	~88	~100	100	~81

a Effect of steam on the syngas composition

b Effect of air on the syngas composition

c Ultimate composition of excreta is similar to glycerol and wood

d AD = after drying

e SBRPG see Eq. (11)

These experimental gasifiers operate at temperatures higher than 800°C. Therefore, these gasifiers can reach thermodynamic equilibrium, and the effect of the gasifying agent on the gas composition can be observed and compared with the equilibrium calculations.

The results of Model I were comparable to those of glycerol using a microwave PG [107]. Here, similar to the present Model I, no O_2 was added for gasification. Model I yielded slightly lower CO_2, equal H_2, and higher CO levels. Model II predicted higher amounts of H_2 and CO than those obtained in the PG by Rutberg et al. [88] because, in their study, more heat is released during the oxidation of biomass as more air is added, reducing the amounts of CO and H_2 and increasing that of CO_2.

The results obtained using the CT model must be demonstrated experimentally to confirm the composition of syngas. However, we concluded that, under comparable operating conditions, the equilibrium syngas composition calculated in the present gasifier model is consistent with the composition obtained from experimental results.

2.3.2 Influence of gasifier operating conditions on system efficiency

Effect of SBR: The SBR significantly influences the product gas composition and electric power input. When the pyrolysis products, including evaporated water, were fed into the PG, these species were converted to CO and H_2. CO in the gas reacts with the residual steam via a water–gas shift reaction (WGSR), increasing the contents of H_2 and CO_2 and decreasing the CO content, slightly reducing the heating value of the syngas, as the WGSR is slightly exothermic. Figure 2.4 shows the net electrical efficiency as a function of the SBRPG at an air/fuel ratio of 0.4 with biomass MCs of 10, 30, and 40 wt.% after drying. At low SBRPG values, electrical efficiency is high owing to the presence of sufficient amounts of H_2 and CO to be electrochemically converted in the SOFC. When the SBRPG increases, electrical efficiency decreases because the generation of additional steam requires high external energy for the plasma torch to heat the extra steam. In addition, an increased steam fraction reduces the voltage and power generated in the SOFC. Although additional power is generated in the MST and additional H_2 is produced at higher SBRPGs, see Figure 2.4, this may not justify the high energy demand for heating the steam.

However, although high CO_2 and H_2O concentrations reduce the SOFC power, less air is required to cool the SOFC at the cathode. The increased CO_2

and H2O contents cool the SOFC stack. This is reflected in the reduced power required to drive air compressor CP1. Generally, the airflow rate is determined by the cooling required to maintain the operating temperature of the SOFC. Furthermore, efficiency is the lowest when the biomass with 10 wt.% MC enters the PG owing to reductions in the amount of H_2 and CO.

The steam requirements for the chemical reaction in the PG are fulfilled by the water vapour released in the pyrolysis reactor from the MC of the biomass and 0.1 gs^{-1} of depleted fuel added to the pyrolysis reactor. This last flow contains water vapour because of the reactions in the fuel cells, where $U_f = 0.51$ for the first and $U_f = 0.58$ for the second fuel cell, giving a total $U_f = 0.84$ (related to the fuel at the inlet of SOFC–1).

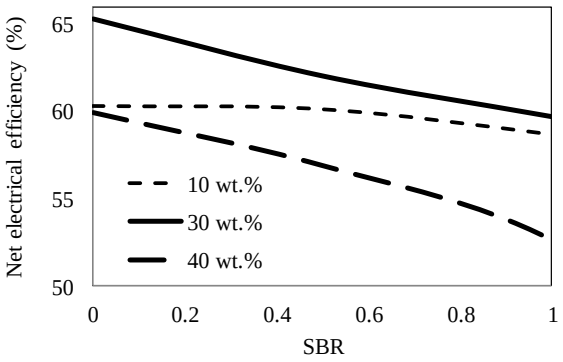

Figure 2.4. Effect of the SBRPG on system net electrical efficiency at 10, 30, and 40 wt.% MC feed to the PG; T = 1100°C.

Effect of air/fuel ratio on net electrical efficiency: When air is added to the PG, the pyrolysis products are partially oxidised and heat is released. Therefore, the heating value of the product gas decreases. Figure 2.5 shows the effect of the air/fuel ratio on the ηel at T = 1100°C, SBRPG = 0, and a biomass MC of 30 wt.% after drying. For high values of the air/fuel ratio, the ηel initially increases. Under these conditions, a relatively high H_2 yield is achieved and energy in the form of heat is released from the partial oxidation of biomass. Owing to high heat production, the PG used less electrical energy to create plasma flames. If a sufficient amount of air is supplied, the ηel decreases because of the low power production in the SOFCs, with less fuel available for electrochemical oxidation. At an air/fuel ratio within the range of 0.4–0.7, the power production in the fuel cell must be reduced by decreasing fuel utilisation to produce enough heat for the

PZR in the PSC. The fuel utilization of the two fuel cells changed from 0.51 and 0.58 to 0.45 and 0.5, respectively, dropping electrical efficiency.

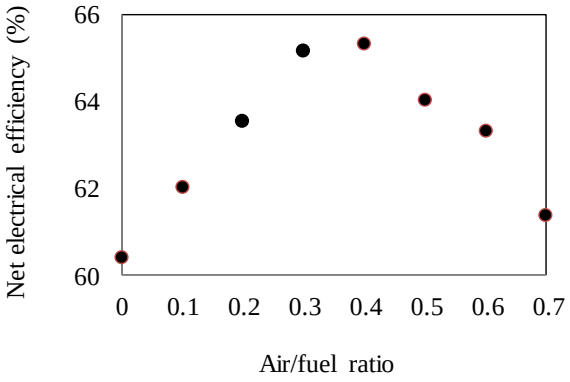

Figure 2.5. Effect of the air/fuel ratio on net electrical efficiency of PG; T = 1100°C and SBRPG = 0.

An air/fuel ratio between 0.3 and 0.4 yields an efficiency of 65%. At this point, sufficient air is supplied to produce heat for the gasifier, reducing the electricity consumption of the plasma torch. The H_2 yield is relatively high, resulting in high electricity production in SOFCs.

2.3.2.1 Gasifier temperature

The plasma power in the PG governs the gasification temperature, and an increase in plasma power increases the temperature of the reactor. Figure 2.6 shows the effects of temperature on the ηel of the system at a constant air/fuel ratio of 0.4, SBRPG = 0, and biomass MC of 30 wt.% after drying. Hypothetically, electrical efficiency decreases as the reactor temperature increases from 950 to 1450°C. This indicates that as gasification temperatures further increase, the amount of heat from electrical energy that must be supplied for the plasma torch to maintain the gasifier at that temperature increases. The plasma power increases from 0.17 to 1.15 kW, and the ηel of the system decreases. Further, at temperatures lower than 950°C, the decomposition of higher hydrocarbons is incomplete, negatively affecting the ηel.

The PZR is one of the most critical components of a biomass gasification system and controls syngas yield. The PZR temperature influences the electrical efficiency by feeding the PG with feedstocks at high temperatures. Thermodynamic calculations suggested an optimal temperature of 700°C for the

PZR. At this temperature, equilibrium can still be considered in the PZR. However, further investigation of the PZR reactor is required, which is reserved for future research.

The provision of heat from the SOFC to the PZR reduces the plasma torch power from 2.7 kW presented in the work of Liu et al. [69] to 0.27 kW in the present study.

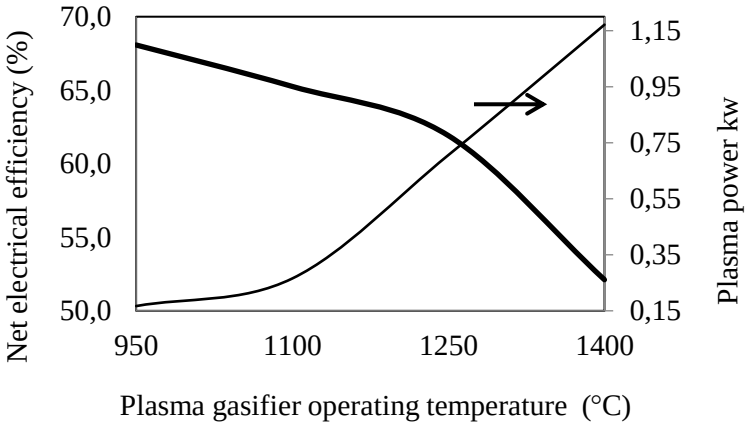

Figure 2.6. Effect of the PG temperature on the net electrical efficiency.

2.3.2.2 Biomass MC

The effect of the initial MC in biomass, which is generally dried to 30 wt.%, on the ηel is shown in Figure 2.7 for an air/fuel = 0.4, SBRPG = 0, and T = 950°C. The system has its highest electrical efficiency of 66.5% with a biomass initial MC of 60 wt.%, which is already lower than the expected minimum MC.

Electrical efficiency decreases with increasing biomass moisture because sufficient power is required to drive compressor CP2, as more steam must be compressed to provide sufficient heat for evaporation in the dryer unit. Thus, less electrical power is produced by the MST. However, although electrical efficiency decreases to 60% when the system is fed with an initial biomass MC of 92 wt.%, the efficiency is still reasonably high compared with those of other available drying technologies.

The incorporation of a superheated steam dryer is a significant advantage of the present system because the MC of biomass does not significantly influence

the electrical efficiency of the system. Therefore, this type of drying technology is well integrated into a combined unit.

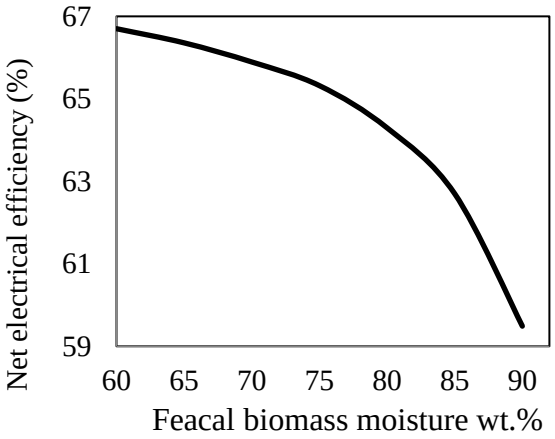

Figure 2.7. Net electrical efficiency as a function of initial biomass MC 60–90 wt.% dried to 30 wt.%.

2.3.2.3 SOFC–1 anode and cathode inlet temperature

The anode–1 inlet temperature depends on the operating conditions of the PZR and SOFC anode–2. The thermal energy of the exhaust gas of anode–1 was transferred to the PZR, and part of the heat of anode–2 was used for the fuel preheating of anode–1, as shown in Figure 2.1. Figure 2.8 shows that the efficiency decreases slightly at lower anode–1 inlet temperatures because fuel utilisation in SOFC–2 is reduced to 0.5 to maintain the temperature of the SOFC–2 at 900°C (cooling purposes). At high anode–1 inlet temperatures, the fuel utilisation in SOFC–2 increased and supply enough heat to reach the anode–1 inlet temperature. An optimum anode–1 inlet temperature of 800°C is obtained, at fuel utilisation of 0.58, resulting in a ηel of over 65%. The cathode–1 inlet temperature depends on the amount of fuel combusted in the PSC. As shown in Figure 2.9, a cathode–1 inlet temperature higher than 650°C causes a decrease in the electrical efficiency of the system because the SOFC–2 fuel utilisation needs to be reduced to produce sufficient heat in the PSC, thereby maintaining the cathode–1 inlet–temperature using HE10 shown in Figure 2.1. Furthermore, as the airflow rate for the SOFC cooling requirement increases, the power required for air compressor CP1 increases and the ηel of the system reduces.

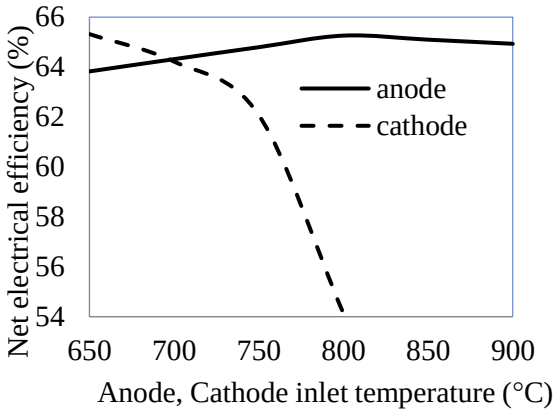

Figure 2.8. Net electrical efficiency as a function of SOFC–1 anode and cathode inlet temperatures, Uf SOFC–1 = 0.51, and Uf SOFC–2 = 0.5–0.58.

2.3.3 Comparison of fuel composition

Figure 2.9 compares the equilibrium composition of the gasifier syngas with that reported by Liu et al. [69]. The increase in H_2 and decrease in CO_2 in the present model are achieved by 1) using steam as a gasifying medium, thus promoting the water–gas shift reaction Eq. (2.9); and 2) reforming of CH_4, Eq. (2.8), and tar in the PG, and 3) using heat from the SOFC for the PZR, thus reducing the partial oxidation of fuel. Thus, a two–stage gasifier contributes to increasing the efficiency of the system.

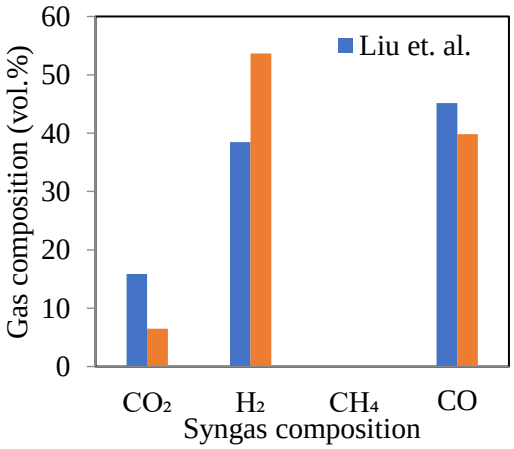

Figure 2.9. Comparison of syngas composition from Liu et al. [69] and the modelled two–stage gasifier, T = 1100°C, air/fuel = 0.4, MC after dryer = 30 wt.%, and plasma power 0.4 kW.

Energy and exergy efficiencies: The performance and key data for the investigated system are listed in Table 2.6. The optimal process parameters estimated in the previous sections are used to assess the system performance: air/fuel ratio of 0.4, no additional steam in the PG, PG temperature of 950°C, biomass MC of 75%, MC after drying of 30%, cathode–1 inlet temperature of 650°C, and anode–1 inlet temperature of 800°C, which reduces SOFC performance.

Table 2.6. Key data system performance.

Parameter	System SOFC ASR 2.5×10^{-5}	System SOFC ASR 5×10^{-5}
Dry biomass flow rate [g/s]	0.56	
Biomass MC [wt.%]	75	
Energy biomass input [kW] (on LHVdry)	9.43	
Exergy biomass input [kW]	10.56	
Turbine net power production [kWel]	0.77	0.83
SOFC1–2 net power production (AC) [kWel]	5.92	5.6
SOFC1–2 net power production (DC) [kWel]	6.10	5.8
Total power production [kWel]	6.69	6.4
Plasma torch power [kW]	0.27	0.27
Auxiliary utilities [kW]	0.26	0.27
Net electrical efficiency [%] (on LHV)	65.3	62.2
Exergy efficiency [%]	57.8	56
SOFC–1 fuel utilization *	0.51	0.51
SOFC–2 fuel utilization *	0.58	0.58
Air factor PSC (λ)	10.05	11.39

* leading total fuel utilization of 84% for the complete SOFC system

A diagram of the exergy flow in the gasifier–SOFC–MST configuration is shown in Figure 2.10, showing exergy destruction due to irreversibility. The values are as follows: in the gasifier 0.5 kW; SOFC 0.6 kW; PSC 0.6 kW, and heat transfer in the multi–HX configuration 1.9 kW, which is the highest value. Better thermal management strategies reduce exergy destruction during gas combustion and heat transfer when steam is generated and air and fuel are preheated. The exergy destruction is high at low SOFC fuel utilisation levels

because of high exergy destruction in the post–combustor and heat transfer. The exergy losses associated with stray heat transfer from the plant components were ignored, except for the exergy losses of the stack (chimney) gases which were 0.36 kW. Calculations are provided for fuel cells with an ASR of 2.5×10^{-5}. For conventional fuel cells with an ASR of 5×10^{-5}, the total efficiency becomes 2.3%–point less, see Table 2.6.

Finally, approximately 50% of the biomass exergy is converted into process heat exergy, which is available to be utilized in the system, and approximately 50% into electric power.

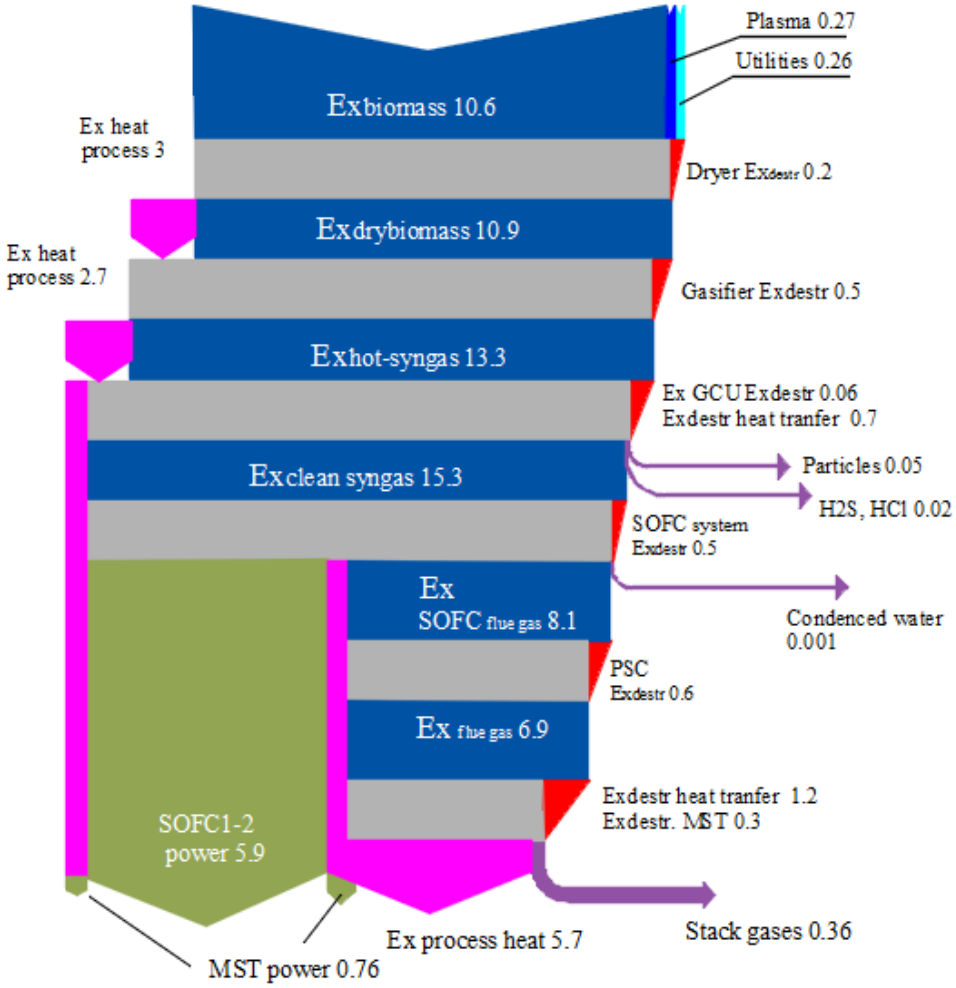

Figure 2.10. Exergy flow diagram (kW).

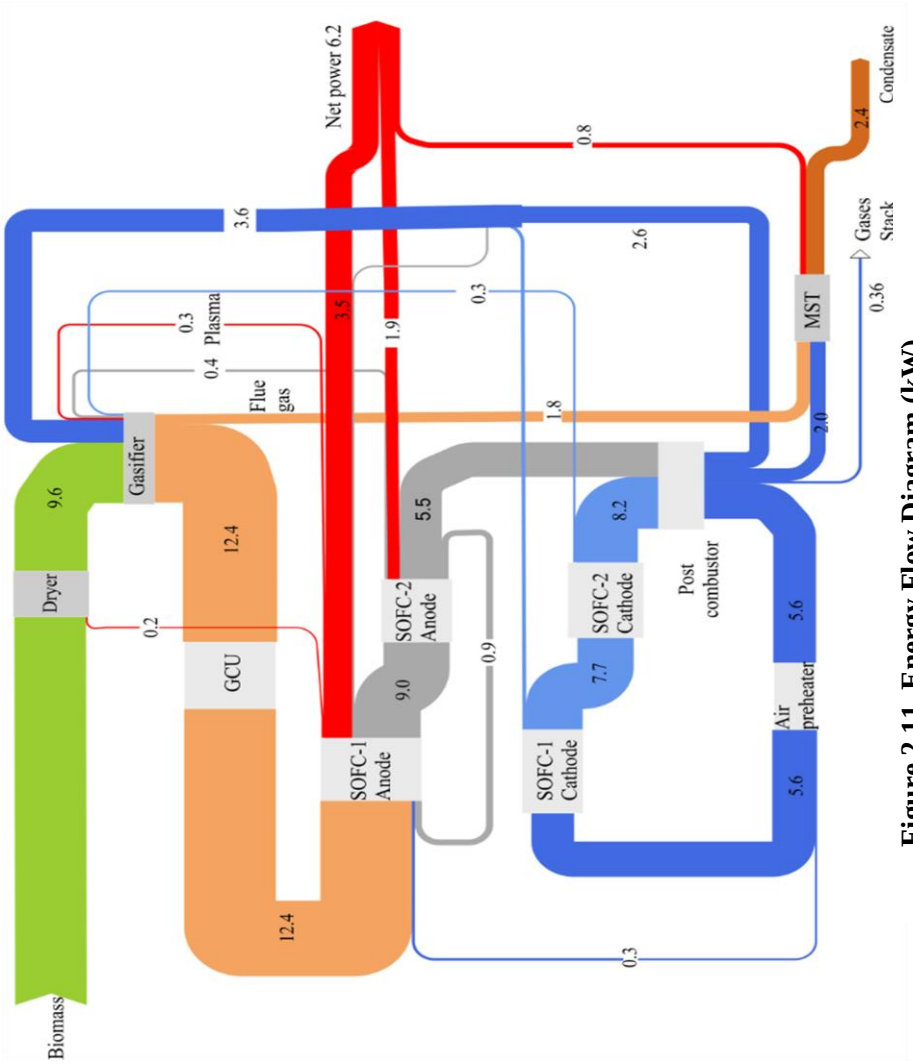

Figure 2.11. Energy Flow Diagram (kW).

The energy flow diagram shown in Figure 2.11 indicates that power production is primarily derived from the SOFC, which produces 85% of the power, and the MST produces 15%. The low power of 0.27 kW used for the PG and the 0.2 kW to drive the compressor for the dryer are noticeable. A loss of energy of 0.4 kW occurs in the flue gas stack (chimney), and a significant amount of heat, 5.6 kW, is used to preheat the SOFC cathode air.

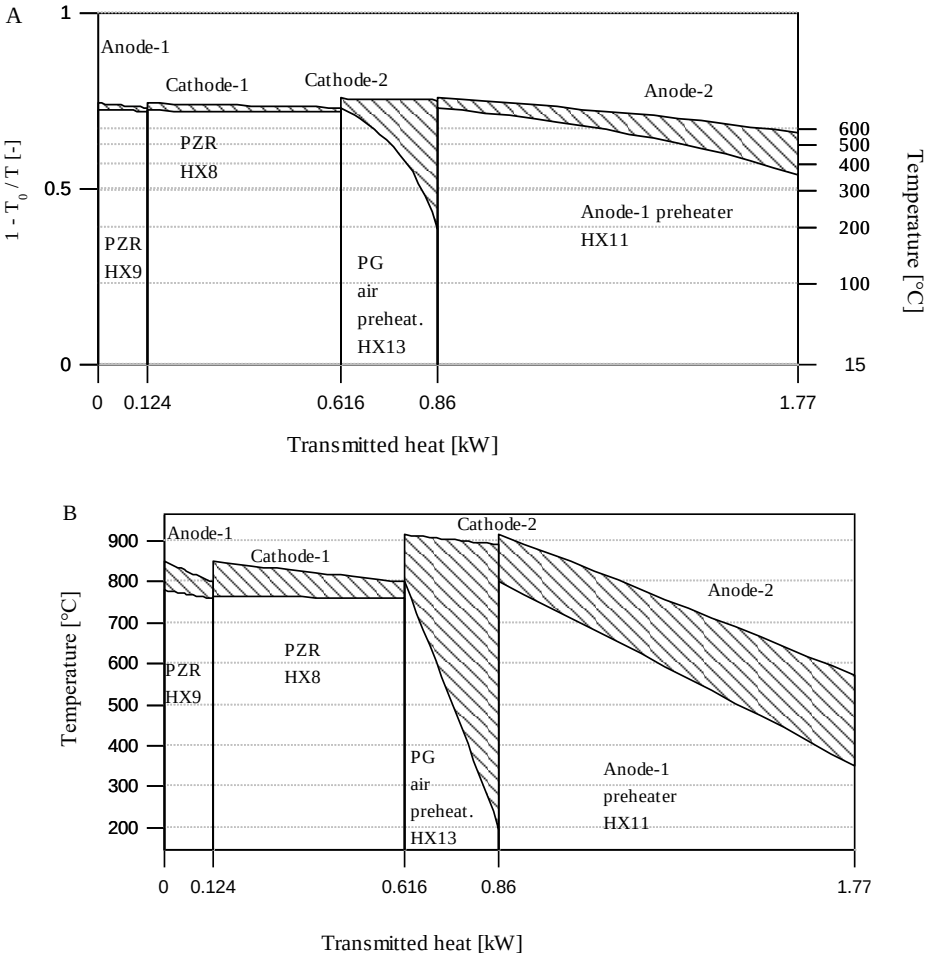

Figure 2.12. QT and value diagrams of the integrated system. SOFC anode and cathode exhaust gases heat transfer to process streams.

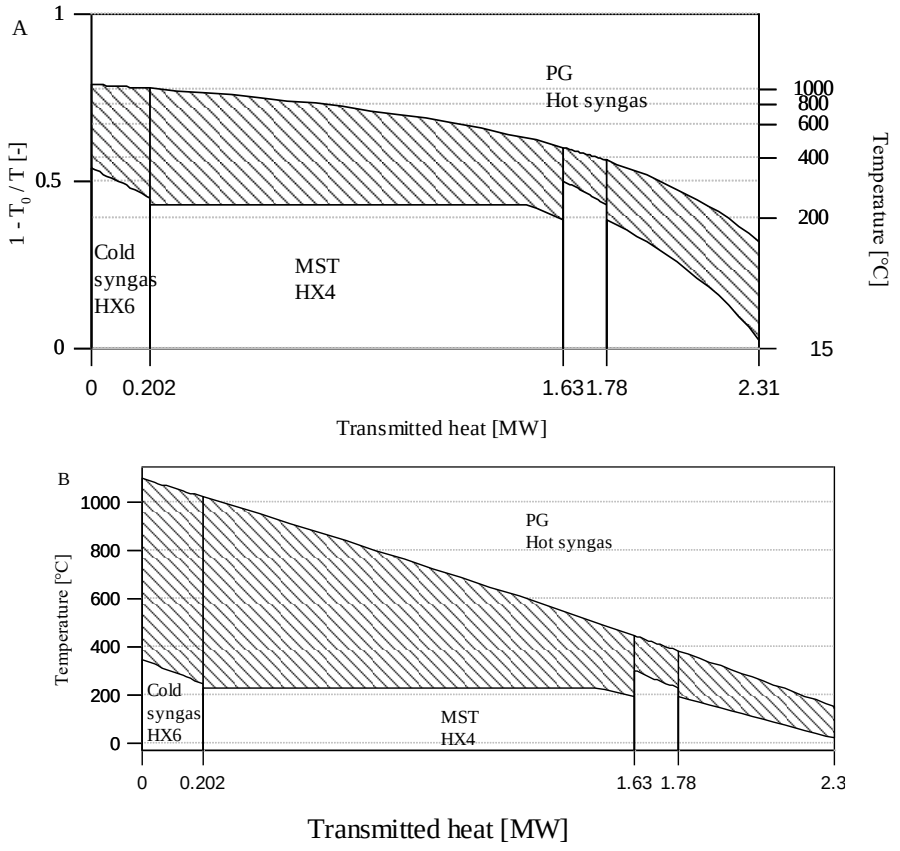

Figure 2.13. QT and value diagrams of the integrated system PG hot syngas.

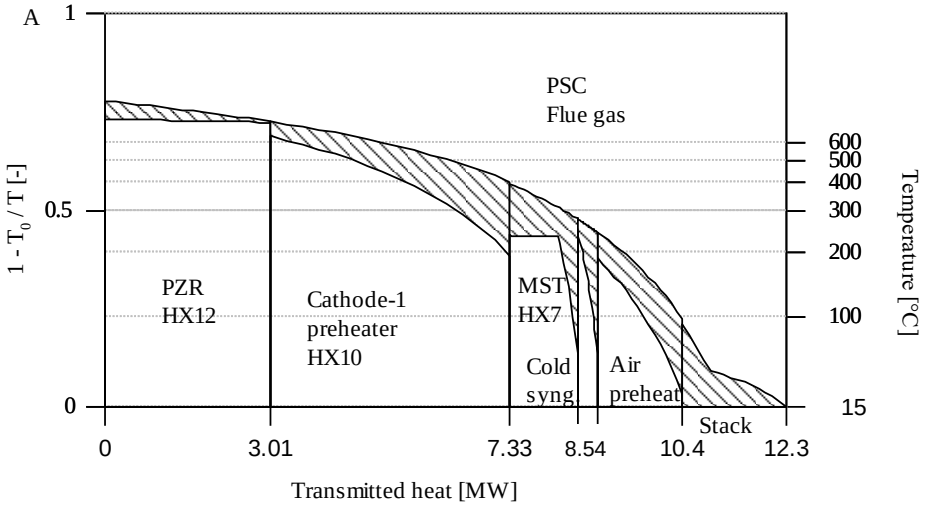

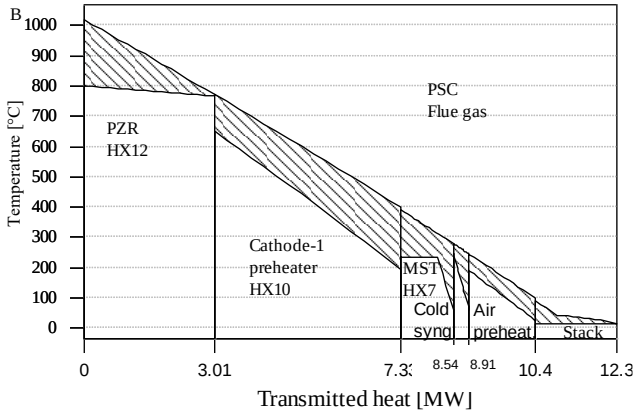

Figure 2.14. QT and value diagrams Post Combustor flue gas.

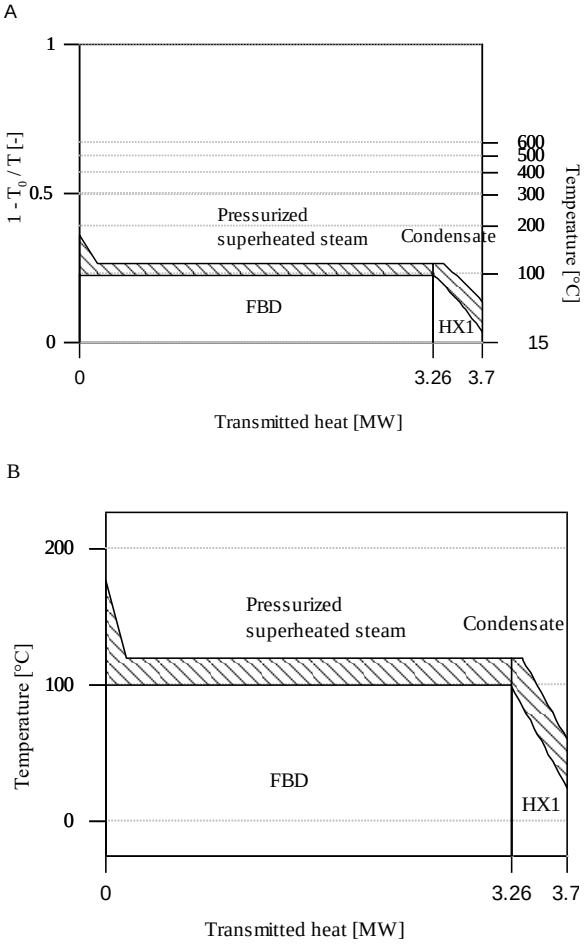

Figure 2.15. QT and value diagram of dryer unit.

The shaded areas shown in the value diagrams in Figures. 2.12–2.15 represent the exergy destruction caused by heat transfer. The significant temperature difference between the streams, as shown in the QT diagram, causes exergy destruction, as demonstrated in the value diagram.

Figures 2.12A and B show the heat transfer from the SOFC anode and cathode exhaust gases to the PZR, anode–1 preheater, and PG air preheater. Figures 2.13A and B show the heat transfer from the PG hot syngas utilized to preheat the cold syngas and produce steam for the MST. Herein, the steam generator HE4 comprises three parts: an economizer, an evaporator, and a superheater. Figures 2.14A and B show the process heat transfer that flows from the PSC flue gas to different process units such as PZR, cathode–1 air preheater, MST steam generation and air preheater.The exergy loss related to stack gases leaving the system is shown on the right. Figures 2.15 A and B represent the heat transfer from the pressurized superheated steam and condensate to the free water in the dryer unit.

The heat transfer from the PG fuel gas stream (Figure 13) has a low exergy recovery of 62% and 0.6 kW exergy destruction. The temperature difference between the two media is high. In contrast, the SOFC exhaust gas streams (see Figure 12) transfer the heat with an exergy recovery of approximately 99% and 0.1 kW exergy destruction. The exergy recovery from the PSC flue gas (Figure 2.14) is 82%, and the exergy destruction is 1.2 kW (for 12.4 kW heat transferred). The exergy recovered in the FBD (Figure 15) is 82%, and the exergy destruction is 0.2 kW.

2.4 Conclusion

The process simulations of this small-scale combined system using faecal biomass as fuel provide the process conditions that are favourable for achieving a high ηel. This work showed an improved system efficiency ηel = 65% and exergy efficiency up to 58% when the system was fed with faecal biomass with an MC of 75 wt.% and biomass dried to obtain an MC of 30 wt.%. The PG is operated with an air/fuel ratio = 0.4 and SBRPZR = 0.6; the calculated SOFCs fuel utilizations are Uf1 = 51% and Uf2 = 58% under atmospheric pressure. The SOFC exhaust gases and hot syngas provide the gasification heat and thermal energy for a steam cycle.

The indirectly heated two-stage gasifier (PZG and PG) produced syngas with a low CO_2 content and a high content of H_2. The chemical energy of these gases is efficiently converted into electricity in the SOFC. The provision of heat from the SOFC to the PZR increases the amount of H_2 from 38 vol. % in the simulation by Liu et al. [31] to 55 vol. % in the present study, and lowered the PG power from 2.7 kW to 0.4 kW. The two SOFC stacks connected in series produced a substantial increase in the ηel of the system, avoiding the need for a CPOX unit and reducing the cooling requirements by the cathode air flow.

The dryer unit reduces the MC from 60–92 wt.% to 30 wt.% without dramatically reducing the electrical efficiency of the system when vapour recompression is used, integrated with an MST.

Heat transfer causes the highest values for exergy destruction in the system, so improvement of the system is mainly expected in this part and is considered as future work. Further modelling and experimental investigation of the integration of microwave plasma gasification and SOFC is necessary to obtain accurate values of conversion efficiency and process heat available for heat integration. Finally, even though the proposed configuration in rather complex, thermodynamically, our study demonstrates that a high-efficiency, environment-friendly sanitation system can be developed using a gasification–SOFC power plant. In contrast to the biochar produced by pyrolysis, syngas from gasification can be fed to an SOFC system for efficient power production. Therefore, a gasifier–SOFC power plant might become a technology that can be commercialized and be financially viable to be used globally for meeting sanitation requirements.

3

Energy Production from Wet Biomass

Oswaldo Guayasamin: Tenderness

More than ten thousand years ago, women in South America discovered and developed the technical and philosophical principles of agriculture. They wanted to feed their families through the Valdivian culture of Ecuador.

3.1 Introduction

SCWG converts wet biomass into CH_4– and H_2–rich gases without drying. Combustible gases are relatively clean and can be fed into SOFCs with limited cleaning. The SCWG of digest sludge, 6 wt.% dry biomass operates with a carbon gasification efficiency (CGE) of 45.8%, and 80.7% solid (phosphorus) is recovered [139]. The assistance of the Ru/C catalyst and a bed of ZnO on top of the gasifier to absorb sulfur and protect the catalyst from deactivation helps achieve a gas composition close to thermodynamic equilibrium.

SCWG converts wet feedstocks such as sewage sludge and manure (moisture content >50 wt.%) into combustible gas. The thermophysical properties of SCW are favourable for the dissolution of organic matter. Low viscosity provides effective mass transfer, a low density promotes high solvation properties, and a low dielectric constant changes SCW to a nonpolar solvent. The high ion production in SCW enables it to act as an acidic or basic catalyst in reactions. Many organic chemicals readily react under the hydrothermal conditions of SCW [140][141], whereas inorganic chemicals do not. Hence, P, K, and lower percentages of Ca, Mg, Fe, and Al can be easily separated [139].

Furthermore, the thermophysical properties of SCW are important for heat transfer and biomass gasification [140]. Above the critical pressure, no phase change is observed. A change in specific heat near the critical point reaches a maximum, and heat recovery is efficient [142]. Thus, the SCWG process typically involves a heat recovery unit.

The chemistry of SCW can be explained through experimental investigations using model compounds. SCWG is kinetically driven, and the measured gas composition is often far from the calculated equilibrium composition [143]. Thermodynamic equilibrium can be effectively approximated at high temperatures, with or without a catalyst.

The SCWG process converts large biomass molecules into smaller gas molecules. The challenge in this process is to reach a near 100% conversion (thermodynamic equilibrium). Nevertheless, a real SCWG system operated with present–day technologies encounters engineering limitations, restricting the conversion of organic matter into gas and other by–products, such as char and higher hydrocarbons. Therefore, catalysts are required. Operating conditions such as biomass concentration, pressure, temperature, reactor residence time, reactor type, and catalyst influence the conversion and composition of the produced gas.

These conditions should be carefully selected when designing SCWG for commercial applications [141][144]. Although technical and economic evaluations indicate that the SCWG of sewage sludge for combustible gas production is feasible [145], challenges associated with high operating costs, reactor plugging, and catalyst deactivation need to be addressed. SCWG may be acceptable for large–scale commercialisation in the future with the development of efficient and stable catalysts at competitive costs [146]. In addition, the recovery of the high–quality heat applied to reactors under supercritical conditions is crucial. Feng et al. [147] reported a thermal energy recovery of 41%.

3.1.1 The operating conditions influence on SCWG system

3.1.1.1 Hydrothermal Process

The hydrothermal process (biomass conversion) is given in Figure 3.1. Hydrothermal carbonization generates hydrochar from wet biomass at mild temperatures and pressures [148]. The gasification process avoids the operating conditions of carbonization. Below the critical point of water, liquefaction hydrolyzes biomass into smaller molecules of acids and phenols. At high temperature, the liquefaction products are reformed and gasified into smaller molecules of CO, H_2, CH_4, CO_2, and so on [149]. The pressure and temperature in the liquefaction process must be sufficient to keep the water in a liquid state. The liquid products are often called bio–oil (water–soluble components).

At near–critical temperatures up to about 400ºC, effective reforming and gasification generally require catalytic enhancement to achieve reasonable rates and selectivity to hydrogen and methane. Homogeneous gasification takes place above 400ºC and higher pressure, producing methane or hydrogen gases in higher yields [149][150]. High temperatures >500ºC generate hydrogen–rich gas without catalyst or with nonmetal catalysts, while at a temperature around 500ºC with catalyst, methane–rich gas is produced.

Biomass is a combination of several components: cellulose, hemicellulose, proteins, lignin, and inorganic. During the hydrothermal process, these components interact with each other, leading to very complicated chemistry. The kinetics of the liquefaction and gasification of these components are being investigated for around 30 years. Some kinetic parameters and reaction pathways are summarized by Yakaboylu et al. [151]. According to the results obtained from a kinetic model, higher residence time increases the CGE [152].

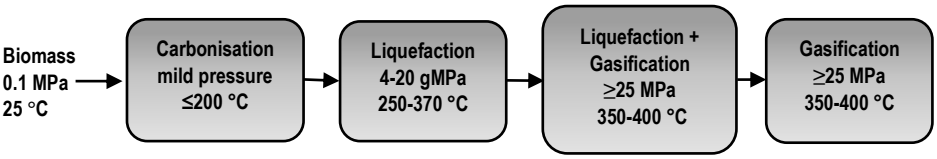

Figure 3.1. Biomass hydrothermal conversion in a typical process configuration

3.1.1.2 Salts

Some salts present in the biomass benefit the conversion in subcritical water, but others poison the heterogeneous catalyst at supercritical conditions, plugging by salt deposition due to the low salt water solubility. On the contrary, alkali salts are active catalysts for the water–gas shift reaction [153] [154]. Only in the presence of such salts are high hydrogen yields at reasonable reaction times possible. The salts influence the reaction pathways during biomass conversion; the probable cause is the basicity of the salts. At ambient conditions, they are neutral, and at near– and supercritical water, the basicity of salts becomes very complex, as presented by Kruse et al. [155].

3.1.1.3 Pressure and Temperature

A simplified explanation of H_2 or CH_4 production from the conversion of biomass into gas in SCWG is given by the stoichiometric Eqs. (3.1)– (3.4) [35]. The formation of H_2 predominates over that of CH_4 at high temperature because high temperature favors endothermic reactions Eqs. (3.1), and (3.2), while low temperature favors exothermic reactions Eqs. (3.3) and (3.4). The increasing pressure decreases the yield of H_2, whereas that of CH_4 increases. Besides, from simultaneous effects of temperature and pressure on hydrothermal gasification of glucose, the CGE increased with the increasing temperature and decreased with increasing pressure [156].

Hydrogen formation

$$C_6H_{12}O_6 + 6H_2O \rightarrow 6CO_2 + 14H_2 \quad (3.1)$$

$$CO + H_2O \leftrightarrow CO_2 + H_2 \quad (3.2)$$

Methane formation

$$C_6H_{12}O_6 \rightarrow 3CH_4 + 3CO_2 \quad (3.3)$$

$$CO + 3H_2 \leftrightarrow CH_4 + H_2O \quad (3.4)$$

3.1.1.4 Feed Concentration

The feedstock moisture content influences the CGE and syngas composition. Most of the research, kinetic modeling, and experiments are done at dry biomass below to 10 wt.% [141]. CGE is low with feedstock at higher content as clarified in Eqs. (3.1) and (3.2) since the formation of H_2 needs water. Therefore, more moderate moisture content theoretically reduces the formation of H_2 and eases the formation of CH_4 [143] Eqs. (3.3) and (3.4). Complete gasification is only achievable with a dry–biomass concentration lower than 5 wt.%, implying a further increase in operating cost [157]. For example, the high heat capacity of water leads to very high heat requirements to heat the aqueous feedstock to ≥400°C. Hence, the very high water content of the feedstock seems to be a significant disadvantage. On the other hand, the H_2 yield of SCWG of sewage sludge, for industrial application, is only obtained with biomass concentration higher than 15 wt.% [158]. The high dry–matter content leads to a high gas production but at low CGE. High reaction temperatures are required to achieve complete gasification for feedstocks with smaller moisture fractions.

3.1.1.5 Resident time and type of reactor

Longer residence time raises the hydrogen yield and the CGE, while CO yield decreases, and favors the complete gasification of biomass, expected within seconds at a temperature above 600°C [145]. However, temperatures higher than 600°C at a pressure >20 Mpa result in high operating costs and limitations on materials [159]. These represent the principal obstacle to the development of this technology.

Continuous reactors operating at high flow rates and fluidized bed reactors are the ones more suitable to control plugging problems during SCWG. The fluidized bed reactor, besides, increases heat and mass transfer during gasification. However, to achieve higher gasification efficiencies, longer residence times, as well as higher reactor temperatures, are needed. Large continuous reactors give high residence times, but there are technical limitations in building such reactors. The preheating section of an SCWG experimental setup constructed with a pipe heat exchanger reaches a total length of 55 m [160]. Furthermore, increasing the residence time by operating the SCW gasifier at low feed flow rates increases the gasification efficiency. However, if the flow rate is too low, it will cause a lack of fluidization inside the reactor, resulting in a very low gasification efficiency [159].

Table 3.1. Comparison of gas composition and carbon gasification efficiencies of various feedstock from supercritical water gasification (SCWG) and SCWG experimental investigations

A	Behnia et al. [162]			Chen et al. [163]		
Feedstock	Glucose			Sewage Sludge + CMC		
Reactor	Continuous flow reactor			Fluidized bed reactor		
Temperature (°C)	500	500	500	500	540	540
Pressure (Mpa)	27.5	27.5	27.5	25	25	25
Concentration (wt.%)	5	5	5	4 +2	12+2	2+2
Catalyst	Ni20% Ru2%/ γ–Al2O3	Ni20 %/γ–Al2O3	blank	blank	blank	KOH 0.9 wt.%
WHSV (h^{-1})	3		–	–	–	–
Gas composition (vol.%)						
H_2	20.9	44.8	40.5	44	18	55
CH_4	38.8	8.2	1.5	5	9	7
CO	0	0	14.7	3	23	1
CO_2	40.2	46.7	41.5	47	44	35
C_2–C_3	0.1	0.3	1.8	1	3	1
CGE (%)	100	70	10	36	31	49

B	Zhang et al. [164]			Zhang et al. [165]		Lu et al. [166]	
Feedstock	Glucose			Glucose	Simul. Waste	corn+CMC	
Reactor	Bench–scale continuous flow			Bench–scale continuous down–flow tubular		Fluidized bed reactor	
Temperature (°C)	600	600	600	600	600	600	600
Pressure (Mpa)	24	24	24	24	24	25	25
Concentration (wt.%)	5	5	5	5	5	10	15
Catalyst	Ni20/g–Al2O3	blank	Ni10/AC	0.1RuNi/c–Al2O3	0.1RuNi/c–Al2O4	blank	blank
WHSV (h^{-1})	3	–	3	6	6	–	–
Gas composition (vol%)							
H_2	58.2	8.7	24.9	48	39.5	36	29
CH_4	10.6	11.5	12.3	12.5	21.4	3	3
CO	0.6	55.1	29.2	0.5	0.3	25	36

Table 3.1. (continue).

CO_2	30.5	18.3	27.3	38.6	38.8	36	32
CGE (%)	99.9	75.2	78.2	99.2	99.9	40	40
C	Zhang et. al. [165]				Lu. Y. et. al. [166]		
Feedstock	glucose			simul. Waste	corn+CMC		corn+ CMC
Reactor	bench–scale continuous down–flow tubular				Fluidised bed reactor		
Temperature (°C)	700	700	700	700	650		650
Pressure (Mpa)	24	24	24	24	25		25
Concentration (wt.%)	7.75	100 g/L	8.22	100 g/L	10		15
Catalyst	blank	0.1RuNi/c–Al2O3	0.1RuNi/AC	0.1RuNi/c–Al2O3	blank		blank
WHSV (h^{-1})		12	~2.5	12	–		–
Gas composition (vol.%)							
H_2	44.7	57.4	54.9	53.8	37		29
CH_4	15.8	7.3	12.1	9.9	9		9
CO	0.7	1.9	0.4	1.8	6		10
CO_2	35	33.4	30.2	34.5	48		52
C_2–C_3					0		0
CGE (%)	90.1	99.6	92.4	>99.9	47		42

3.1.1.6 Catalyst

The appropriate physicochemical properties of SCW help the reactions [146]. Addition of suitable catalyst in SCW enhances gasification and is especially important at lower temperatures. Nevertheless, most catalysts get poisoned, and the destruction of their support takes place with real biomass.

Biomass decomposition in SCWG is investigated in numerous experimental studies. This gives limited reported data regarding the gas composition and CGE, in particular when the SCWG operates in continuous reactors with real biomass at higher than 10 wt.%. According to the kinetic results of Yakaboylu et al. [152], the hydrothermal decomposition of biomass constituents (cellulose, hemicellulose, lignin, and protein) representing manure at 10 wt.% dry biomass gives a CGE of 50%, the reactor residence time is 60 s at 500ºC, 25 MPa. Kinetic models in the catalytic SCWG of glucose, gives a CGE variation from 80 to 100%, the feed biomass fraction is 5–35 wt.% [161].

Table 3.1 compares the gas composition and CGE of different types of feedstock at varied operating conditions in SCWGs. The influence of the catalyst,

feedstock concentration, and temperature on the CGE is visible. The CGE of glucose conversion in SCWG reaches near 100% with the assistance of a catalyst at low feedstock biomass fraction 5 wt.% and 500ºC. A CGE of 99.9% is achieved for simulated waste at 5 wt.% feedstock at 600ºC, with the assistance of a catalyst. The CGE of corn + CMC is 40% at 600ºC, 15 wt.%, and have nonassistance of a catalyst. It is noticeable that the amount of CO_2 in all cases is significant.

3.1.2 Gasifier–SOFC Integrated System

The gas produced by gasification processes is a potential fuel for a SOFC. The SOFC converts the chemical energy of the gas into electricity. The gasification of organic waste integrated with the high–temperature electrochemical process is attractive from the thermal point of view since gasification also operates at high temperature. Heat integration allows the generation of power with a high system efficiency.

A SOFC is an electrochemical device that comprises a solid electrolyte, a fuel electrode, and an oxygen electrode. The electrolyte allows the transport of oxygen ions, and the electrodes transport charge and are a heterogeneous catalyst. A charge transfer takes place among a gas, electrolyte, and electrodes and results in fuel oxidation [167]. Fuel oxidation generates heat and electricity. Furthermore, the heterogeneous catalyst in the fuel electrode promotes the reforming and partial oxidation of hydrocarbons.

The efficiency of the SOFC system depends on the thermal strategy of the balance of the plant (BOP) and SOFC design. Process heat must replace the external energy required for air and fuel preheating in the BOP. The SOFC exhaust gases mostly contain CO_2 and H_2O. Potential exists for the capture and storage of these gases for further application, such as the electrochemical conversion of CO_2 into CO [168] or to feed a photobioreactor [115].

Thermodynamic calculations demonstrate a net electrical efficiency of 50% reached by a manure SCWG combined with a SOFC and gas turbines (GT) [91]. The efficiency increased to 63% by integrating an SCWG–SOFC–Rankine cycle–Fuel processing turbines–GT [92]. On the other hand, n comparison, for a plasma gasification–based plant, including a fecal sludge drier, gasifier, gas cleaning unit, and SOFC–steam turbine combined system, the net electrical efficiency reaches 65% [169]. The efficiency calculated in these works assumed complete conversion of the chemical energy of the biomass into synthesis gas at thermodynamic equilibrium.

3.1.3 Perspective of the SCWG–SOFC

The variation of the effectiveness of catalysts and variations in process conditions in the SCWG influence syngas compositions and quantities and hence the overall system efficiencies. Such influences are not yet studied in detail. This work, as far as the authors are aware of, for the first time, evaluates the influence of such variations on the efficiencies of SCWG integrated high–efficiency power plants in which SOFCs are employed for power production.

The performance of an SCWG at different operating conditions and the thermal strategy applied to the SCWG–SOFC combined system strongly influence the efficiency of the system. In particular, the combination of high temperature and high biomass moisture. Those parameters are favorable to reach almost full biomass conversion but negatively affect the thermal management and represent a challenge in the field of construction materials. On the contrary, operation of the SCWG at lower temperature and biomass moisture, expected in a real gasifier, makes it difficult to achieve complete conversion (thermodynamic equilibrium) in SCWGs. It results in lower conversion efficiency and lower production rate of syngas, which has an influence on the final results. These conditions are stopping the industrial development of the SCWG technology for the treatment of the unappealing wet biomass. Considering the mentioned drawback is compulsory to find new ways to improve the performance of an SCWG–SOFC system. Therefore, this study develops a parametric analysis of the SCWG–SOFC system to determine the influence of the mentioned gasifier condition on the energy and exergy performance of the system. The energy and exergy analysis will allow identifying potential process streams to combine bottoming cycles as a possible route to improve system performance.

As a result, the performance of a fecal sludge SCWG–SOFC power plant for industrial applications depends on the gasifier design with several engineering limitations and the thermal strategy applied in the system. No high H_2 purity is required for an SOFC because of the internal heterogeneous reactions achieved in an SOFC. In this work, a thermodynamic model, developed in Aspen Plus™, simulates the performance of an SCWG–SOFC power plant. Two models estimate the net electrical efficiency of the combined system, one operated with a real SCWG gasifier and another with a gasifier at thermodynamic equilibrium. Both systems are modeled according to the scheme in Figure 3.2, to be discussed in the next chapter. The data used in the model is from SCWG experimental plants designed with present–day engineering limitations. The current work assesses the influence of the operating conditions on the system net electrical efficiency and

the impact of the SCWG operating conditions on the biomass conversion. Finally, the present work compares the system performance with the performance of another similar system, that is, a plasma–assisted two–stage gasifier–SOFC–Micro steam turbine (MST) presented by the author in a previous publication [169].

3.2 System description

Figure 3.2 depicts a schematic flow sheet of the SCWG–SOFC ystem. Biomass at ambient conditions is pressurized in pump P1 and P2 to 12 and 25 MPa, respectively; HX1 and HX2 increase the temperature to around 110 and 320ºC, respectively.

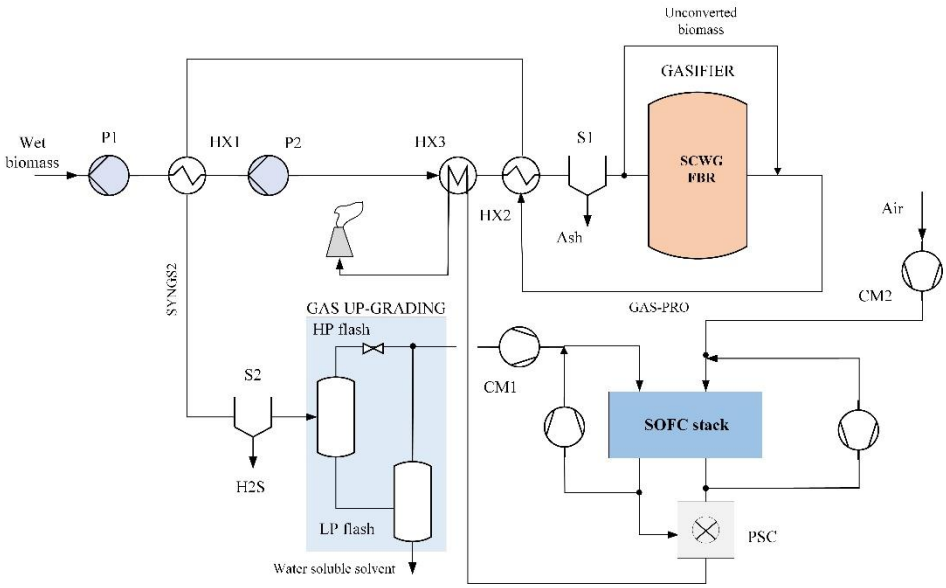

Figure 3.2. Layout of the supercritical water gasification (SCWG)–solid oxide fuel cell (SOFC) integrated system.

HX3 heats the hot pressurized biomass to reach a value below the reaction temperature, around 400ºC. The flow is fed into the SCWG, where the conversion reaction is taking place at 500 or 600ºC and 25 MPa. Unconverted biomass is sent around the reactor. The solid separator S1 removes the ash to clean the gas. HX2 and HX1 recover the heat of the produced gas, leaving the SCWG, to use it for biomass preheating. Then the gas is cooled down below to 200ºC in HX4. The gas upgrading unit separator 1 (HP flash) at 10 bar separates fuel gas from water, which contains the higher hydrocarbons. Further separations take place in LP

flash at 25ºC and low pressure of 1 bar. The fuel gas contains CH_4, H_2, CO, and a small concentration of CO_2 and H_2O.

The gas cleaning unit S2 removes H_2S from the upgraded gas at ambient conditions. The clean syngas is fed with steam, then is heated up to 850°C with recirculated syngas and fed into the SOFC anode. Internal reforming of CH_4 will take place in the SOFC anode. Air is heated to 650°C with the exhaust gas from the SOFC cathode poststack combustor (PSC) and fed into the SOFC cathode. The SOFC stack converts a large part of the chemical energy of syngas into electricity and heat. The PSC combusts the exhaust gas from the SOFC anode with the air from the cathode exhaust. Then, the flue gases heat the hot pressurized biomass in HX3.

3.3 Thermodynamic model

Reactions (3.1)–(3.4) explain the complete conversion of biomass in SCWG, where $C_6H_{12}O_6$ represents biomass.

The reactions that might occur in a SOFC anode operated with syngas are the oxidation of fuel, Eq. (3.5); the water–gas shift reaction, Eq. (3.6); the internal steam reforming of fuel Eq. (3.7). The electrochemical conversion of the fuel is carried out according to reactions Eqs. (3.5) and (3.9), generating electrical energy and heat (the heat given is for both Eqs. (3.5) and (3.8).

At the fuel electrode

$$H_2 + ½O_2 \text{–}\!\!\rightarrow H_2O + 2e\text{–} \qquad \Delta H = -242\ kJ/mol \qquad (3.5)$$

$$H_2O + CO \leftrightarrow H_2 + CO_2 \qquad \Delta H = \pm 41 kJ/mol \qquad (3.6)$$

$$CH_4 + H_2O_{(gas)} \leftrightarrow 3H_2 + CO \qquad \Delta H = \pm\ 206\ kJ/mol \qquad (3.7)$$

At the oxidant electrode

$$O2\text{–} + 4e\text{–} \rightarrow 2O2\text{–} \qquad (3.8)$$

3.3.1 Energy and Exergy Analysis of the SOFC

Eq. (3.9) determines the power and heat generated by the reactions (3.5 and 3.6), where ΔH is the change of enthalpy, T is the reaction temperature, ΔS is the change of entropy, $T\Delta S$ is the heat, and ΔG is the Gibbs free energy change, giving the power [170].

$$\Delta H = \Delta G + T\Delta S \qquad (3.9)$$

The reversible cell voltage of the SOFC refers to the transfer of charged species, electrons, or ions across the interface in a SOFC and is given by Eq. (3.10). Where n describes the number of moles of electrons transferred for every mole of chemical species reacting, and F is Faraday's constant.

$$E = -\frac{\Delta G}{nF} \tag{3.10}$$

The Nernst equation describes the reversible cell voltage of the SOFC as a function of the partial pressure of the system species, applied to the chemical reactions Eqs. (3.5) and (3.8) gives:

$$E_r = E + \frac{RT}{nF}\frac{P_{H_2}P_{O_2}^{1/2}}{P_{H_2O}} \tag{3.11}$$

During operation, the resistance to the flow of an electric current in the cell generates Ohmic overpotential η_{ohm}. Additionally, the charge transfer reactions cause activation overpotential η_{act}, and the transport limitations of gases through the porous electrodes to the TPB cause concentration/diffusion overpotentials η_{conc}. The total overpotential reduces the final voltage of the cell, being a function of the current density j

$$V_{SOFC} = E_r - \eta_{act}(j) - \eta_{ohm}(j) - \eta_{conc}(j) \tag{3.12}$$

The cell resistance of an electrolyte–supported SOFC is governed mainly by the Ohmic type overpotentials, which depends mostly on the cell temperature. In this work, the SOFC temperature is assumed constant. Hence, the polarization overpotential is constant and is represented by the area specific resistance of the cell (ASR)

$$V_{SOFC} = E_r - ASR(j) \tag{3.13}$$

Faraday's Law, Eq. (3.14), describes the maximum current that a SOFC generates. Assuming the electrochemical oxidation of H_2 and the internal reforming of CH_4 and CO:

$$I_{SOFC} = 2 \cdot F \cdot N_{fuel} \cdot U_f \tag{3.14}$$

$$N_{fuel} = 2 \cdot N_{H_2} + 8 \cdot N_{CH_4} + 2 \cdot N_{CO} \tag{3.15}$$

where the N_{fuel} [mol.s^{-1}] is the moles of reactants on SOFC, and Uf is the fuel utilization for the requirements of an excess of fuel to avoid Ni oxidation.

The current density result:

$$j_{SOFC} = \frac{I_{SOFC}}{A_{SOFC}} \tag{3.16}$$

where A_{SOC} is the area of the stack. The oxygen usage is calculated considering that each mole of oxygen transfers four moles of electrons:

$$O_2 usage = \frac{I_{SOFC}}{4F} \text{moles } s^{-1} \tag{3.17}$$

The power of the SOFC is calculated by:

$$P_{SOFC} = V_{SOFC} \cdot I_{SOFC} \tag{3.18}$$

From the energy balance Eq. (3.19) describes the heat generated by the SOFC, where Δh_{CH_4}, Δh_{WGS} are the reaction enthalpies of the SOFC anode heterogeneous reactions respectively, methanation and water gas shift reaction; the term η_{SOFC}*I is the heat generated by the cell overpotential, which is equal to the ASR times the current I [kW]. The enthalpy of the oxidant flow rate (in general air), Δh_{ox}, fed to the SOFC cathode, acts as temperature regulator removing the excess heat from the SOFC. $\dot{N}$ is mol flow rate of the chemical species:

$$\dot{N}_{mol,ox} \cdot \Delta h_{ox} = \dot{N}_{mol,H_2} \cdot T\Delta S + (\dot{N}_{mol,CH_4} \cdot \Delta h_{CH_4} + \dot{N}_{mol,CO} \cdot \Delta h_{WGS} + \eta_{SOFC} I) \tag{3.19}$$

3.3.2 Exergy Analysis of System

The exergy analysis estimates the work obtained from the SCWG–SOFC system and determines the components where the exergy destruction and losses take place.

The exergy balance [171] of the SCWG–SOFC at steady state is represented by Eq. (3.20). The exergy enters the system with the biomass. The system is well insulated; in this regard, there is no exergy transfer accompanying heat transfer (except by the GUP), and the SOFC generates power:

$$0 = -E_r + \sum_i \dot{m}_i e_{fi} - \sum_e \dot{m}_e \dot{e}_{fe} - \dot{E}_d \tag{3.20}$$

where $\dot{E}_d$ is the rate of exergy–destruction within the system, e_{fi} is the total specific flow exergy at inlet i, and e_{fe} is the specific flow exergy at exit e.

$$\dot{e}_f = h - h_0 - T_0(s - s_0) + \bar{e}^{ch} \tag{3.21}$$

where h and s represent the specific enthalpy and entropy, respectively, at the inlet or exit under consideration; h_0 and s_0 are the properties at the reference conditions T_0, p_0

The chemical exergy for an ideal gas mixture at T_0, p_0, is given by:

$$\bar{e}^{ch} = \sum_{i=1}^{j} y_i \bar{e}_i^{ch} + \bar{R}T_0 \left(\sum_{i=1}^{j} y_i \ln y_i \right) \quad (3.22)$$

where $\bar{e}i^{ch}$ is the chemical exergy for each gas component i, and y_i denotes the mole fraction of component i in the mixture.

3.3.3 Efficiencies

Eq. (3.23) defines the net electrical efficiency of the power plant ηel, where P_{SOFC} is the electricity generated by the SOFC stack (kW), P_{BOP} is the total power consumption of auxiliary components, including compressors and pumps (kW); $\dot{m}_{biomass}$ is the mass flow of the biomass fed into the system (kg s^{-1}); LHV (dry) biomass is the lower heating value of the biomass on a dry basis (kJ kg^{-1}).

$$\eta_{el} = \frac{\dot{P}_{SOFC} - \dot{P}_{BOP,sys}}{\dot{m}_{biomass} \times LHV_{biomass}} \quad (3.23)$$

The exergy efficiency ηex–sys is the ratio between the power generated in the SOFC exergy minus the BOP of the system and the exergy in the biomass.

$$\eta_{ex-sys} = \frac{\dot{P}_{SOFC} - \dot{P}_{BOP,sys}}{\dot{m}_{biomass} \times Ex_{biomass}} \quad (3.24)$$

The CGE is the ratio of the total amount of carbon in the gas phase divided to the total amount of carbon in the feedstock, where N_C is the mole of carbon.

$$CGE = \frac{\dot{N}_{C.syngas}}{\dot{N}_{C,biomass}} \quad (3.25)$$

3.3.4 Aspen Model

Figure 3.3 illustrates the Aspen model of the SCWG–SOFC system. The equation of state Peng Robinson is applied in the Aspen model because it is more favorable for describing thermodynamic behavior at temperatures above the critical point of water. The SCWG model utilizes processes with solids according to the procedure presented in Ref. [172], represented by the reactors DECOMP and SCWG. The SCWG product gas composition at thermodynamic equilibrium is calculated by applying the Gibbs free energy minimization method using the Gibbs Reactor in Aspen Plus™. The gasifier at nonthermodynamic equilibrium

uses the RYield Reactor in Aspen Plus™. The gas upgrading unit (GUP), modeled by the HPFLASH and LPFLASH, separates the unconverted components from the gas, which are water–soluble (acetic acid as a representative component for the present models).

The present SOFC model was built based on the work of Tanim et al. [173], Zhang et al. [174], and Tanim et al. [175]. Gibbs reactor REFOR describes the heterogeneous reaction WGSR, the electrochemical oxidation of H_2 with the Gibbs reactor ANODE–1. The heat and power produced by ANODE–1 is calculated by applying a calculator block; the total value describes the POW–HEAT stream. The air flow rate represented by the C–AIR stream carries the heat generated in ANODE–1, calculated by Eq. (18). The stream HEAT–CAT takes the heat to the CATH, modeled as a Flash in Aspen. The C–AIR flow rate changes to maintain the SOFC system isothermal at 850ºC. The molar flow rate of stream O2 is calculated by Eq.(16).

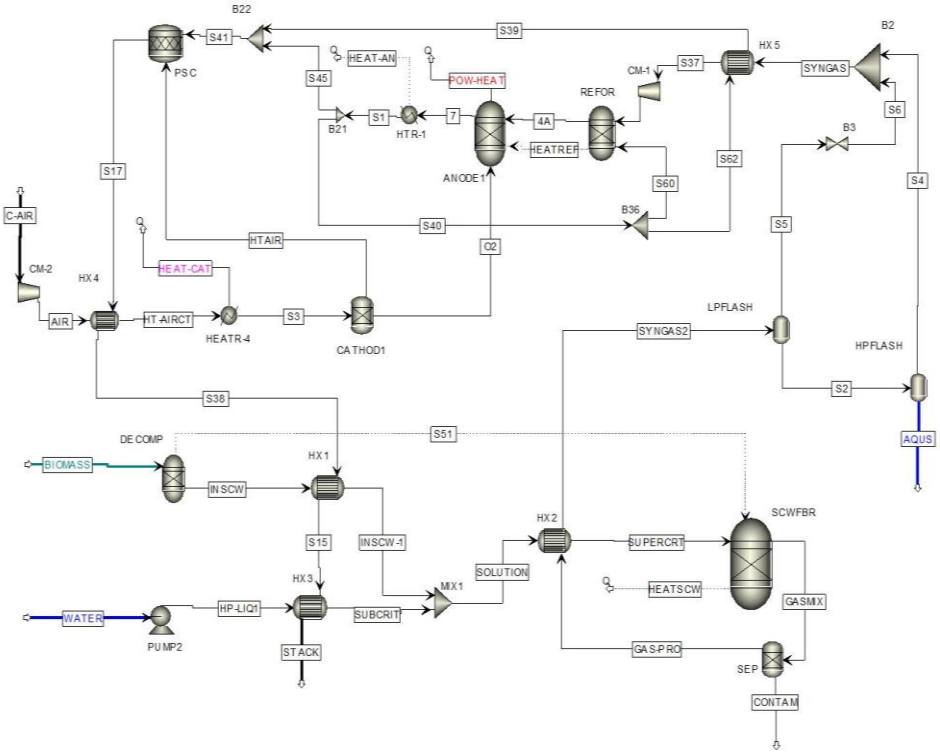

Figure 3.3. Aspen Plus process flow diagram of the supercritical water gasification (SCWG)– solid oxide fuel cell (SOFC) system.

3.4 Results and discussion

3.4.1 Model Comparison

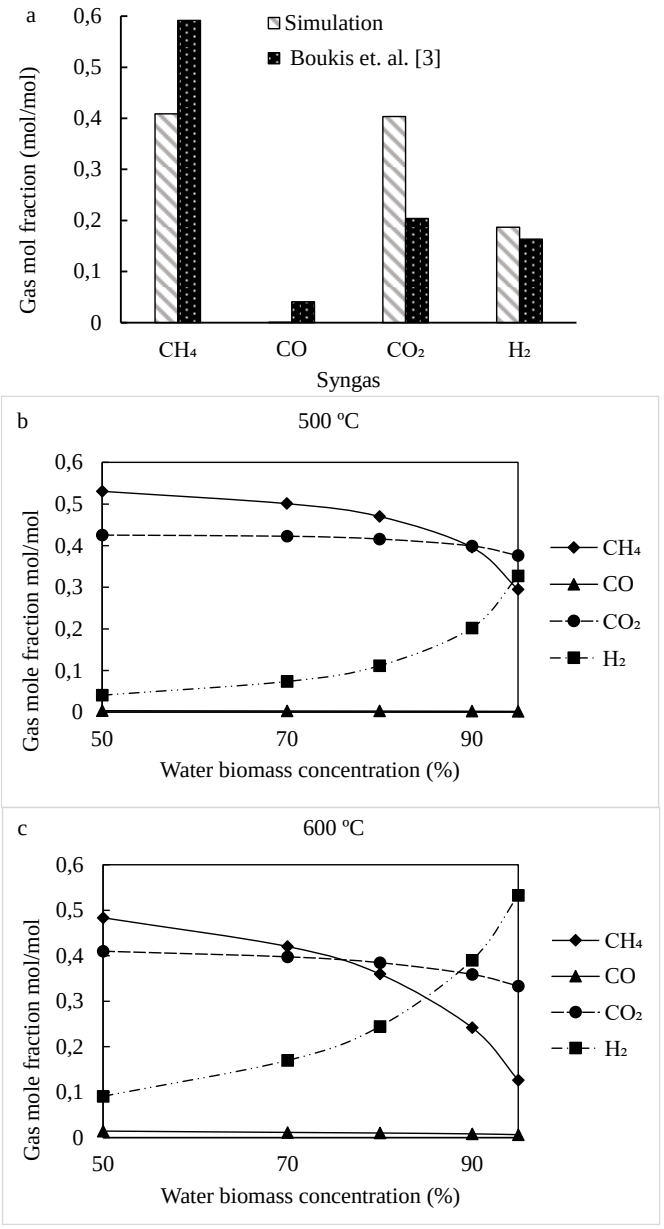

Figure 3.4. Product gas composition compared with reference gas product concentration at reactor temperature 450°C, pressure is 25 MPa, 6.7 wt.% moisture content at thermodynamic equilibrium (TE) and at nonequilibrium.

Table 3.2. Comparison of the simulation results of the supercritical water gasification (SCWG)–solid oxide fuel cell (SOFC) system with the data obtained from reference

Parameter		Facchinetti et Al. [92]	Present work
SCWG			
Feedstock composition	(C, H, O, N)	51.1, 5.8, 42.9, 0.2	
Dry biomass concentration	wt.%	80	
Pressure	bar	300	
Temperature	ºC	400	
Syngas chemical composition	m.%		
H_2		1.5	1.7
CH_4		33.6	44.7
H_2O		34.3	10.1
CO_2		30.6	43.5
CO		–	0.0
SOFC			
Pressure	bar	1.0	1.0
Temperature	ºC	800; 850	850
Fuel utilization		0.7; 0.8	0.8
SOFC efficiency	%	62.2	58.2
SCWG–SOFC			
Net electrical efficiency	%	49.5	50.3
Exergy efficiency	%	47.8	47.8

Figure 3.4A compares the SCWG syngas composition reported by the experimental work of Boukis et al. [139] with the calculated gas composition at thermodynamic equilibrium, temperature 450ºC, 25 MPa, 6.7 wt.% dry biomass concentration. The difference in gas concentrations might be due to the experimental results presented by Boukis that gives a CGE of 45.8%; this generally occurs in SCWG real systems due to the natural constraints [176], according to Yakaboylu et al. [144]. The CGE is the most essential additional constraint that might affect the gas composition. The presence of CO at temperatures lower than 500 ºC is the result of the insufficient residence time to complete the water gas shift reaction [160].

Table 3.3. Ultimate analysis of fecal sludge

Ultimate Analysis (wt.%–dry basis)	
H	6.3
C	42.96
N	2.36
S	0.10
O (by difference)	35.78
Ash	12.50
Moisture (%)	85–95
Energy content LHV (dry), (MJ/kg)	16.84

Table 3.4. Gasifier and solid **oxide fuel cell (SOFC) stack parameter and operating conditions**

Parameters and Operating Conditions		
Supercritical water gasification (SCWG)		
Reaction temperature	°C	500–600
Reaction pressure	MPa	25
Dry biomass flow rate	g/s	0.56
Dry biomass concentration	wt.%	20 – 5
HP – LP flash pressure [177]	bar	10 – 1
HP – LP flash temperature [177]	°C	100 – 25
Pump efficiency [178]	%	80
SOFC		
Number of cells	–	371
Area of a cell	m2	0.01
Fuel Utilization Uf	–	0.65 –0.95
Current Density	A/m2	2000 – 2500
Cell Resistance [179]	Ωm	5e–5
Operating Temperature	°C	850
Operating Pressure	bar	1.013
DC–AC inverter efficiency	%	95
Fuel compressor isentropic efficiency[180]	%	82
	%	82
Air compressor isentropic efficiency [180]	K	10
Minimum approach temperature		

The simulation results of the SCWG–SOFC system are compared with the simulation data reported by Facchinetti et al. [92]. Table 3.2 gives the input parameters and the results. The syngas chemical composition, in dry basis, is comparable in both works. The different operating conditions of the GUP result in a higher content of H_2O on the syngas composition presented by Facchinetti, operating the GUP at 70 and 1–6 bar. Whereas in this work, the operating pressures are 10 and 1 bar. In general, the SCWG–SOFC system performance has a good agreement with the reported value.

3.4.2 Analysis of the Process Parameters on SCWG–SOFC system

This section presents the results of the thermodynamic analysis of the proposed system. The impact of temperature and biomass moisture, SOFC fuel utilization, and CGE on system performance is investigated. The feedstock used for this analysis is fecal sludge. Table 3.3 gives the ultimate analysis. Table 3.4 gives the SCWG and SOFC operating conditions.

3.4.3 Fuel Utilization and Biomass Moisture Content

The product gas at thermodynamic equilibrium, temperature 500 and 600ºC and 250 bar is illustrated in Figures 3.4B and C. The significant increment of H_2 and reduction of CH_4 concentrations at biomass water content higher than 85 wt.% are noticeable. Figure 3.5 shows the net electrical and exergy efficiency of the SCWG–SOFC system as a function of SOFC Uf (fuel utilization) and biomass moisture content.

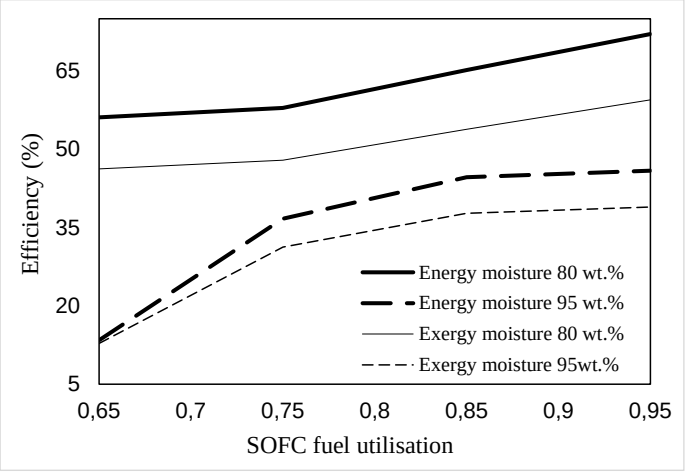

Figure 3.5. Efficiency of the supercritical water gasification (SCWG) solid oxide fuel cell (SOFC) system as a function of Uf and biomass moisture content.

The system net electrical efficiency is maximum at higher Uf and low biomass moisture content. Uf variation from 0.65 to 0.95 changes the net electrical efficiencies from 56 to 72% at moisture content 80 wt.%, and from 13.4 to 46% at 95 wt.%. Higher Uf generates additional power and heat in the SOFC, and the heat efficiently preheats the air and fuel inlet streams. Also, high Uf reduces the fuel fed to the PSC, and thus the exhaust gases that preheat the feedstock entering the SCWG, leading to lower exergy destruction, because of the reduction of the temperature difference between the streams. The highest net electrical efficiency and exergy efficiencies of 72 and 59%, respectively, are obtained at 80 wt.% moisture, Uf 0.95. The efficiencies decrease significantly to 46 and 39% at 95 wt.%, since extra heat is required to maintain the reaction temperature, due to the significant increment of water fed to the system.

For lower moisture content in the biomass, the SOFC off gas, after combustion, provides enough heat for gasification but at the expense of reducing SOFC Uf to 0.65 and consequently decreasing the SOFC power generation. On the other hand, the hot syngas efficiently preheats biomass by the recovery of the high–quality heat produced in SCW. The higher moisture in the biomass favors the H_2 production. However, the influence in the chemical exergy is minor; at 95 wt.%, the chemical exergy of syngas after the GPU reaches 9,499 kW and decreases to 9,342 kW at 80 wt.%.

Figure 3.6A illustrates the contribution of each process unit in the exergy destruction at 80 and 95 wt.% biomass moisture. The most significant contributions are from SOFC–air preheater, SCWG, gas GUP, and fuel preheater. The total exergy destruction is higher in the case of higher biomass moisture content at 95 wt.% because of the significant increase in exergy losses in the SCWG. The SCWG exergy destruction increases from 1,054 kW at 80 wt.% to 2,335 kW at 95 wt.%. The high exergy destruction in the SCWG is principally caused by variations in the thermochemical exergy. The chemical exergy has a lower influence (changes from 9.3 MW at 80 wt.% to 9.5 MW at 95 wt.%; Figure 3.9. Irreversibilities in the SOFC–air processing and fuel processing are associated with the heat transfer between the high– and low–temperature fluids in the heat exchangers. Exergy destruction in the air compressor and pumps is considerably lower. Exergy loss occurs in the GUP (Figure 3.2) due to heat transfer. The water separation is an endothermic process, and thus heat is transferred from the HP flash to the surroundings. LP flash operates at ambient temperature, 25ºC, and the exergy loss is negligible. The exergy destruction in the fuel–processing unit is higher at 95 wt.%, 1,153 kW when compared to 390

kW at 80 wt.%. Higher water flow rate at increased biomass moisture increases significantly the thermochemical exergy in the fuel streams and, hence, the exergy destruction in heat exchangers.

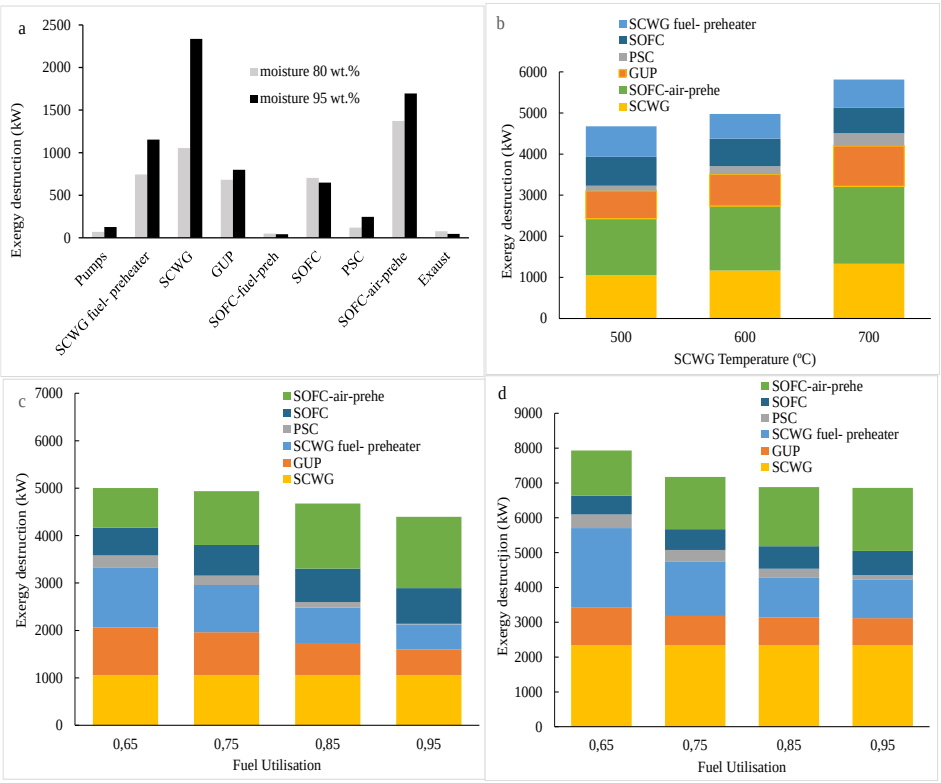

Figure 3.6. Exergy destruction attribution of each section to the total exergy loss as a function of: (A) 80 wt.% and 95 wt.% biomass moisture (B) gasifier temperature (C) Uf in supercritical water gasification (SCWG)–solid oxide fuel cell (SOFC) system at 95 wt.%.

Figures 3.6c and d shows the contribution of each process unit in the total exergy destruction of the combined system at 80 and 95 wt.% biomass moisture as a function of the Uf. The total exergy destruction of the combined system decreases with increasing Uf. The exergy destruction in the SCWG has almost no influence on the Uf. But the exergy destruction in the SOFC–air preheater increases with increased Uf because higher fuel utilization increases the heat produced by the SOFC. Thus, the more heat carried out the by air stream, the more power required to drive the air compressor CM2. Besides, the increase in air flow rate increases the exergy destruction in the air preheater heat exchangers, since the SOFC cathode air is recirculated and fed to the PSC (Figure 3.2). The

exergy destruction in the SOFC increases slightly at increased Uf as more fuel is processed. On the contrary, the exergy destruction in the PSC, fuel–preheater, and GUP decreases with increasing Uf. Higher fuel utilization reduces the fuel combusted in the PSC, hence, the stream available for fuel–preheater has less difference in temperature, and thus less exergy destruction. Similarly, the temperature of the stream fed the GUP is low and thus lower exergy destruction accompanying heat transfer. The exergy destruction in the SOFC at 95 wt.% at increasing Uf is lower than that at 80 wt.%. The higher concentration of H_2 at higher moisture content increases the thermochemical exergy and reduces the exergy destruction.

The PSC produces heat at high temperature and at low Uf, which results in high exergy destruction in heat exchangers, affecting the performance of the SCWG–SOFC combined system. The integration of the system, operating with biomass moisture lower than 90 wt.%, with bottoming cycles to recover the heat is a subject for further simulations.

3.4.4 Heat Recovery on the System Efficiencies

The energy and exergy efficiency strongly depends on the heat recovery from the product gas generated in the SCWG. The heat exchanger HX2 recovers the heat from the stream GAS–PRO by heating the feed to the SCWG. The temperature of the hot stream SYNGAS2 reflects the amount of heat recovered (Figure 3.2). According to the design presented in the work of Fiori et al. [181], the temperature of the stream SYNGAS2 maintains the vapor fraction equal to one at 350ºC. While in the work of Feng et al. [147], the liquid fraction of the stream SYNGAS2 is equal to one at 100ºC. In this work, the estimation of the minimal temperature of SYNGAS2 depends on the process heat available. Figure 3.7 shows the influence of the SYNGAS2 temperature on system efficiency. At 80 wt.% biomass moisture, the maximum heat recovered is at SYNGAS2 temperature 278ºC, reaching energy and exergy efficiency of 65 and 53%, respectively. At higher SYNGAS2 temperature (375ºC), less heat is recovered and the efficiencies decrease to 31 and 27%. At 95 wt.%, the minimum temperature is 137ºC, at high moisture, there is less process heat available. Higher SYNGAS2 temperature than 137ºC makes the combined system no longer energetically sustainable since the system requires additional external heat for fuel preheating.

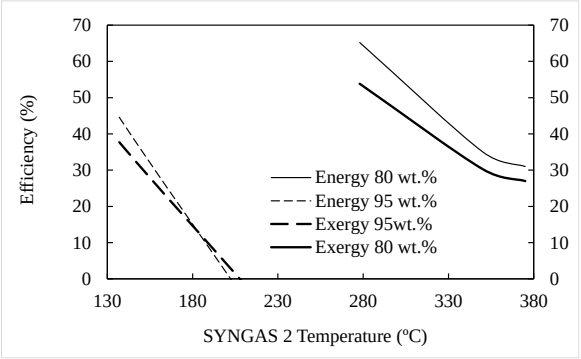

Figure 3.7. Influence of the heat recovery on the supercritical water gasification (SCWG) solid oxide fuel cell (SOFC) efficiency

3.4.5 SCWG operating temperature

The variations in the efficiencies of the combined SCWG–SOFC system with the SCWG operating temperature and biomass moisture are presented in Figure 3.8 (at Uf 0.85). The exergy and net electrical efficiencies decrease when the operating temperature increases, since high operating temperature increments the heat demanded by the gasifier, while the chemical exergy of the product gas slightly increases. At 80 wt.%, the energy and exergy efficiencies reach a maximum of 65% and 54%, respectively, at 500ºC. These are significantly higher than the efficiencies at 95 wt.%, 44 and 37%. The combination of high moisture and high temperature considerably reduces system efficiency. At operating temperatures higher than 650ºC and 95 wt.% the system is not self–sustainable. The power generated by the SOFC is significantly lower than the total power consumption by the auxiliary components of the system due to the high energy demanded by the SCWG.

Figure 3.9 illustrates the variation in the heat needed by the SCWG and the chemical exergy variation of the product gas as a function of the gasifier temperature and biomass moisture. The chemical exergy of the product gas slightly increases with the temperature at 80 and 95 wt.%. The SCWG is, to some extent, exothermic at lower temperature and low moisture. Since the exothermic reactions (3) and (4) are favourable, the gasifier requires less heat. The gasifier generates 0.5 MW of heat at 500ºC and 80 wt.%. The heat demanded by the gasifier slightly increases with the temperature. At higher moisture levels, the gasifier is very endothermic. The heat needed by the SCWG at 95 wt.% and 500ºC increases to 2.2 MW and significantly increases with temperature to 5 MW at 700ºC. At high moisture levels, the endothermic reactions (1) and (2) dominate,

and because of the high moisture levels, the gasifier requires a higher amount of heat.

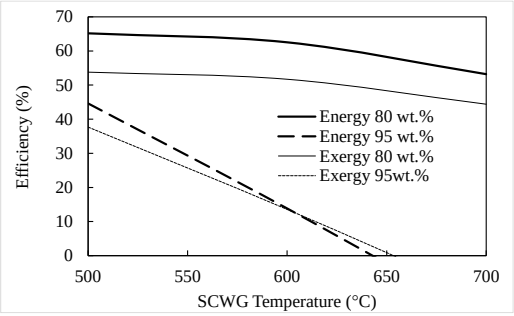

Figure 3.8. System efficiency as a function of the gasifier temperature at 80 and 95 wt.% moisture

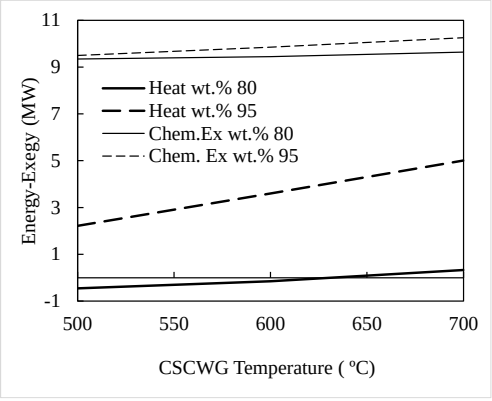

Figure 3.9. Supercritical water gasification (SCWG) heat needed and chemical exergy of stream SYNGAS as a function of the gasifier temperature

Figure 3.7B shows the effects of SCWG temperature on the irreversibilities in the primary process units of the SCWG–SOFC combined system and their contributions to the total exergy destruction at Uf 0.85. Higher temperatures increase the heat demanded by the gasifier; hence, the total exergy destruction in the system increases. The exergy destruction in the SOFC air–preheater accounts for the most substantial amount. The high temperature increases the H_2 production, increasing the heat carried by the air stream. This increases the air flow rate and thus the thermochemical exergy and exergy destruction in the heat exchangers. Consequently, the exergy destruction in the PSC increases as well. The increased temperatures in the gasifier rises the exergy destruction in the GUP

since the product gas fed to the GUP has a higher thermochemical exergy. On the other hand, the exergy destruction in the SOFC decreases with the increased gasifier temperature. High temperature favors an increment of H_2 and decrement of CH_4 in the gas product. Higher production of H_2 in the gasifier reduces the requirement of heat in the SOFC for the endothermic CH_4 internal reforming reaction. Thus, more heat is available in the SOFC to be utilized for air and fuel processing.

3.4.6 CGE of SCWG

Figure 3.10 shows the net electrical efficiency of the SCWG–SOFC as a function of Uf at gasifier CGE of 40% (non–thermodynamic equilibrium) and CGE of 100%. The non–equilibrium process parameters are selected from available experimental data of SCWG of biomass, taking into account the projection to industrial application and considering the current technical and catalytic limitations to build a reactor. Dry biomass content is 15 wt.%, 600°C, 25MPa. The gas concentration and CGE are assumed the same as the ones reported in the work of Lu et al. [166] (Table 3.1).

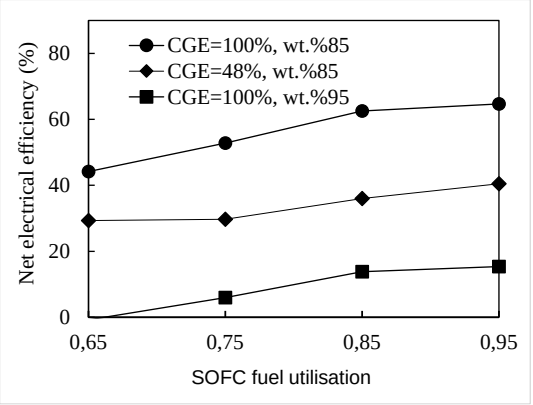

Figure 3.10. System net electrical efficiency as a function of the Uf at different gasifier carbon gasification efficiency (CGE).

At nonequilibrium, the efficiency reaches 29 to 40% at Uf 0.65–0.95, which is significantly lower compared with the equilibrium calculations. The main reason is the low CGE of the SCWG, in the order of 40%, resulting in a high amount of unconverted biomass discharged in the GUP.

The net electrical efficiency is in the order of 44 to 65% at thermodynamic equilibrium and the SOFC operating at Uf varying from 0.65 to 0.95. According to experimental results from the literature, gasifier operating temperatures higher

than 600°C can improve the CGE at dry biomass around 15 wt.%, but materials restriction is still an impediment [158]. Besides, the CGE at 600°C with the support of a catalyst can be close to 100% at dry biomass lower than 5 wt.%, but the gasifier requires careful design to avoid low conversion. This work finds a system efficiency of 14% at 95 wt.%, 600°C, Uf 0.85, (Figure 3.9). In spite of the low efficiency, if a complete conversion of biomass can be achieved at moisture 95 wt.%, it represents an advantage. The gas product rich in H_2O at SCW conditions is a valuable product. It can be integrated with a bottoming cycle and recover the thermochemical exergy of the product.

3.5 Gasifier–SOFC System Performance Comparison

3.5.1 SCWG–SOFC Combined System

The work of Toonssen et al. [91], SCWG of 20 wt.% (dry) manure content, at 600°C and 24 MPa, reported a net electrical efficiency of the order of 50%. The gasifier is at equilibrium and 100% CGE; however, this is not yet possible to achieve with current technology at dry biomass content higher than 10 wt.%.

3.5.2 Competing Technologies

Table 3.5 gives the necessary data of the SCWG–SOFC integrated system compared with the results of a dryer–plasma–assisted two–stage gasifier–SOFC–micro steam turbine (MST) combined system, as both systems are developed for similar purposes (production of electricity with high efficiency from wet biomass streams). According to thermodynamic calculations, the combination of a superheated steam dryer and plasma–assisted two–stage gasifier–gas cleaning unit (GCU)–SOFC–MST [169] gives a net electrical efficiency of the order of 50–65%. The system is fed with biomass at 60 to 92 wt.% moisture. The syngas contains a higher amount of H_2 and CO and a lower amount of CO_2 than the gas product in SCWG. The gasifier is at equilibrium, and 100% of the carbon is gasified. The cold gas efficiency, which is the chemical energy of the syngas as a proportion of the chemical energy of the biomass and energy input to the gasifier, is 88%,.

Thermodynamic calculations and experiments demonstrate that a CGE near 100% is possible with a plasma–assisted two–stage gasifier. The gasifier receives additional energy from the plasma torch. The moisture content of the biomass, higher than 90 wt.%, is not a barrier to reach system efficiency higher than 50%, with the application of an efficient dryer unit. The integrated system constituted with a drier, plasma–assisted two–stage gasifier, GCU, SOFC, and

MST is relatively complex and needs further technology development and experimental demonstration.

Table 3.5. Key data and results from supercritical water gasification (SCWG)−solid oxide fuel cell (SOFC)

Process	SCWG–SOFC	plasma–assisted two–stage gasifier–SOFC–MST [169]
Reactor	FBR	NA
Temperature (°C)	600	950
Pressure (bar)	250	1.013
Dry biomass flow rate g/s	0.56	0.56
Concentration (wt.%)	15	15
Gas composition (vol.%)		
H_2	29	56
CH_4	3	0
CO	36	39.5
CO_2	32	3.16
Carbon gasification (%)	40	100
Cold gas efficiency (%)	46	88
Carbon concentration in water soluble solvent	>50%	0
Energy biomass input [kW] (LHVdry)	9.43	9.43
SOFC net power production [kWel]	3.6	6.4
SOFC fuel utilisation Uf	0.65 – 0.95	0.5
Energy auxiliary components [kWel]	0.2	0.54
Net electrical efficiency (%)	29 –40	63

In contrast, the limited results available from SCWG thermodynamic calculations or experiments demonstrating the possibility to reach a CGE near 100% utilizing real biomass at dry biomass content higher than 10 wt.%. High CGE is only possible to achieve at dry biomass content lower than 10 wt.%. However, the SCWG–SOFC is not energetically suitable at this concentration. Furthermore, the product stream contains relatively high CO_2 (>20 vol%). The generation of high amounts of water–soluble compounds (>40 wt%) at dry biomass higher than 10 wt.% is responsible for the significantly low system efficiencies.

However, this study reveals that the optimal combination of the operational conditions of the SCWG–SOFC system could make the integrated system more competitive. The process streams may combine thermal power plants. Besides, an advantage of the SCWG is the production of a stream rich in steam at high temperature and pressure; the energy of this stream can be recovered with more efficient methods. In the current system, this energy is not recovered entirely due to heat transfer limitations, which also influence the efficiency of the system. The products generated in the real SCWG gasifier, CO_2, steam, and water–soluble compounds could be utilized in different processes, for example, the electrochemical reduction of CO_2 and H_2O into CO, H_2, and O_2 when excess electrical energy is available [182]. The reforming or partial oxidation of the water–soluble compounds is also a possibility to produce more useful products. Those are methods that may make both systems appear as appealing but face challenges.

3.6 Conclusions

A thermodynamic model is developed in Aspen Plus™ to evaluate the performance of the SCWG-SOFC combined system. The gasifier model is considered first at thermodynamic equilibrium and subsequently at nonequilibrium. The model assesses the effect of several gasifier operating parameters and the SOFC Uf on the net electrical and exergy efficiencies, as well as on the total and process unit wise exergy destruction.

The SCWG operating parameters varied are temperature, biomass moisture, residence time, and the percentage conversion of biomass in the gasifier. Thermodynamic equilibrium simulation of SCWG assuming a CGE is equal to 100% results in higher system efficiency. However, near 100% conversion of real biomass into a gas product in SCWG is only possible at solid contents lower than 10 wt.% at temperatures higher than 500ºC and long residence times. However, due to the operating conditions, there are material limitations and difficulties in the reactor construction. Besides, at low solid content, the remarkably high energy needed to increase the temperature of the water reduces the energetic sustainability of the combined system. At 95 wt.% moisture, 600°C, 250 bar, Uf 0.85, the net electrical efficiency is 14% at thermodynamic equilibrium. Nevertheless, the almost full biomass conversion at these conditions make the SCWG product gas suitable for using in bottoming cycles as a way to increase the system efficiencies.

Dry biomass contents higher than 10 wt.% gives higher net electrical efficiency. However, near 100% biomass conversion into product gas is not found experimentally for higher dry biomass content in SCWG systems. At these conditions, the CGE is around 40%, the combined system net electrical efficiency reduces to 29 and 40% at SOFC fuel utilization of 0.65 and 0.95, respectively, fed with biomass, with a solid content of 15 wt.% at 600°C and 25 MPa. The low conversion of the solid biomass into product gas in a real SCWG and the low heating value of syngas (CO_2 >20 vol%) are the main reasons for the low net electrical efficiency of the SCWG- SOFC systems. The product gas composition of the SCWG reactor is from reported experimental data, where the gasifier has not reached thermodynamic equilibrium. On the contrary, at thermodynamic equilibrium, the system reaches a higher net electrical and exergy efficiency of 63 and 52%, respectively, at Uf = 0.85 for the SOFC and 600ºC and 25 MPa in the gasifier for a dry biomass content of 20 wt.%. The SOFC-air preheater causes the highest exergy destruction. The lower moisture results in excess thermochemical exergy available in the system for using in bottoming cycles, and this could improve the system efficiency.

A potential exists for improving the gasification process by employing a suitable catalyst and increasing the residence time and materials quality, and so on. Such improvements, though not easy to achieve, might lead to efficient gasifiers and efficient systems. On the other hand, the variation of operational parameters such as biomass moisture content, SCWG operating temperature, SOFC fuel utilization generates process stream. That has a high potential for its integration with other processes. Thus, in spite of the engineering limitations of the SCWG, the performance of the combined system can be improved. In this regard, the product gas rich in steam and CO_2 obtained at high biomass moisture in the gasifier can be integrated with an electrochemical process to produce fuel. While at low biomass moisture, the high heat produced combined with bottoming cycles, such as thermal power plants, is a route to improve the system performance. The water-soluble compounds generated in the SCWG process, being useful by-products, might also increase the competitiveness of real SCWG syste

4

SCWG – rSOC system

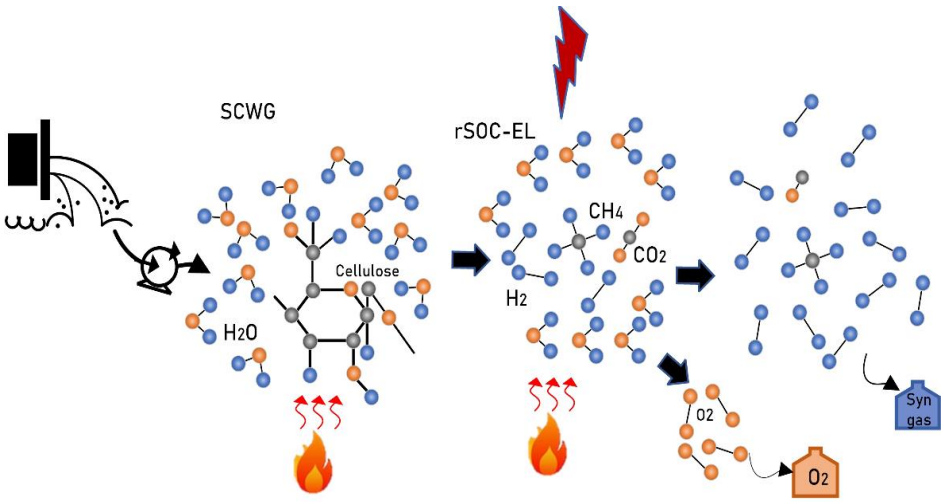

Everything should be made as simple as possible, but not simpler (Albert Einstein)

4.1 Introduction

According to previous studies [183] renewable energy will constitute 14% of global energy sources worldwide by 2040 under current policies for a faster–growing energy source than oil or natural gas [184]. As a result, the price of renewable electricity is falling globally and is already quite low in some areas; for example, it is 13.5 USD MWh^{-1} in the United Arab Emirates [185]. However, renewable energy sources such as wind and solar are intermittent. Therefore, there is a need for development of efficient energy storage solutions.

A high–temperature electrolysis process utilises electricity and heat to produce hydrogen (or syngas) from steam and CO_2, which can be used directly as a fuel, or raw material for production of other synthetic fuels. Any process that generates a high concentration of steam or CO_2 is a potential source of these reactants for electrolysis. The electricity and heat required for the electrochemical reaction may come from sources such as solar, wind, industrial process waste heat, geothermal, or nuclear energy.

Solid oxide fuel cells (SOFC) are high efficiency devices used to produce electricity directly from fuels by electrochemical oxidation, without NOx production. For stationary power generation, SOFC–GT (gas turbine) combined cycles are the systems with the highest efficiency [187]. At present, SOFC technology has reached high TRL (Technological Readiness Level) levels (8 or above), prompting various companies to offer SOFC products, Solid Power, Sunfire, etc. [188].

A combination of SOEC and SOFC systems can be used to convert renewable electricity to synthetic fuels, and later utilise these fuels to produce electricity again; thus, acting like a renewable energy storage system. In the recent years, there has been increasing research on the concept of reversible solid oxide cells (rSOC). The main advantage of this concept is that the same SOC device can operate both in fuel cell (FC) and electrolysis (EL) mode, and in some cases, the same balance–of–plant (BOP) component can also be used in both modes. This reduces the capital cost of such a renewable energy storage system, while retaining the high efficiency benefits of SOC systems.

Some researchers have studied the integration of biomass gasification with SOEC systems. Sigurjonsson et al. [73] investigated the integration of rSOC with biomass gasification for hydrogen or power generation. The system reaches an efficiency of 46% for fuel production from biomass with a moisture content of 45 wt.%. Clausen et al. [189] examined the combined gasifier and pressurized

SOEC system. The energy efficiency achieved was 84% for syngas production from wood pellets. In another research, Anghilante [190] proposed the upgrading of bio–syngas through steam electrolysis and catalytic methanation achieving an energy efficiency in the range of 78.5–81.8%. Ali et al. [191] investigated straw biomass gasification and SOEC combined system for methanol production. The system reaches an energy efficiency of 72.08%, at a biomass moisture content of 7.9 wt.%. Yi et al. [192] analysed and optimized a biomass–fuelled polygeneration system for electricity, hydrogen, and freshwater generation. The system combined a Rankine cycle, a multi–effect desalination, and a solid oxide electrolyser and achieved a total exergy efficiency of 17.64%. Habibollahzade et al. [193] analysed and optimized the integrated hybrid biomass–based solid oxide fuel cell/solid oxide electrolyser cell/gas turbine using different gasification agents. The system achieves an exergy efficiency of 45.25% for power and hydrogen production. For the systems mentioned above it is difficult to compare the efficiencies since for poly–generation systems the definition of efficiency requires a different approach.

According to the literature review, the integration of gasification technology with SOEC technology combines the advantages of the two. Heat integration improves thermal performance. The oxygen by–product of electrolysis acts as a gasifying agent. Therefore, the fuel is produced with high energy efficiency > 70% [189], [190], [191]. However, the efficiency of fuel and power production in the poly–generation system reduces to < 50% [192], [193]. There is a lack of studies on highly efficient fuel and/or power generation using wet biomass feedstock. The integrated systems analysed are limited to conventional biomass with a moisture content lower than 10 wt%. Higher moisture in biomass requires an energy demanding dryer unit, reducing the efficiency of the systems. It is reflected in the efficiency of 46% found in the work of Sigurjonsson et al. [73].

SCWG is a process that converts wet biomass into combustibles with useful minerals as by–products [194]. A separation system can easily recover the minerals contained in the biomass, given that minerals have low solubility in water at supercritical conditions. A gas cleaning unit at temperature > 374°C, and pressure > 221 bar recovers the salt [195], [196]. The addition of a ZnO bed in the SCWG reactor enables sulphur removal [197] [139]. Hence, the product gas is relatively clean to feed a SOC without causing degradation of the SOC anode. This process operates at relatively low temperatures between 400°C and 600°C and pressures above 220 bar. The variation of thermo–physical properties of

supercritical water (SCW) significantly influences the heat transfer and the biomass gasification [198,199]. The main advantage of SCWG is that it does not need an energy–intensive biomass–drying step since it uses water as both the reactant and the reaction medium.

Table 4.1. Fuel and power SCWG combined system

Integrated System	**P bar**	**T °C**	**con. wt. %**	**η %**	**η_{ex} %**	**Prod.**	**Ref.**
SCWG–SOFC–GT	250	600	21.52	50	50	Power	[91]
Hydrothermal gasification–Catalytic fixed–bed gasific SOFC–RNK–FP–GT	300	350–450	20	63	60	Power	[92]
SCWG–direct expansion in a gas supercritical turbine–combined cycle.	250	650	25	54.38		Power	[210]
Solar SCWG – SMR	240	605	25	45	45	syngas	[204]
SCWG–syngas chemical looping (SCL)–power generation		650	15	73		Power + H_2	[207]
Solar SCWG – SMR	240 – 250	590–605	13–15.4	81.26	50.31	syngas	[202]
SCWG – syngas separation Rankine cycle	250	650	20	8	89.18 20	Power +syngas	[2]

The SCWG technique is still not widely commercialised and needs some research and development because it is hindered by high operating costs and multiple engineering challenges. Nearly 100% conversion of biomass (minimization of char formation) into syngas requires high temperatures (> 600°C without catalyst), feasible residence time and low feedstock concentration [200], [201], [157]. The thermodynamic efficiency is affected by high energy requirements, which requires a heat recovery system [201]. The resulting gas

contains high concentration of steam and CO_2. Chen et al. [1] suggested increasing the system capacity, feedstock concentration, improving the heat transfer efficiency and energy recovery, etc. to contribute to the reduction in hydrogen production cost and the improvement in the thermodynamic efficiency.

Table 4.1 shows the operating conditions and performance of several integrated SCWG systems for fuel and/or power production. The energy efficiency reached by these systems is in the range of 50 to 82%. The feedstock concentration is between 13% and 25%. Thermal efficiency and CGE (cold gas efficiency) are favoured at feedstock concentrations > 10 wt.% [43], [202] because of the higher CO and CH_4 content in the syngas [203]. But the exergy efficiency decayed due to increased char formation [204], [202]. In this regard, high feedstock concentration harms the gasification, since water influences the physics and chemistry that determines supercritical water gasification [205], [206]. It is demonstrated nearly complete gasification of 99.2% CE (carbon gasification efficiency) at feedstock concentration of 9 wt.% chicken manure at 620°C [43]. On the contrary, the high moisture content leads to a high energy requirement for increasing the temperature to supercritical conditions, substantially reducing the exergy efficiency. Chen et al. [2] reported a decrease in the SCWG exergy efficiency from ~90% at 20 wt.% biomass to ~20% at 8wt.% biomass. Thus, a trade–off between complete gasification and thermal efficiency is required.

The SCWG product gas, with high exergy, contains a high amount of steam, which is usually condensed out (gas upgrading unit) before utilisation of the gas as fuel. The systems indicated in Table 4.1 recover the exergy of the product gas, before entering a gas upgrading unit, with a HE (heat exchanger) or with chemical looping (oxy–fuel combustion using a solid–state oxygen carrier). These units recover the sensible heat of the product gas to recirculate in the process. Ajiwibowo et al. [207] uses chemical looping in co–production of H_2 and recovers the heat for power generation. The system reaches an energy efficiency of 73%. Chen et al. [2] uses a HE for heat recovery and power generation. The HE recovers most of the sensible heat of the gasification product gas. The heat recovered pre–heats the water entering the SCWG and heats the water that feeds a Rankine cycle. The system reaches an exergy efficiency of 89.18% at 20 wt.% biomass (80 wt.% water) but reduces to 20% at 8 wt.% biomass. The exergy destruction of the energy recovery units accounts for a significant fraction of the total exergy destruction in the system [2], [202]. Guo et al. [208] presented direct mass transfer system as an alternative to the HE. The

highest exergy efficiency, around 90%, is reached at feedstock concentration of 70.6 wt.% biomass; at 30 wt.% biomass the efficiency reduces to 30% approximately. In addition, the oxygen demand by the system will imply additional operation costs.

The gas upgrading unit negatively influences the overall system efficiency. It depends on the high–water content and the inlet gas–product temperature. High inlet temperature of the gas upgrading unit results in high waste heat production in the system [204], [209]. The syngas obtained after the condensation still contains a high volume of CO_2 (22 vol.%, SCWG operating at 420°C, 280 bar) [139], which reduces its calorific value. Onigbajumo et al. [202] fed the product gas to a reforming reactor promoting, simultaneously, the water gas shift reaction. However, the reactors represent 60% of the total exergy destruction of the process [202] and [204]. The higher the system complexity the higher exergy destruction. It is reflected in the exergy efficiency of 50.31% in the work of Onigbajumo.

From this perspective, feedstock concentration lower than 10 wt.% can be an alternative to address the char formation issue, achieving a high conversion of feedstock in SCWG, despite the high energy demand to increase the temperature to supercritical conditions. Process integration makes heat recovery feasible and reduction of exergy destruction in HE, gas–liquid separation unit and reforming reactors, by applying simpler system configuration. In this context, the gasifier product gas (salt separation in the gas cleaning unit Temperature > 374°C, Pressure > 221 bar [195], [196]), when excess renewable electricity is available, can be directly fed to an rSOC in EL mode. The fuel electrode promotes the electrochemical reduction of H_2O into H_2 and O_2. It increases the exergy of the produced gas and thus the capacity of the system. SOEC anode is able to support electrolysis. Additionally, it also supports water–gas shift reaction and methanation reaction (the latter at pressurised operation [211]).

The combustible gas and the air–based streams release heat during the downstream cooling process. This provides the energy required to pre–heat the feedstock to supercritical conditions. Heat is also provided for SOEC air preheating. The water content of the product syngas is significantly reduced thanks to electrolysis. The high–value syngas generated can be stored for later use in the rSOC in FC mode. When there is a deficit of renewable electricity, the stored syngas is mixed with the fresh syngas from the SCWG system (after gas upgrading), and used in the rSOC in FC mode to generate electricity.

The objective of this study is to develop a process design for a combined SCWG–rSOC system that significantly increases the system capacity for hydrogen production, which could reduce operating costs and achieve high thermodynamic efficiency by reducing exergy destruction. The integration enables intermittent syngas or power production from wet biomass SCWG. Syngas generation from wet syngas generated in SCWG using an rSOC in EL mode, and power generation from mixed syngas using an rSOC in FC mode. In addition, by aligning with the objectives towards the sustainable development of society, this novel system can be a potential solution that addresses a threefold need: sustainable sanitation, power generation from wet biomass waste, and energy storage.

To evaluate the performance of the SCWG–rSOC system, process simulations were conducted. The efficiency of the combined system in each mode was calculated. The effects of several parameters such as biomass moisture content, rSOC stack temperature and pressure, and current density on the system efficiency were studied. Finally, an exergy analysis was carried out to identify the sources of greatest exergy destruction.

4.2 System concept

4.2.1 Integration of SCWG with rSOC

Figure 4.1 shows a feed diagram of the proposed system, in which wet biomass is used to feed an endothermic SCWG. The gasifier generates a steam–rich gaseous mixture (Line 1, in Figure 4.1) under supercritical water conditions. The rSOC stack operating in the electrolyser mode is directly fed with the pressure–regulated gaseous mixture coming from (Line 1, in Figure 4.1) of the SCWG. Figure 4.2A shows the process heat integration of the SCWG–rSOC EL mode. The high–temperature and high–pressure steam and CO_2 in the gaseous mixture are recovered and electrochemically reduced into H_2 and CO in the fuel electrode of the SOEC using electricity from the grid, which can be produced by solar and/or wind power systems. The heat required for the SOEC can be partly obtained from the heat generated by *in situ* methanation and partly from the heat generated from the rSOC losses (cell overpotential). Additional heat can be supplied by an external thermal source and process heat. An air stream feeds the oxygen electrode and is used as a sweep gas to remove the oxygen generated during electrolysis. The air stream is also used as a sink or source of heat for exothermic or endothermic SOEC operation. The expander E1 recovers any energy from the hot airflow. The SCWG is highly endothermic; heat exchangers

are employed to facilitate the heat flow from the high temperature stream to the low temperature feedstock.

After SOEC operation, the unconverted H_2O is condensed in separator S1 upon cooling to remove it from the fuel gas produced in the electrolyser. It is then pressurizer and stored in a tank for future use.

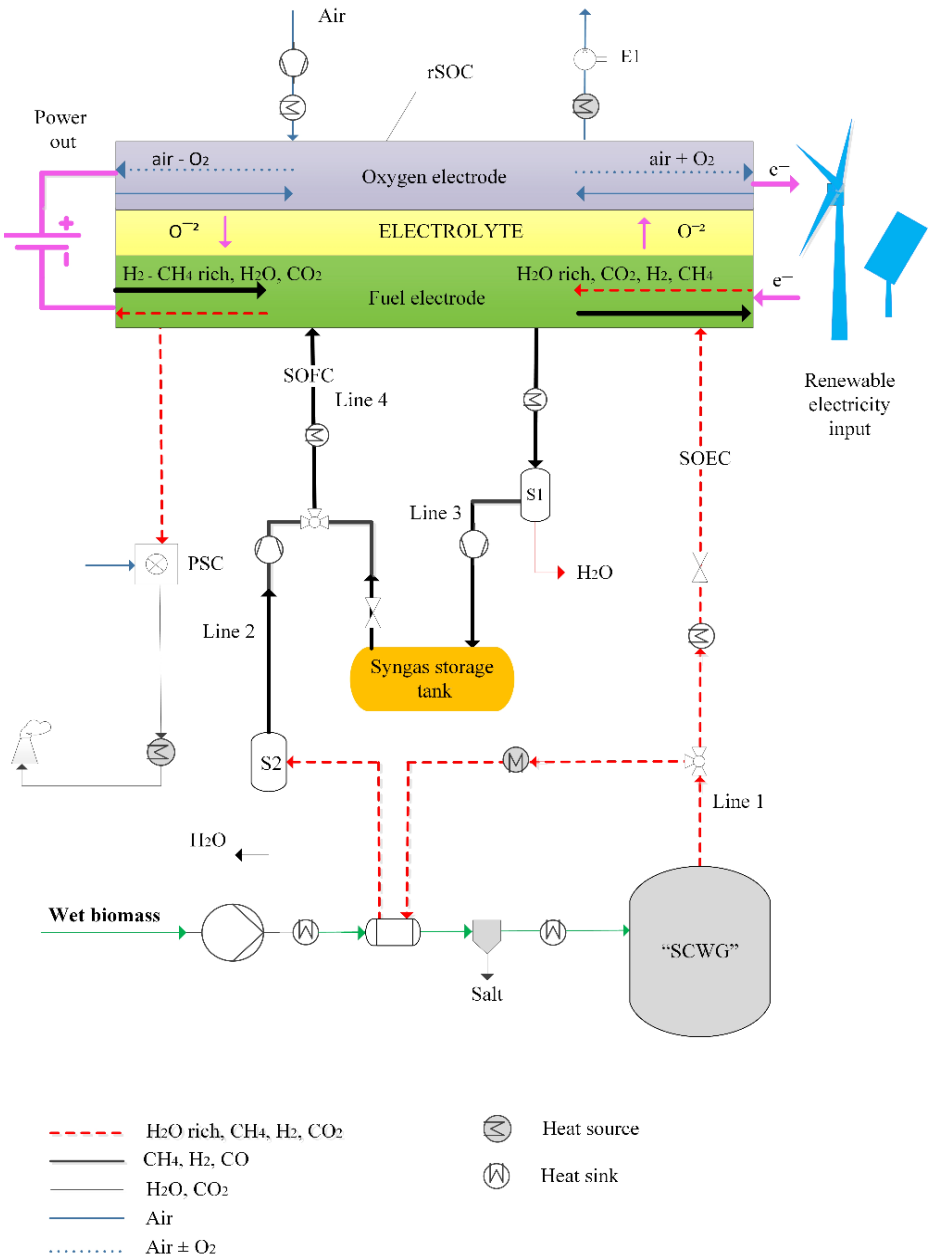

Figure 4.2. Feed system of the SCWG–rSOC process

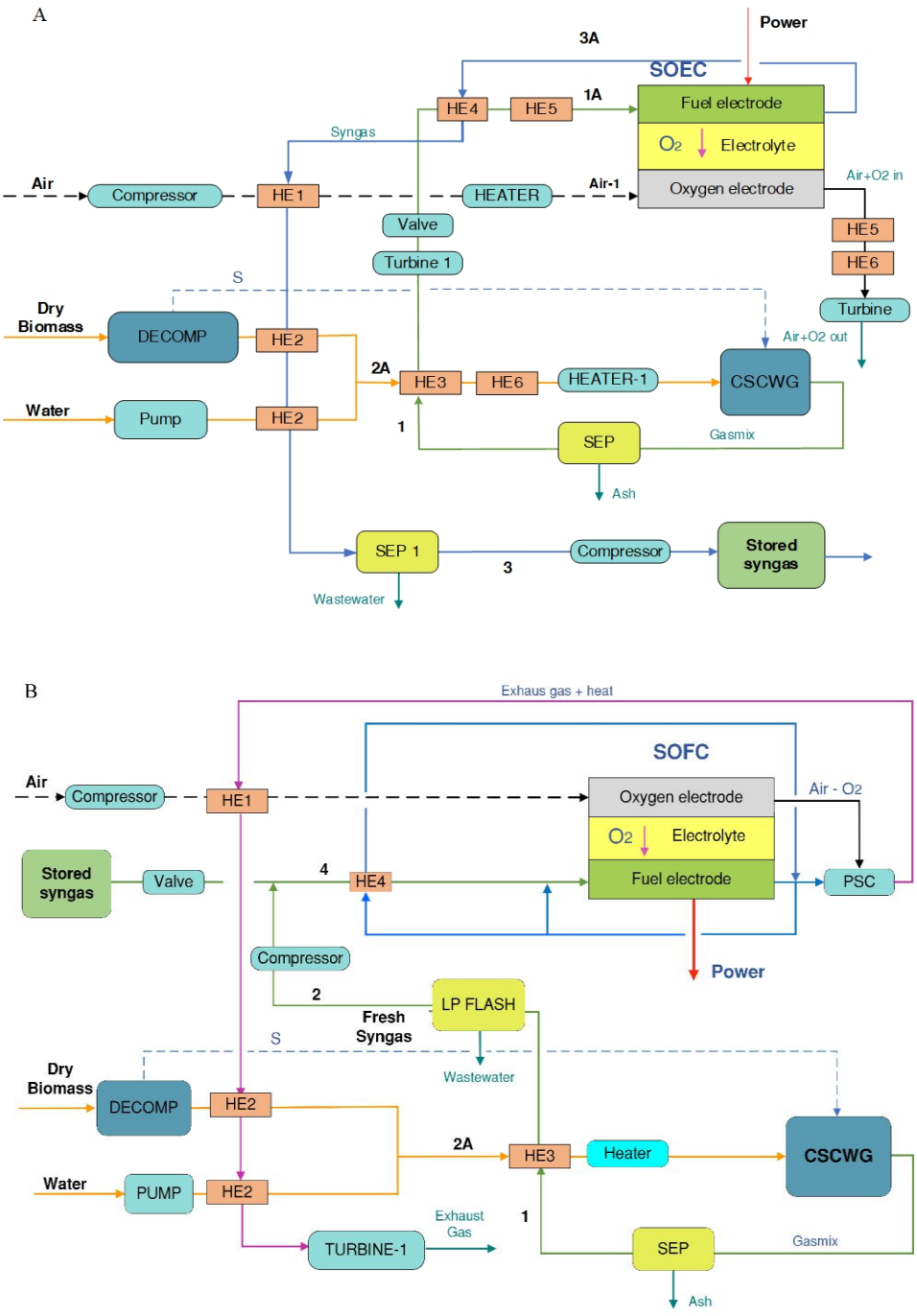

Figure 4.2. Aspen Plus SCWG–rSOC feed system simulation. A) SCWG–rSOC–EL Mode, B) SCWG–rSOC–FC Mode

In the SOFC operation mode, two fuel sources are fed to the fuel electrode of the rSOC: the syngas from the SOEC, which is stored in the storage tank (Line 3 in Figure 4.1), and the fresh syngas from the SCWG (Line 2 in Figure 4.1), which is upgraded in a gas/liquid separator (S2) that removes the water from the gaseous mixture. The gaseous mixture is pressure–regulated before being fed to the SOFC stack, where the process heat preheats the fuel and air streams. Then, the gaseous mixture is electrochemically oxidised on the fuel electrode of the SOFC, producing electricity, heat, and exhaust compounds. The airflow provides oxygen for the electrochemical reactions and regulates the stack temperature, removing excess heat. Combustion takes place in the post–combustor (PSC) between the high–temperature airflow from the oxygen electrode and the exhaust species from the SOFC fuel electrode. Figure 4.2B shows the process heat integration of the SCWG–rSOC FC mode.

Main assumptions of this study are:

- All processes are in steady–state equilibrium; the system is well insulated (i.e. no energy or exergy is lost to the environment from the process units).
- Low solubility of the inorganic compounds (ash) in supercritical water at thermodynamic equilibrium. NH_3 and SO_2 is transported by water in the gas–liquid separation units [212].
- Co–electrolysis of H_2O and CO_2 takes place at the fuel electrode of the rSOC in EL mode [213], [214].
- The ASR estimation uses a gaseous mixture of H_2O and H_2 [215].
- External heat supplied to the system is electric heat.

4.3 Thermodynamics of the SCWG–rSOC system

4.3.1 Chemical analysis

Non–traditional biomass feedstocks such as wet animal manures, human waste, sewage sludges, food industry waste, aquaculture residues and algae are potential feedstock for SCWG. These feedstocks are large renewable residual streams, continuously generated. These feedstocks must be treated to guarantee the protection of the environment. However, the high degree of heterogeneity in the form, composition and water content of biomass is a disadvantage for almost all applications [17]. Real biomass is quite challenging due to the complex nature containing cellulose, hemicellulose and lignin. For the SCWG, equations (1,2) describe the complete conversion of biomass into a mixture of H_2, CH_4 and CO_2, where the organic matter of biomass is assumed as $C_6H_{12}O_6$ as a representative

model biomass compound used to understand the gasification process. Table 2 shows a sample composition of the biomass. We assume low solubility of the inorganic compounds (ash) in supercritical water at thermodynamic equilibrium [212]. It is separated in the salt separator unit, Figure 1.

Table 4.2. Main biomass properties

Parameters	
Ultimate Analysis biomass (wt.%–dry basis)	[216]
H	6.3
C	49.1
N	5.9
S	2.0
O (by difference)	36.7
Proximate analysis (wt.% dry basis)	[216]
Volatile fraction (%, db)	46.46
Ash (%, db)	49.03
Moisture content (%, fresh weight)	90–95
Energy content LHV (dry), (MJ/kg)	16.84

The sulphur content is converted to H_2S, while nitrogen content is converted to NH_3 [177]. The addition of a ZnO bed in the reactor allows the removal of H_2S [139,197] in the SEP unit described in Figures 2A and 2B. NH_3 is assumed to be transported by water in the SEP 1 and LPFLASH water separation units in Figures 2A and 2B, respectively. The temperature, pressure, residence time, and amount of water in the biomass all influence the product gas composition. Furthermore, hydrogen production is favoured at high temperatures, whereas methane generation is facilitated by high pressures [143]. Note that the reaction in Equation (4.2) is exothermic and thus contributes to reducing the heat required for the gasification process.

$$C_6H_{12}O_6 + 6H_2O \rightarrow 6CO_2 + 12H_2 \qquad \Delta H = 360\ kJ \cdot mol^{-1} \qquad (4.1)$$

$$C_6H_{12}O_6 \rightarrow 3CH_4 + 3CO_2 \qquad \Delta H = -132\ kJ \cdot mol^{-1} \qquad (4.2)$$

Details of the thermodynamic analysis of the FC operation mode can be found in [209]; the analysis of electrolysis and thermochemical reactions is detailed in Equations (4.3)–(4.9). The excess electrical energy—available from

renewable sources—and a residual heat supply (external or internal) serve as energy inputs for high temperature electrolysis. Equations (4.3) and (4.4) represent the reduction of H_2O and CO_2; thus, electrical energy is stored in the chemical form. The generated CO and H_2 react to form methane following Equation (4.8) (methanation reaction) at low temperature and high pressure (600 ^oC, 20 bar). Methanation has a considerable impact on cell thermal management because of the relatively high amounts of heat released (ΔH) due to its exothermic nature [217], which contribute to satisfying the heat requirements of the SOEC. Operating conditions also allow the reverse water–gas shift reaction (the reverse of Equation (4.7)) to be predominant, which results in the reduction of CO_2 by H_2 [218].

Full cell reactions in the rSOC:

$$H_2O_{(gas)} \leftrightarrow H_2 + \tfrac{1}{2}O_2 \qquad \Delta H = 242\ kJ\cdot mol^{-1} \tag{4.3}$$

$$CO_2 \leftrightarrow CO + \tfrac{1}{2}O_2 \qquad \Delta H = 283\ kJ\cdot mol^{-1} \tag{4.4}$$

Reactions at the fuel electrode:

$$H_2O + 2e^- \leftrightarrow H_2 + O^{2-} \tag{4.5}$$

$$CO + O^{2-} \leftrightarrow CO_2 + 2e^- \tag{4.6}$$

$$H_2O + CO \leftrightarrow H_2 + CO_2 \qquad \Delta H = -41\ kJ\cdot mol^{-1} \tag{4.7}$$

$$3H_2 + CO \leftrightarrow CH_4 + H_2O_{(gas)} \qquad \Delta H = -206 kJ\cdot mol^{-1} \tag{4.8}$$

Reactions at the oxidant electrode:

$$O^{2-} \leftrightarrow \tfrac{1}{2}O_2 + 2e^- \tag{4.9}$$

4.3.2 Energy analysis of the rSOC system

The overall energy required to spur a chemical reaction [170] in the rSOC is given by:

$$\Delta H_{SOEC} = \Delta G + T\Delta S \tag{4.10}$$

where ΔH is the change in enthalpy; ΔG is the change in Gibbs free energy, which, at a constant pressure and temperature, determines the maximum value of the useful electrical work of the system required to initiate the reaction; and $T\Delta S$ is the product of the temperature and change in entropy, which determines the reversible transfer of heat.

The reversible cell voltage of the rSOC is related to ΔG through the Nernst equation as a function of the species partial pressure of the system. This equation represents a case in which an electrochemical reaction facilitates the charge transfer between phases [219]. This transfer of charged species (electrons or ions) across the interface in an rSOC depends on the amount and nature of the electrode/electrolyte/gas triple–phase boundaries (TPB). Assuming that co–electrolysis of H_2O and CO_2 takes place at the fuel electrode of the rSOC in EL mode [214], the reversible cell voltage, E_r, is the average of the Nernst equation applied to the chemical reactions in Equations (4.3) and (4.4) as follows [213]:

$$\mathrm{E_{r,H_2O}} = \mathrm{E_{0,H_2O}} + \frac{\mathrm{RT}}{\mathrm{nF}} \frac{\mathrm{p_{H_2} p_{O_2}^{1/2}}}{\mathrm{P_{H_2O}}} \tag{4.11}$$

$$\mathrm{E_{r,CO_2}} = \mathrm{E_{0,CO_2}} + \frac{\mathrm{RT}}{\mathrm{nF}} \frac{\mathrm{p_{CO} p_{O_2}^{1/2}}}{\mathrm{p_{co_2}}} \tag{4.12}$$

$$\mathrm{E_r} = \frac{1}{\mathrm{x_{H_2O} + x_{CO_2}}} \left(\mathrm{x_{H_2O} E_{r,H_2}} + \mathrm{x_{CO_2} E_{r,CO}}\right) \tag{4.13}$$

where the quantity nF expresses the amount of charge transferred for every mole of reactant species.

The reversible voltage calculated by the Nernst equation is equivalent to the open–circuit voltage (OCV), which can be measured as the difference between the electrode potentials of the anode and cathode when no current is flowing.

The rSOC reversible voltage varies with the electrical current flowing through the system, and its nature depends on the direction of the current [219].

Resistance to the flow of charge in a cell leads to Ohmic losses. The charge transfer reactions cause activation losses, whereas the transport limitations of gases through the porous electrodes to the TPB cause concentration/diffusion losses. These resistances affect the final voltage of the rSOC. Thus, the operating voltage is higher than the OCV for the case of an SOEC as follows:

$$\mathrm{V_{SOEC}} = \mathrm{E_r} + \eta_\mathrm{a}(\mathrm{j}) + \eta_\mathrm{ohm}(\mathrm{j}) + \eta_\mathrm{conc}(\mathrm{j}) \tag{4.14}$$

The total overvoltage η is equal to the area–specific resistance (ASR) times the current density of the cell, resulting in the following expression for SOEC operating voltage [220]:

$$V_\mathrm{SOEC} = E_\mathrm{r} + ASR * j \tag{4.15}$$

For the ASR estimation, it is assumed that the rSOC stack is fed with a gaseous mixture of H_2O and H_2. The SOEC stack ASR is described using the models developed by [221] and [215]. Table A1 provides the simulation parameters to fit the I–V curve of a two–electrode supported solid oxide cells with structure of "Ni–Sm doped CeO_2 infiltrated porous $La_{0.9}Sr_{0.1}Ga_{0.8}Mg_{0.2}O_3$ (LSGM) dense LSGM/$SmBa_{0.5}Sr_{0.5}CO_2O_5$ infiltrated porous LSGM" tested in the work of Wang S. et al. at 600°C [222]. Appendix A gives supplementary information about ASR estimation.

Table A1 Simulation parameter of the SOC

Parameter		Unit	Fit. Value	Ref.
Anode – cathode				
Thickness anode	dan	μm	2.10E–04	[222]
Thickness cathode	dcat	μm	2.10E–04	[222]
Particle diameter	d_p	[nm]	200	[222]
Porosity	ε		0.3	[221]
Tortuosity	τ		5	[221]
Empirical constant	$i^*_{H_2}$	A/cm2	2.8	[221]
Pre–exponential of desorption	A_{des}	s cm2/mol	5.59E+19	[221]
Surface site density	Γ	mol/cm2	2.60E–06	[221]
Sticking probability	γ_0		0.01	[221]
Activation energy of desorption	E_{des}	kJ/mol	88.12	[221]
Empirical constant	i^*_{O2}	A/cm2	0.4	
Pre– exponential factor	A_{O_2}	atm	4.90E+08	[221]
Activation energy	E_{O_2}	kJ/mol	200	[221]
Electrolyte				
Thickness	del	μm	1.60E–05	[222]
Pre– factor of O^{2-}	so,el	W–1cm–1	333.3	[221]
Activation energy	E_{el}	J/mol	85.63	[221]

4.3.3 Current density

When operating in EL mode, the amount of current through the external circuit depends on whether reduction of CO_2 at the fuel electrode occurs through steam electrolysis followed by reverse water–gas shift reaction or via direct co–

electrolysis. It also depends on structural and operational parameters, which determine if direct CO_2 electrolysis will have a significant or negligible influence on the process [215]. According to [223], a surface ratio β, derived based on the applied experimental method, splits the active surface area for the H_2O and CO_2 electrochemical reductions. In this study, the approach of [213] was considered which is as follows:

$$\mathrm{I_{SOEC/H_2O}} = 2F\dot{n}\beta \cdot U_\mathrm{f} \tag{4.16}$$

$$\mathrm{I_{SOEC/CO_2}} = 2F\dot{n}(1-\beta) \cdot U_\mathrm{f} \tag{4.17}$$

$$\beta = \frac{y_{\mathrm{H_2O}}^{\mathrm{TPB}}}{y_{\mathrm{H_2O}}^{\mathrm{TPB}} + y_{\mathrm{CO_2}}^{\mathrm{TPB}}} \tag{4.18}$$

The current density is estimated by:

$$\mathrm{j_{SOEC}} = \frac{\mathrm{I_{SOEC}}}{\mathrm{A_{SOEC}}} \tag{4.19}$$

A single SOEC stack consisted of parallel connected cells. Each cell of the SOEC has an active area equal to 0.1 m^2. For each biomass moisture content, the required number of cells is obtained with the objective of operating the cell with the highest system efficiency.

The power supplied to the electrolysis operation can be calculated by:

$$\mathrm{P_{SOEC}} = \mathrm{V_{SOEC}} \cdot \mathrm{I_{SOEC}} \tag{4.20}$$

4.3.4 Thermoneutral voltage

The theoretical thermoneutral voltage in electrolysis mode is obtained as [218]:

$$V_\mathrm{TN} = \frac{\Delta H_\mathrm{SOEC}}{nF} \tag{4.21}$$

In SOEC mode, V_{TN} is the cell voltage provided to the SOEC system. The heat generated in the cell meets the heat balance of all cell reactions, both chemical and electrochemical [218], thereby resulting in both adiabatic and isothermal operations [224]. At operating voltages less than or greater than V_TN, the system operates in the endothermic mode or the exothermic mode, respectively. The molar change of the enthalpy ΔH of the reactions promoting charge–transfer (Equations (4.3) and (4.4)) depends on the external supply of power, ΔG, and heat, $T\Delta S$, as expressed in Equation (4.10). The energy balance diagram of the SOEC shown in Figure 4.3 depicts all the energy (heat and power)

sources and sinks influencing the thermal energy required by the reactions defined in Equations (4.3) and (4.4).

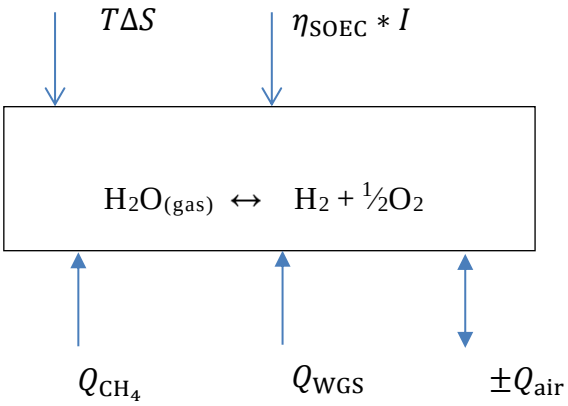

Figure 4.3. rSOC electrolysis mode heat balance

In Figure 4.3, Q_{CH_4} and Q_{WGS} are the reaction enthalpies of the spontaneous reactions for methanation and water–gas shift, respectively, at the fuel electrode. The heat liberated by the cell losses is equal to the overpotential, η_{SOEC}, times the current, I. The air fed to the air electrode acts as a temperature regulator, adding or removing heat, Q_{air}, from the SOEC. Thus, based on the energy balance equation, Q_{air} can be computed by:

$$Q_{air} = T\Delta S - (Q_{CH_4} + Q_{WGS} + \eta_{SOEC} I) \quad (4.22)$$

Combining Equation (4.22) with Equations (4.10) and (4.14) results in

$$Q_{air} = \Delta H_{SOEC} - V_{SOEC} \cdot I - (Q_{CH_4} + Q_{WGS}) \quad (4.23)$$

The Aspen Plus™ reactor blocks provide the values for Q_{CH_4}, Q_{WGS}, and ΔH_{SOEC}. When $Q_{air} = 0$, the SOEC is in thermoneutral mode, and the operating voltage is equal to the thermoneutral voltage. In this case, the oxygen electrode supplies a small amount of air to release the product O_2, since there is no heat to provide to or remove from the SOEC. When $Q_{air} > 0$, the net operation in the SOEC is endothermic, and air at a higher temperature than the SOEC operating temperature provides the heat required by the cell. When $Q_{air} < 0$, the net SOEC operation is exothermic and sweep air at a lower temperature than the SOEC operating temperature drains the excess heat.

4.3.5 Exergy analysis of the SCWG–rSOC system

Eq. (4.24) describes the exergy balance of the SCWG–SOEC system at steady state [225]. The exergy enters the system in the form of biomass and electricity. The system is well insulated; there is no exergy transfer accompanying heat transfer.

$$0 = \dot{W}_{\mathrm{cv}} + \sum_{\mathrm{i}} \dot{m}_{\mathrm{i}} e_{fi} - \sum_{\mathrm{e}} \dot{m}_{\mathrm{e}} e_{fe} - \dot{E}_{\mathrm{d}} \tag{4.24}$$

The total specific flow exergy is the sum of the thermomechanical and chemical exergies:

$$e = e_{\mathrm{f}} + \bar{e}^{\mathrm{ch}} \tag{4.25}$$

The thermochemical exergy is given by:

$$\mathrm{e_f} = \mathrm{h} - \mathrm{h_0} - \mathrm{T_0}(\mathrm{s} - \mathrm{s_0}) \tag{4.26}$$

The chemical exergy for an ideal gaseous mixture at the reference environment (T_0, p_0) is given by:

$$\bar{\mathrm{e}}^{\mathrm{ch}} = \sum_{\mathrm{i}} (\mathrm{y_i} \bar{\mathrm{e}}_{\mathrm{i}}^{\mathrm{ch}} + \mathrm{y_i} \overline{\mathrm{R}} \mathrm{T_0} \ln \mathrm{y_i}) \tag{4.27}$$

4.3.6 Efficiency definitions

The SCWG–rSOC system's efficiency:

$$\mathrm{P_{BOP,system}} = \Sigma \mathrm{P_{heat}} + \Sigma \mathrm{P_{power}} \tag{4.28}$$

$\mathrm{P_{heat}}$ is the external heat supplied to the system (heaters), assuming electric heat, and $\mathrm{P_{power}}$ is the power of the auxiliary components (pumps, gas compressors). Aspen Plus™ blocks provide values for each $\mathrm{P_{heat}}$ and $\mathrm{P_{power}}$ component of the system. In the equations below, the subscript (i) refers to the components relevant to the subsystem whose efficiency is being calculated.

SCWG efficiency:

$$\eta_{\mathrm{SCWG}} = \frac{\dot{n}_{\mathrm{fuel}} LHV_{\mathrm{syngas,SCWG}}}{\dot{m}_{\mathrm{biomass}} LHV_{\mathrm{biomass}} + P_{\mathrm{BOP},(i)}} \tag{4.29}$$

$$\eta_{\mathrm{ex-SCWG}} = \frac{Ex^{ch}_{syngas} + Ex^{f}_{gas\ mixture}}{\dot{m}_{\mathrm{biomass}} Ex^{ch}_{biomass} + P_{\mathrm{BOP},(i)}} \tag{4.30}$$

rSOC efficiency:

$$\eta_{\mathrm{SOEC}} = \frac{\dot{n}_{\mathrm{fuel}} HHV_{\mathrm{syngas,SOEC}} - \dot{n}_{\mathrm{fuel}} HHV_{\mathrm{syngas,SCWG}}}{P_{\mathrm{SOEC}} + P_{\mathrm{BOP},(i)}} \tag{4.31}$$

$$\eta_{\mathrm{SOFC}} = \frac{P_{\mathrm{SOFC}} - P_{\mathrm{BOP},(i)}}{\sum \dot{n}_{\mathrm{fuel}} HHV_{\mathrm{syngas},(i)}} \quad (4.32)$$

The system energy efficiency:

$$\eta_{\mathrm{SCWG-SOEC}} = \frac{\dot{n}_{\mathrm{fuel}} HHV_{\mathrm{syngas,SOEC}} - \dot{m}_{\mathrm{biomass}} HHV_{\mathrm{biomass}}}{P_{\mathrm{SOEC}} + P_{\mathrm{BOP,system}}} \quad (4.33)$$

$$\eta_{\mathrm{SCWG-SOFC}} = \frac{P_{\mathrm{SOFC}} - P_{\mathrm{BOP,system}}}{\dot{n}_{\mathrm{fuel}} HHV_{\mathrm{syngas,SOEC}} + \dot{m}_{\mathrm{biomass}} HHV_{\mathrm{biomass}}} \quad (4.34)$$

Exergy efficiency of the system:

$$\eta_{\mathrm{ex-SCWG-SOEC}} = \frac{Ex^{ch}_{syngas} - Ex^{ch}_{biomass}}{P_{\mathrm{SOEC}} + P_{\mathrm{BOP,SCWG-SOEC}}} \quad (4.35)$$

$$\eta_{\mathrm{ex-SCWG-SOFC}} = \frac{P_{\mathrm{SOFC}} - P_{\mathrm{BOP,SCWG-SOFC}}}{Ex^{ch}_{syngas,SOEC} + Ex^{ch}_{biomass}} \quad (4.36)$$

4.4 Simulation of the CSCWC rSOC model in Aspen Plus™

Table 4.3. SCWG operating conditions

Parameter		
SCWG		
Temperature (ºC)	500	
Pressure (bar)	250	
Biomass mass flow rate (dry) (g/s)	0.56	
Biomass water flow rate (80, 90, 95 wt.%) (g/s)	2.24, 5.04, 10.64	
HP–LP flash pressure (bar)	10–1	[177]
HP–LP flash temperature (ºC)	100–25	[177]
Pump isentropic efficiency (%)	85	[226]
Biomass moisture content (wt.%)	95	
Energy biomass input (on HHV) (kW)	8.92	
Energy biomass input (on LHV) (kW)	8.25	
Exergy biomass input (kW)	10.56	

Figures 4.2A and 4.2B depict the feed system model of the SCWG–rSOC operation as simulated on Aspen Plus™. The rSOC model was built based on the work in [227], [228], [175]. This model considers the following assumptions: all processes are in steady–state equilibrium; the system is well insulated, and no energy or exergy loss occurs in the process units.

Table 4.4. rSOC operating conditions

Parameters	
rSOC	
Temperature (ºC)	680–850
Pressure (bar)	1–20
Fuel utilization	0.95 – 0.65
Number of cells	260 – 370
Area of a cell (m2)	0.01
Current density SOFC (A cm^{-2})	<2
Current density SOEC (A cm^{-2})	>2
Storage fuel tank temperature (ºC)	25
Storage fuel tank pressure (bar)	400 [229]
DC/AC inverter efficiency (%)	95 [230]
Fuel compressor isentropic efficiency (%)	85 [226]
Air compressor isentropic efficiency (%)	85 [226]
Heat exchanger minimum approach temperature (°C)	10
Process units pressure drop (bar) *	0.02

* Each process unit of SCWG–rSOC system

The Aspen model consists of three sections: SCWG, SOFC, and SOEC. In the SCWG, the gasifier model uses the procedure available in the Aspen Plus process simulation using solids. Table 4.3 lists the operating parameters of the SCWG. The RGibbs block used to represent the SCWG predicts the final gas product concentration from the gasifier based on the minimisation of the total Gibbs free energy. Table 4.2 lists the elementary composition of the dry biomass described by the Dry biomass stream, Figure 4.2A and 4.2B. The biomass decomposes into its constituent elements in the RYield block, DECOMP, at ambient temperature and a pressure of 250 bar. The heat of reaction, which is a product of the decomposition of the biomass, is considered in biomass gasification. Heat stream S then carries the reaction heat from the RYield block to the RGibbs block in the SCWG. The WATER stream is used to simulate the water content of the biomass. The pressure of the WATER stream is increased to 250 bar at PUMP and mixed with decomposed biomass stream 2A. The heat exchangers HE2, HE3 and HE6 and HEATER–1 preheat solution stream 2A, and the preheated species enter the reactor SCWG. The GASMIX fuel stream is then directed to either the SOFC or SOEC block, depending on the desired operation mode defined by the availability of electricity.

In the SOFC, as shown in Figure 4.2B, the SOEC stored syngas and the fresh syngas from the SCWG (stream 2) are mixed to form stream 4, and fed into the system. The turbine TURBINE–1 recovers part of the energy from the exhaust. For a complete discussion of the SCWG–SOFC simulation, the reader is referred to [209].

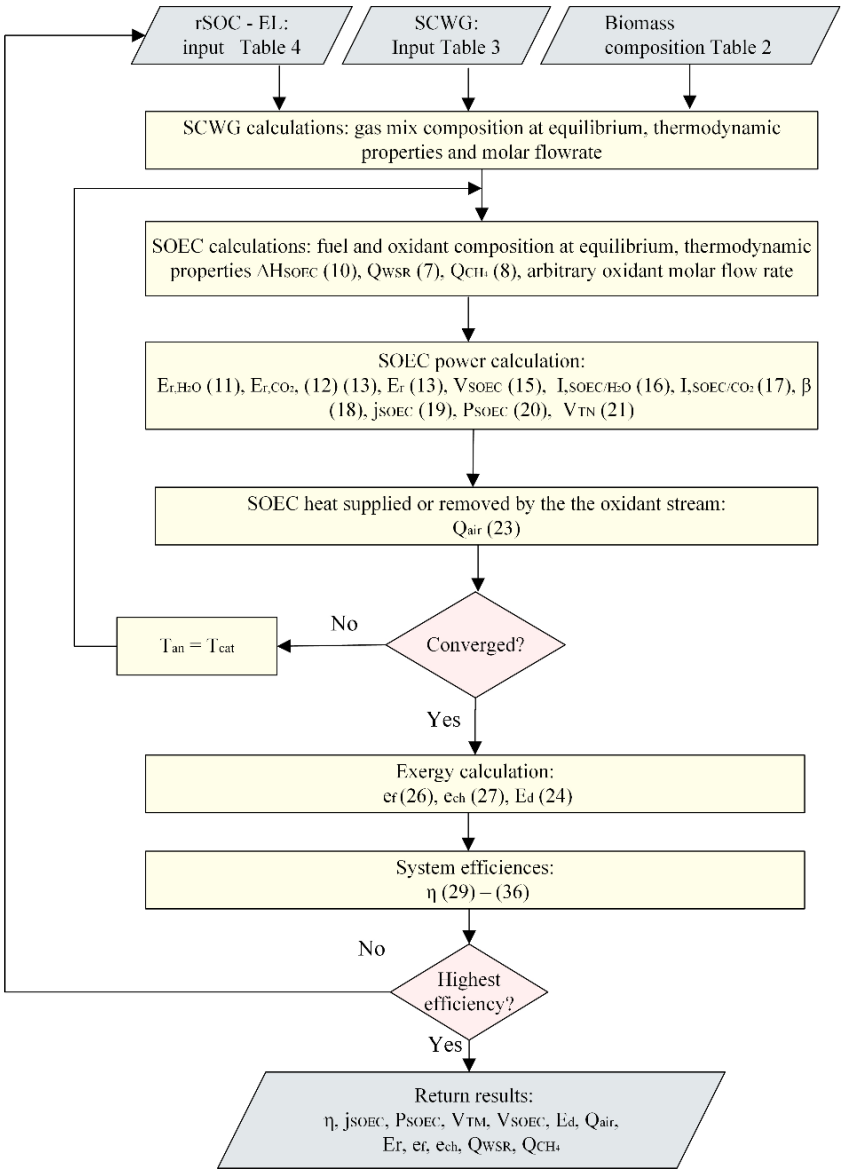

Figure 4.4. Calculation workflow for estimating the highest efficiency of the SCWG–rSOC–EL (numbers in parentheses refer to equations in this paper)

The SCWG–rSOC–EL model is shown in Figure 4.2A and Table 4.4 provides the operating parameters of the rSOC. The SCWG–rSOC–EL model (see Figure 4.S1 supplementary material) employs three blocks to describe the fuel electrode: WGSR, CATHODE, and METH. The RGibbs blocks WGSR and METH account for the heterogeneous reactions on the catalytic material of the fuel electrode: the forward and reverse water–gas shift reaction (WGSR) and methanation reaction (METH). The stoichiometric block CATHODE defines the electrochemical reduction of H_2O and CO_2 into O_2, H_2, and CO. The separator block ANODE1 and heater Q6 simulate the air electrode. The block ANODE1 separates the oxygen and syngas from CATHODE. The heat in the fuel electrode is added to or removed from the SOEC using block heater Q6. An Aspen Fortran calculator computes total heat entering or leaving block Q6 according to the energy balance shown in Figure 4.3 and defined in Equation (4.23). The airflow rate of the stream AIR and temperature of stream 17 by means of electric heater Q7 changes to keep the temperature of the outlet air stream 18 equal to the SOEC operating temperature.

The enthalpy of the electrochemical reaction is estimated using the net DUTY of CATHODE. The enthalpy of the heterogeneous reactions, WGSR, and METH are determined by the DUTY of block WGSR and METH, respectively. The calculation sequence for estimating the efficiency of the is shown in Figure 4.

4.5 Results and discussion

4.5.1 rSOC results comparison

The ASR of the rSOC is compared with the experimental I–V curve presented by Wang et al. [222] as shown in Figure 4.5A and Figure 4.5B. Table 4.1A provides the fitted cell parameters to obtain the experimental results. The model accurately simulated the rSOC experimental results of Wang, at 600 ºC, at atmospheric pressure 50% H_2O and 70% H_2O. The higher the gas concentration, the higher the cell exchange current density [231]. This is reflected in the variation of the slope curve.

The predicted value of the ASR, rSOC operating at 20 bar, 680 ºC and 70% H_2O is shown in Figure 4.5B. Concentration losses in the SOEC are reduced at higher operating pressure and higher H_2O concentration, while the increased temperature reduces Ohmic losses. Therefore, increasing pressure, gas concentration and temperature are favourable for the rSOC performance, obtaining stable ASR, which is shown in Figure 5B. This trend coincides with the

results presented in the work of Hauck et al. [215]. The ASR value of rSOC, at temperature > 800°C and ambient pressure, used in this work is equal to the value presented by Banner et al. [232] for LNO–LDC50 and LSM–YSZ oxygen electrodes. As a result, the following analysis uses an ASR in the range of 0.11 to 0.16 Ω cm^{-2}.

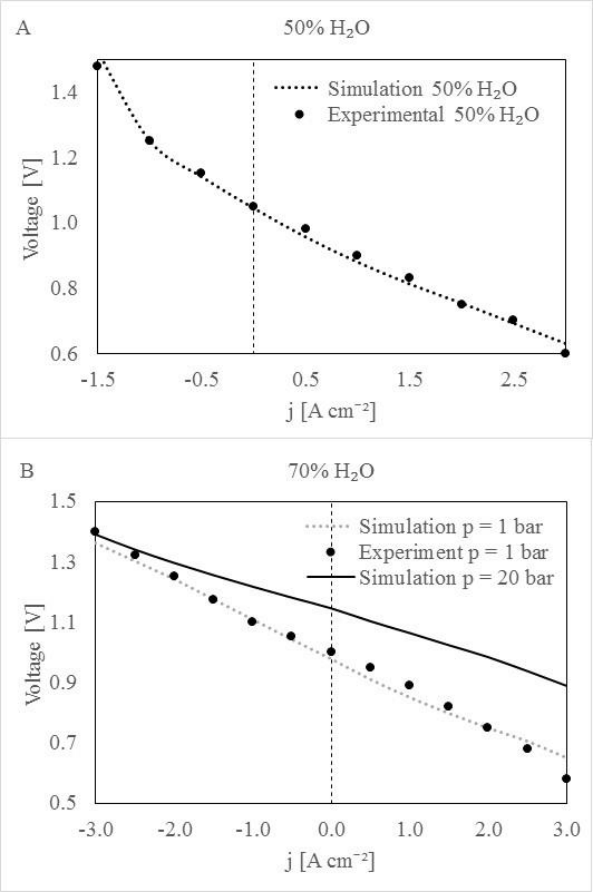

Figure 4.5 A – B Experiments by Wang et al. [222] **and present simulation results.**

At 95 wt.% biomass moisture, the pH_2O/pCO_2 ratio of the gas mixture SCWG (see Table 4.5) is around 53. According to recent findings of Ioannidou et al. [233], the H_2O/CO_2 co–electrolysis process in pH_2O/pCO_2=1 is 100% selective towards H_2O electrolysis. A similar behaviour is expected at pressurized operation [234]. Therefore, the influence of CO_2 electrochemical reduction is negligible for 95 wt.% biomass moisture. The surface ratio β is almost one calculated with Eq. 4.18.

The exergy efficiency of the SOEC at 95 wt.% biomass moisture, 1 bar and 850°C, (see Table 4.6) is 78%. This value is in agreement with the findings of [235]. At 20 bar and 680°C, feedstock with a moisture content of 80, 90 and 95 wt.% the thermoneutral voltage found in this work is in the range of 1.24–1.25 V and the reversible voltage is around 1.1 V. These values are in the same range of the findings of [218] at 20 bar and H/C ratio higher than 40.

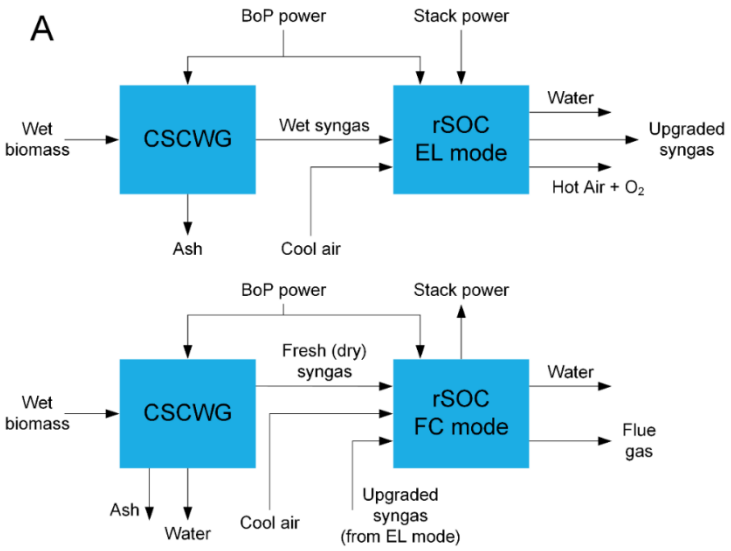

Figure 4.6. Schematic for energy/exergy flows in each mode

4.5.2 SCWG–rSOC operation

The performance analysis of the proposed SCWG–rSOC system based on energy, exergy, and mass balances for power or syngas generation (i.e., FC mode and EL mode, respectively) are summarized here. The performance is studied by making use of an exergy flow diagram, which indicates the exergy losses occurring in the various processes; the diagram also indicates additional external heat requirements, process heat recovery and the power consumed by the auxiliary units. Subsequently, the changes in the energy efficiency of the SCWG–rSOC are analysed as a function of i) biomass moisture, ii) rSOC pressure, iii) rSOC temperature, iv) syngas flow rates, v) current density. Table 5 reports the key data describing the system performance. Figure 4.6 shows a schematic of energy/exergy flows of the SCWG–rSOC in FC and EL mode. Figure 4.7 A–C shows the flowsheet of the system and Table 4.5 present the main gas compositions. The thermochemical and chemical exergy flows are shown in Figure 7, at j = 3.4 A cm^{-2}, T = 680°C, P = 20 bar, biomass moisture content = 95 wt.%.

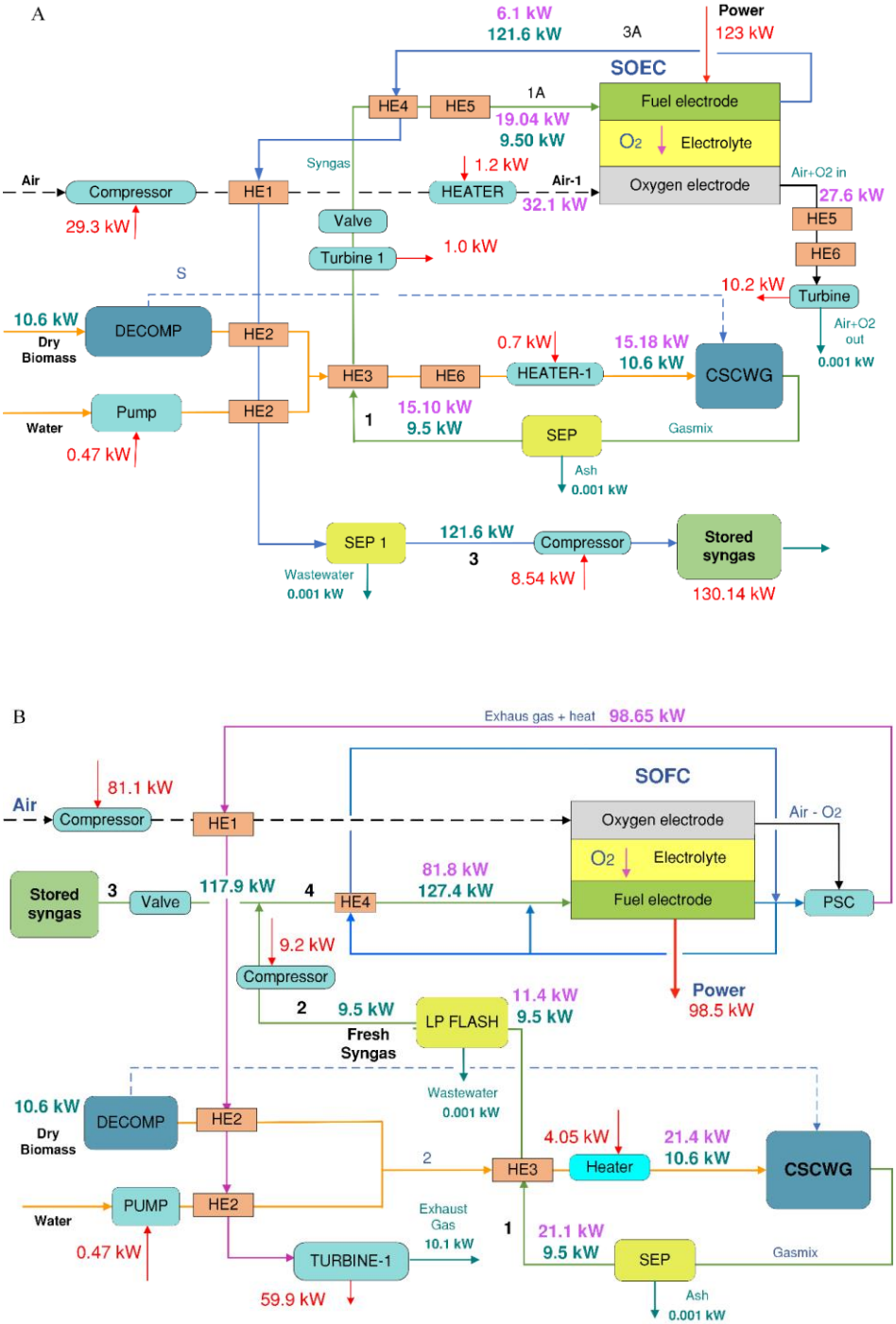
A
6.1 kW
121.6 kW
3A
Power
123 kW
SOEC
HE4
HE5
1A
Fuel electrode
19.04 kW
9.50 kW
O2
Electrolyte
Syngas
1.2 kW
Air
Compressor
HE1
HEATER
Air-1
Oxygen electrode
Air+O2 in
27.6 kW
32.1 kW
HE5
29.3 kW
Valve
HE6
Turbine 1
1.0 kW
10.2 kW
Turbine
S
Air+O2
out
0.001 kW
10.6 kW
Dry
Biomass
DECOMP
HE2
0.7 kW
15.18 kW
10.6 kW
HE3
HE6
HEATER-1
CSCWG
Water
Pump
HE2
1
15.10 kW
9.5 kW
SEP
Gasmix
0.47 kW
Ash
0.001 kW
SEP 1
121.6 kW
Compressor
Stored
syngas
3
Wastewater
0.001 kW
8.54 kW
130.14 kW
B
Exhaus gas + heat
98.65 kW
SOFC
81.1 kW
Air
Compressor
HE1
Oxygen electrode
Air - O2
O2
Electrolyte
Stored
syngas
3
Valve
117.9 kW
4
HE4
81.8 kW
127.4 kW
Fuel electrode
PSC
9.2 kW
Compressor
Power
98.5 kW
2
9.5 kW
Fresh
Syngas
LP FLASH
11.4 kW
9.5 kW
Wastewater
0.001 kW
10.6 kW
Dry
Biomass
DECOMP
HE2
4.05 kW
21.4 kW
10.6 kW
2
HE3
Heater
CSCWG
PUMP
HE2
Water
Exhaust
Gas
10.1 kW
1
21.1 kW
9.5 kW
SEP
Gasmix
0.47 kW
TURBINE-1
59.9 kW
Ash
0.001 kW

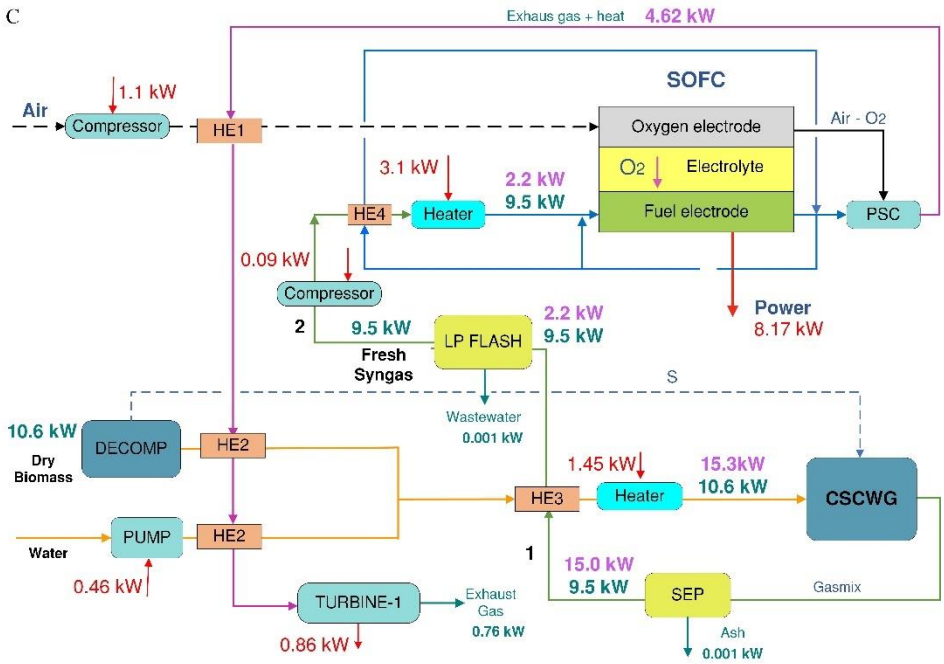

Figure 4.7. Flowsheet of the SCWG–rSOC system at j = 3.4 A cm^{-2} , T = 680°C, P = 20 bar, biomass moisture content = 95 wt.%. The figures include electricity consumption and production (red), as well as chemical exergy flows (green), thermochemical exergy flow (pink). Stream numbers refer to Table 5 with gas compositions. A) SCWG–rSOC – EL. B) SCWG–rSOC – FC. C) SCWG–SOFC.

4.5.3 SCWG–rSOC operating in EL mode

Figure 4.8A shows an exergy flow diagram of the results of the performance analysis of the syngas generation. The system is fuelled by SCWG product gas mixture (Line 1 in Figure 4.1) and electricity, and the system generates biofuel (Line 3 in Figure 4.1). Table 4.5 summarizes the results of analysis of flow rates, gas composition, pressure, temperature of the gases labelled in Figure 4.1, Line 1. In Figure 4.8A and Table 4.5, the SCWG–rSOC EL operation is at j = 3.4 A cm^{-2}, T = 680°C, P = 20 bar, and biomass moisture content = 95 wt.%.

The system efficiency depends on the external power and heat supplied to the system, and the efficient utilisation of the process heat in the SCWG fuel, air, and fuel preheating. The generated process heat almost satisfies the heat required by the SCWG, fuel and air preheaters. The energy supplied to the electrolyser is used to electrochemically reduce steam and CO_2 from the gas mixture, generating

H_2 and CO (syngas). The use of rSOC in EL mode results in an amount of syngas (Line 3, Figure 4.1) that is around thirteen times the fresh syngas generated exclusively in the SCWG gasifier (Line 2, Figure 4.1).

Some energy is recovered as electricity using the turbine, although with high exergy destruction. The fuel generated by the SCWG–rSOC system in EL mode contains approximately 69% of the total exergy input to the entire system.

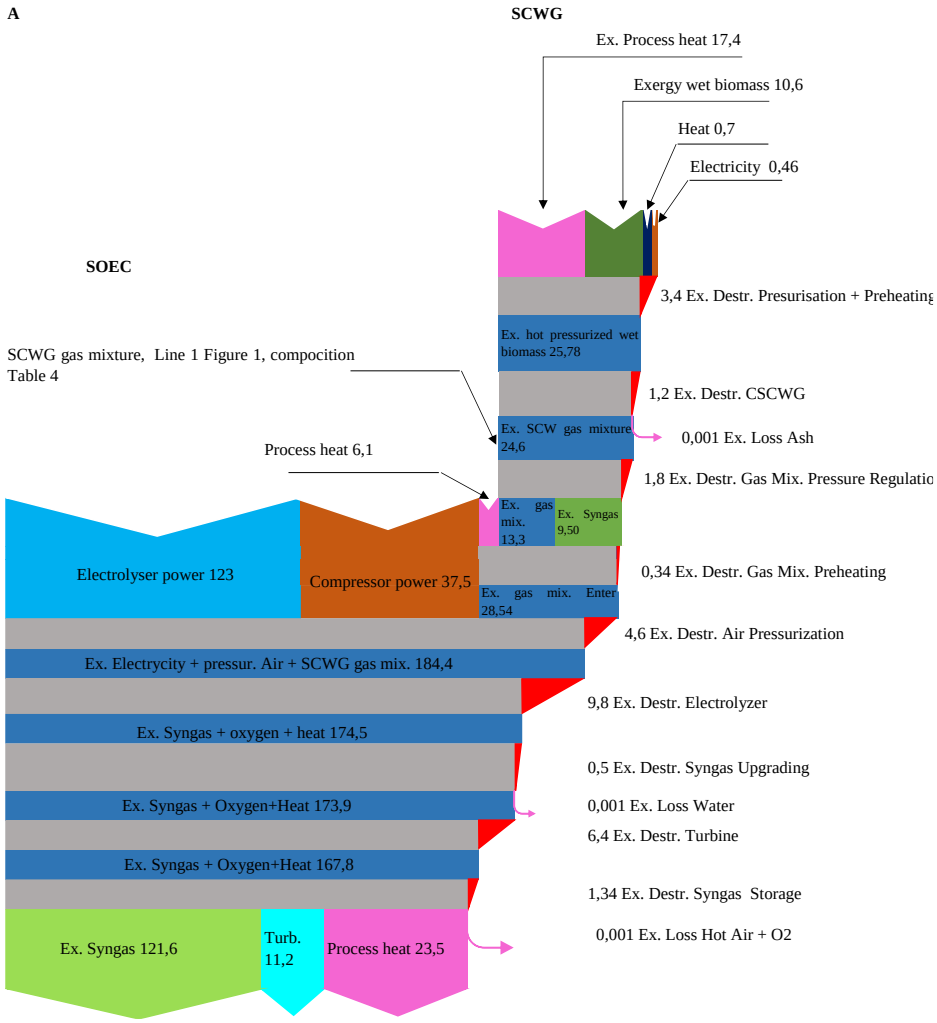

Figure 4.8. Exergy flow diagram (kW) of the SCWG–rSOC system at j = 3.4 A cm^{-2} , T = 680°C, P = 20 bar, biomass moisture content = 95 wt.%. A) SCWG– rSOC EL mode, B) SCWG– rSOC FC mode with mixed syngas, and C) SCWG–rSOC FC mode with fresh syngas.

Table 4.5. Performance results of SCWG–rSOC

Chemical composition

		Gas mix. SCWG		**Fresh SCWG syngas**		**SOEC syngas**	**Mixed gas**			
stream in Figure 2A		Line 1	Line 1A	Line 2	Line 3A	Line 3	Line 4	Air–1	Air+O2 in	Air+O2 out
H_2	%mol	1.6	1.6	29.0	73.0	95.3	90.7	–	–	–
CH_4	%mol	1.4	1.4	26.2	3.3	4.4	5.8	–	–	–
H_2O	%mol	95.1	95.1	9.9	23.5	0.1	0.8	–	–	–
CO_2	%mol	1.8	1.8	33.4	trace	trace	2.3	–	–	–
CO	%mol	trace	trace	–	trace	trace	–	–	–	–
NH_3	%mol	trace	trace	–	trace	trace	–	–	–	–
N_2	%mol	trace	trace	1.28	trace	trace	0.16	71.0	67.1	67.1
O_2	%mol	–	–		–	–	–	21.0	32.9	32.9
Total flow	mol s^{-1}	0.611	0.611	0.033	0.589	0.451	0.48	1.309	1.541	1.541
	g s^{-1}	11.1	11.1	0.726	3.7	1.2	1.94	37.8	45.2	45.2
LHV (ref. 15°C)	kJ mol^{-1}	15.4	15.4	280.9	203.5	265.7	266.7	–	–	–
Chemical exergy	kJ mol^{-1}	15.5	15.5	300.4	198.6	261.1	262.4	–	–	–
Temperature	°C	500	680	97	680	25	680	569	680	–12
Pressure	bar	250	20	1.013	20	20	20	20	20	1.013
Specific Enthalpy	kJ mol^{-1}	–226.7	–214.2		–38.6	–3.7		16.6	20.3	–1.1

The exhaust gas emitted to the environment is at ambient temperature, thus its exergy loss (that eventually becomes exergy destruction in the atmosphere) is negligible. In contrast, the exergy destruction of the electrolyser and turbine (9.6 and 6.4 kW respectively) have significant influence in reducing the system performance. The rSOC stack in EL mode must operate at a current density higher than 2 $A \cdot cm^{-2}$. This current density was derived considering that the system must operate near the thermoneutral voltage to attain the highest possible efficiency. The system achieves an energy efficiency of 91% which can be compared with and efficiency of biomass and electricity by gasification with pressurized SOEC of 84% [189].

4.5.4 SCWG–rSOC FC operation

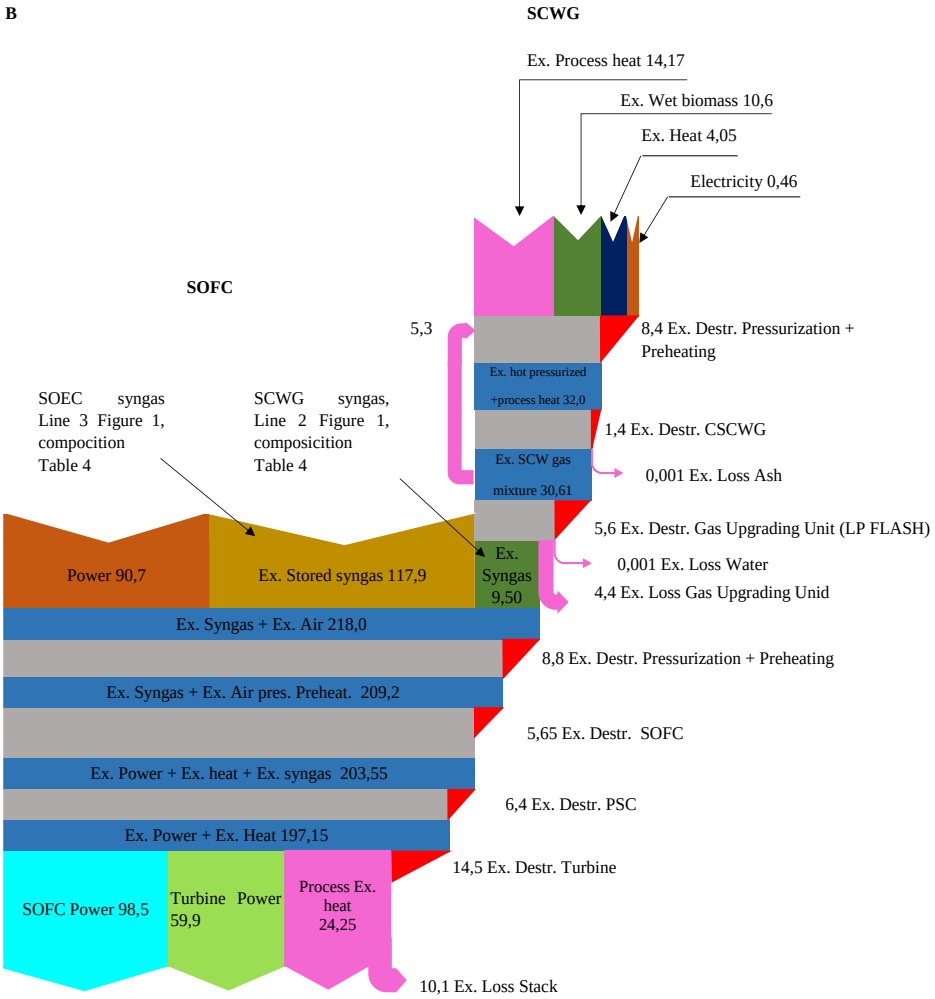

Figure 4.8. (continued).

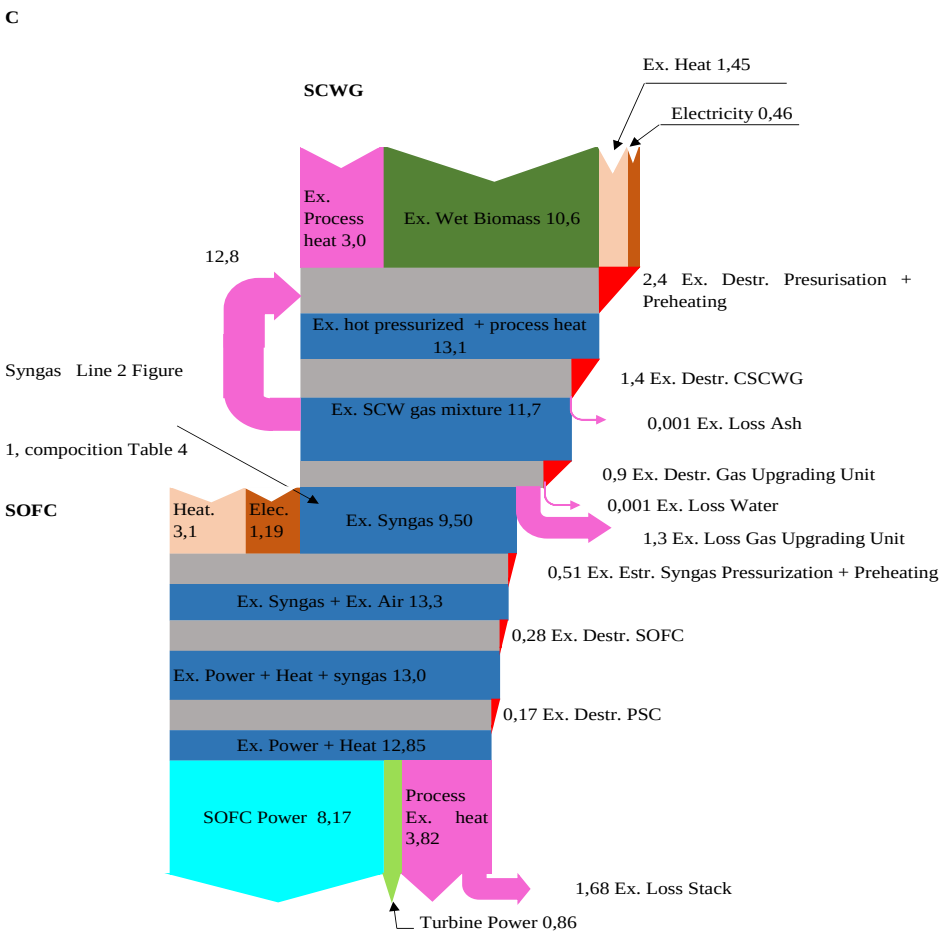

Figure 4.8. (continued).

Figure 4.8B shows an exergy flow diagram of the results of the performance analysis of the SCWG–rSOC operating in FC mode for power generation. In Figure 4.8B and Table 4.5, the SCWG–rSOC FC operation is at j = 3.4 A cm^{-2}, T = 680°C, P = 20 bar, biomass moisture content = 95 wt.%. The fuel used can either be: Part i) only syngas produced by SCWG (while system is running in FC mode), hereafter called "fresh syngas" Part ii) fresh syngas + stored syngas which was produced in rSOC in EC mode. This mixture is hereafter called "mixed syngas".

Table 4.5 summarizes the results of flow rates, gas composition, pressure, temperature of the gases labelled in Figure 4.1 as Line 2 and Line 3. Figure 4.8C and Table 4.5 shows the results of the analysis of power generation by the rSOC in FC mode fuelled exclusively by fresh syngas (Lines 2 in Figure 4.1).

It can be seen from Figure 4.8B and Figure 4.8C, that the twelve times higher power is produced when the rSOC uses mixed syngas, when compared with using only fresh syngas. This is owing to the higher flow rate of the mixed syngas, as well as its higher calorific value. The rSOC fuelled by the mixed syngas has higher exergy losses and exergy destruction than the rSOC fuelled by fresh syngas. This is because the system fuelled by the mixed syngas is not configured for optimal utilisation of the heat produced in the rSOC and PSC. Therefore, improving the heat integration can have a scope for significant reductions in the exergy losses and exergy destruction. The current density was derived considering the amount of produced heat to be distributed in the system to reach the minimum exergy loss and destruction in the exhaust and process units respectively.

4.5.5 Sensitivity analysis of SCWG–rSOC–FC operation

4.5.6 Effect of pressure and temperature and moisture content on the energy efficiency of the SCWG–rSOC–FC mode system

Figure 4.9A shows the influence of the operating pressure and temperature of the rSOC on the energy efficiency of the SCWG–rSOC system in FC mode, at biomass moisture contents of 80 and 95 wt.%, with current densities of 0.47 and 1.5 $A \cdot cm^{-2}$, respectively. The feed to the rSOC consists of the "mixed syngas".

At a high biomass moisture content (95 wt.%) the gasifier was endothermic because the high moisture content favours the production of H_2, which is an endothermic reaction. The energy consumed by the gasifier under this condition was approximately 2 kW. However, at a moisture content of 80 wt.%, the gasifier was exothermic and generated 0.453 kW of heat since low moisture promotes the exothermic methanation reaction. Additionally, the energy required by the gasifier preheater to take the biomass to the reaction temperature was exceptionally high at 95 wt.% moisture, due to high flow rates.

High operation pressures increased the rSOC power output due to the higher Nernst voltage. The external heat demand for the preheating of air and fuel decreased because of the increase in gas temperatures caused by the air and fuel compressors, respectively. However, the adverse effects of increased compressor power requirements overrode both these benefits, and the overall system efficiency decreased.

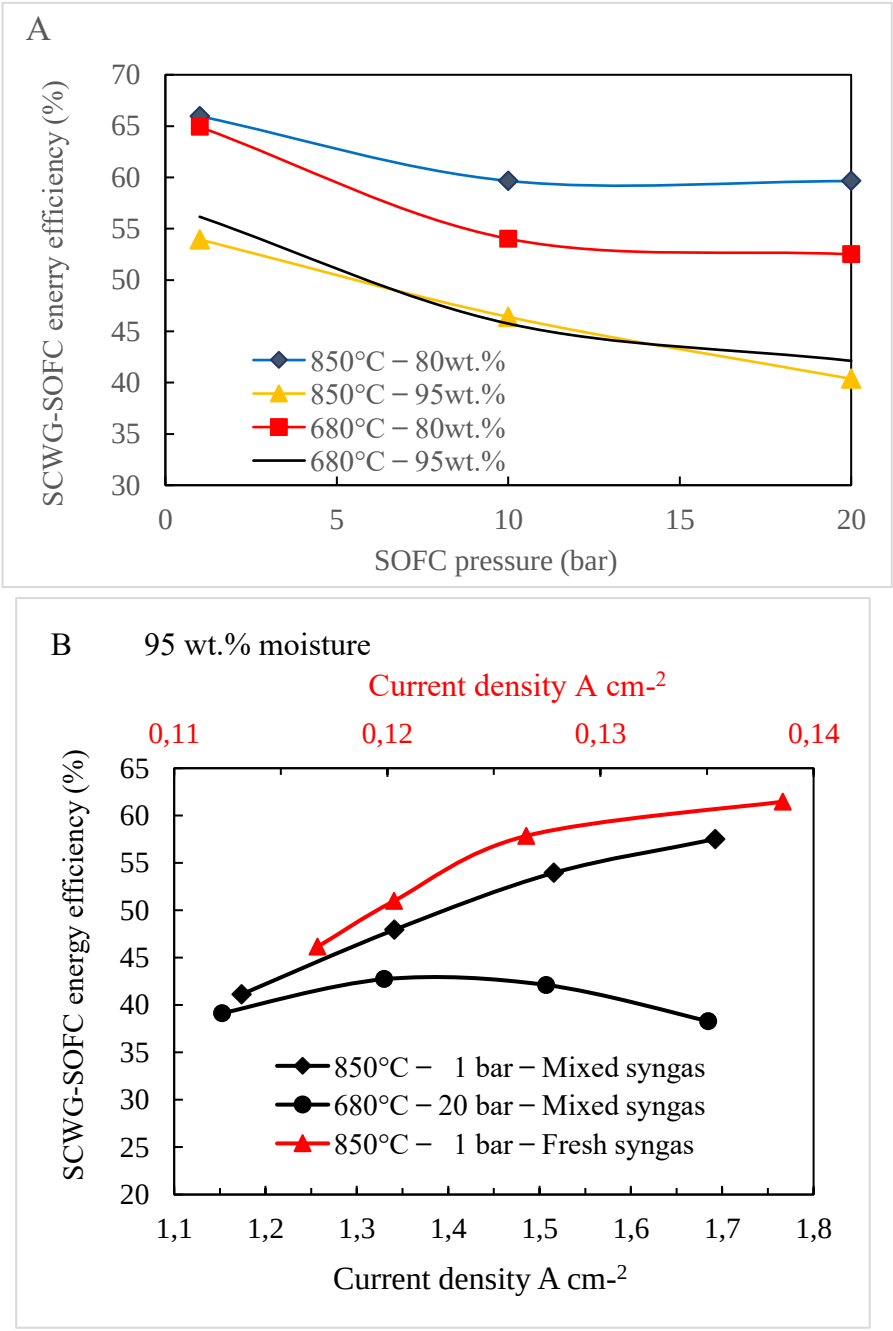

Figure 4.9. A) Effect of SOFC pressure and temperature on the SCWG–rSOC–FC mode system's efficiency. B) Effect of current density on the SCWG–rSOC–FC mode efficiency at different pressures, temperatures, and fuel flow rates (SCWG–stored syngas, and SCWG syngas) at 80 wt.% and C) 95 wt.% biomass moisture content.

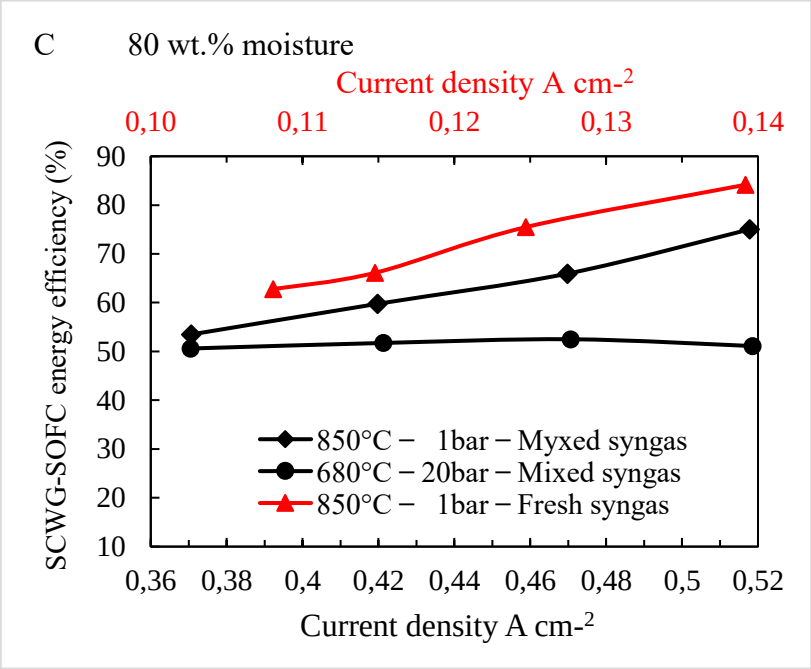

Figure 4.9. (continued).

The reduction in efficiency with increasing stack pressure was more severe at 95 wt.% moisture content than at 80 wt.% because, at 95 wt.%, the air compressor required more power to remove excess heat from the rSOC. This was the result of greater heat generation in the stack at 95 wt.% due to the higher fuel consumption rate. Indeed, at 95 wt.%, the syngas molar flow rate was almost five times that at 80 wt.% (0.48 kmol·s^{-1} compared to 0.1 kmol·s^{-1}) because as mentioned before, the mass flows are higher at higher biomass moisture levels. The higher fuel consumption also required a higher current density (0.47 A·cm^{-2} at 80 wt.% and 1.5 A·cm^{-2} at 95 wt.%) that increased the overpotentials, further contributing to greater heat generation in the rSOC at higher biomass moisture contents.

At 80 wt.%, the reduction in efficiency with increased pressure was less severe at 850°C than at 680°C because a high temperature favours the endothermic reformation of methane in the rSOC, reducing the heat generation and thus requiring lower cooling airflow. At a lower airflow, the increase in compressor power with pressure was less severe, and so was the decrease in efficiency. At 680°C, however, the opposite effect was observed: low temperature and high–pressure favour exothermic methanation, which increased

Table 4.6. Key data – SCWG–rSOC performance

Parameter	Unit	SCWG–rSOC–FC	SCWG–rSOC–EL	SCWG–SOFC	SCWG–rSOC–FC	SCWG–rSOC–EL	SCWG–SOFC
Reactant		Mix syngas	Gas mixture	Fresh syngas	Mix syngas	Gas mixture	Fresh syngas
SOC operating pressure	bar	1			20		
SOC operating temperature	°C	850			680		
rSOC ASR	Ω.cm^{-2}	0.11			0.16		
SCWG Exergy efficiency	%	76.4	69	68.9	32.4	78.1	61.4
Individual mode simulations							
Current density	A cm^{-2}	1.5	3.4	0.13	1.5	3.4	0.14
Stack active area	cm^{-2}	60000	26250	60000	60000	26250	60000
Turbine net power production	kW				56	9.6	
SOFC net power production (AC)	kW	80.42		6.8	64		7.76
SOFC net power production (DC)	kW	84.65		7.2	68		8.17
SOEC fuel production (on HHV)	kW		147			145	
SOEC fuel production (on LHV)	kW		124			124	
System efficiency (on HHV)	%	56.4	87	57.8	42	89	21.0
System efficiency (on LHV)	%	65.9	73	62.6	46	77	22.7
System exergy efficiency	%	61.6	70	52.3	49	73	48.8
Exergy efficiency rSOC–FC/EL	%	59.4	77.9	68.5	72.6	74.5	70
System with same area in both modes							
Current density	A cm^{-2}	2.7			2.7		
Stack active area	cm^{-2}	33750			33750		
Energy efficiency of the system	%	44.9	88.56		31.1	88.4	

the heat generation in the stack. Thus, the compressor power required to drive the cooling air increased more sharply with pressure at a temperature of 680°C, and the accompanying decrease in efficiency was more severe. However, at 95 wt.%, the curves in Figure 4.9B for 680°C and 850°C are very close because the methane reforming or methanation reactions are negligible at higher moisture contents, and therefore the effects described at 80 wt.% are not apparent at 95 wt.%.

The maximum efficiency of the SCWG–rSOC system in FC mode was found to be 66% at the following conditions:

rSOC pressure of 1 bar
moisture content of 80 wt.%
rSOC temperature of 850°C

At 95 wt.% and 1 bar, the efficiency decreased to 56% at 680°C and 54% at 850°C.

4.5.7 Effect of current density on the efficiency of the SCWG–rSOC system in FC mode

Figure 4.9B and Figure 4.9C illustrate the effect of current density (j) on the SCWG–rSOC system energy efficiency in FC mode at 95 and 80 wt.% biomass moistures, respectively, at varying rSOC operating pressures and temperatures. Two different situations were evaluated for the rSOC in FC mode: a) fresh syngas as fuel, and b) mixed syngas as fuel. While the current density was varied, the fuel flowrate and the stack area were constant. Therefore, fuel utilisation factor also increased proportionally with current density. However, due to the different flow rates of fresh and mixed syngas, the achievable current densities for those two cases was very different. In order to make a proper comparison between the trends in the same figure, the X–axes of Figures 4.9B and 4.9C use the current density between the minimum and maximum current densities for each case in the figure.

At 95 wt.% biomass moisture, and rSOC pressure of 1 bar, and rSOC temperature of 850°C, the power generated by the rSOC fed by fresh syngas was 7.2 kW. However, the rSOC power increased to 86.25 kW when the mixed syngas was fed to the rSOC. This was due to the higher flow rate and calorific value of the mixed syngas.

At a higher temperature (850°C) and lower pressure (1 bar), the system efficiency monotonically increased with increasing *j*. At higher *j* values, a greater portion of the fuel was consumed in the stack. Therefore, stack power output increased, while the PSC had to burn less fuel. Lower fuel combustion in the PSC led to smaller combustion losses and lower exhaust gas temperatures. Lower exhaust gas temperatures, in turn, led to a lower fuel temperature at the HE1/HE2 outlets (in Figure 4.2B). Therefore, HE3 recovered more heat from the gasifier outlet, and less heat was lost in the gas/liquid separator (LPFLASH). The lower exhaust gas temperatures also led to more efficient heat transfer with the incoming air and fuel due to the smaller temperature differences in the heat exchangers (HE1/HE2/HE4). All these factors led to higher efficiency at higher *j* values. On the other hand, at lower *j* values, the PSC had to combust more fuel and additional air was supplied to limit the gas temperature to less than 1000°C. The additional heat generated in the PSC was lost to the environment via exhaust gas and LPFLASH, leading to lower efficiency.

At 95 wt.% moisture, the current density was only between 0.12 and 0.14 $A \cdot cm^{-2}$ when fresh syngas was used. The maximum system efficiency is not reached at 850°C and 1 bar at current density < 0.14 $A \cdot cm^{-2}$, contrary to at 680°C and 20 bar. By contrast, the current density varied between 1.2 and 1.7 $A \cdot cm^{-2}$ when mixed syngas was used. Therefore, more heat was generated in the rSOC with mixed syngas due to the higher fuel consumption and higher overpotentials. This excess heat was lost through the air exhaust and the liquid/gas separator.

However, at a lower temperature (680°C) and higher pressure (20 bar), the system efficiency reached its maximum at $j \approx 1.5$ $A \cdot cm^{-2}$ and then decreased with further increase in *j*. At $j < 1.5$ $A \cdot cm^{-2}$, an increase in *j* improved efficiency for the same reasons stated in the previous paragraphs. But at $j < 1.5$ $A \cdot cm^{-2}$, the rSOC became highly exothermic owing to the higher fuel consumption and current overpotentials. Therefore, the required cooling airflow and air compressor power grew very large, reducing the efficiency despite the other benefits mentioned above. The maximum system efficiency depend on the fuel utilization and thus the current density [236].

The trends for lower biomass moisture content (80 wt.%), Figures 4.6C, were similar to those for higher biomass moisture content as discussed above, but the efficiencies were higher at lower moisture contents. This occurred for several reasons:

The syngas flow rate was lower at lower moisture contents, leading to decreased heat generation in the rSOC and smaller heat losses to the environment, as mentioned above;

The lower moisture and the accompanying lower biomass flow rate meant that the gasifier required less external heat for preheating and for driving the reactions in the gasifier.

The higher content of CH_4 in the flow promotes endothermic side reaction such as CH_4 reforming, thus reducing the energy utilized for heat removal by the air compressor.

These effects resulted in a higher efficiency at a lower biomass moisture content.

4.6 Sensitivity analysis of SCWG–rSOC EL operation

4.6.1 Effect of rSOC pressure and temperature on the efficiency of the SCWG–rSOC system

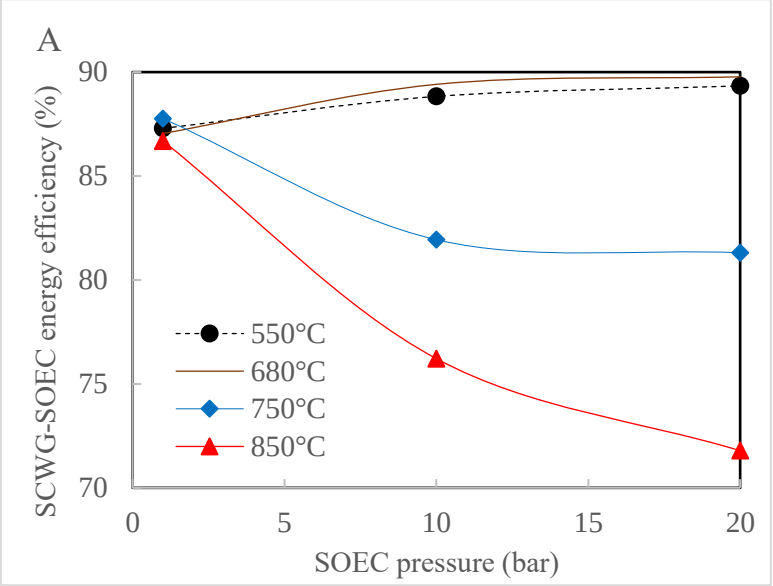

Figure 4.10. A) Effect of rSOC operating pressure and temperature on the SCWG–SOEC energy efficiency at 95 wt.% biomass moisture content. B) Effect of the current density on the SCWG–SOEC system energy efficiency at 680°C and 20 bar. C) A comparison of the effect of current density on both operating modes

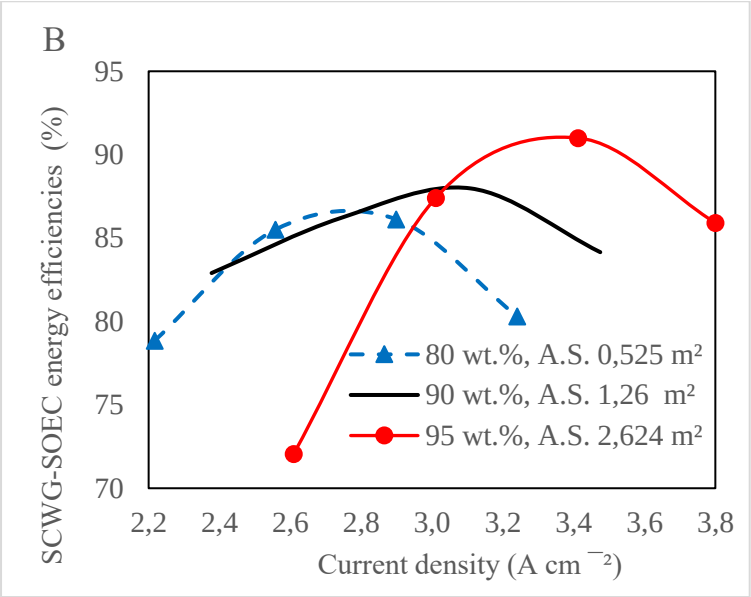

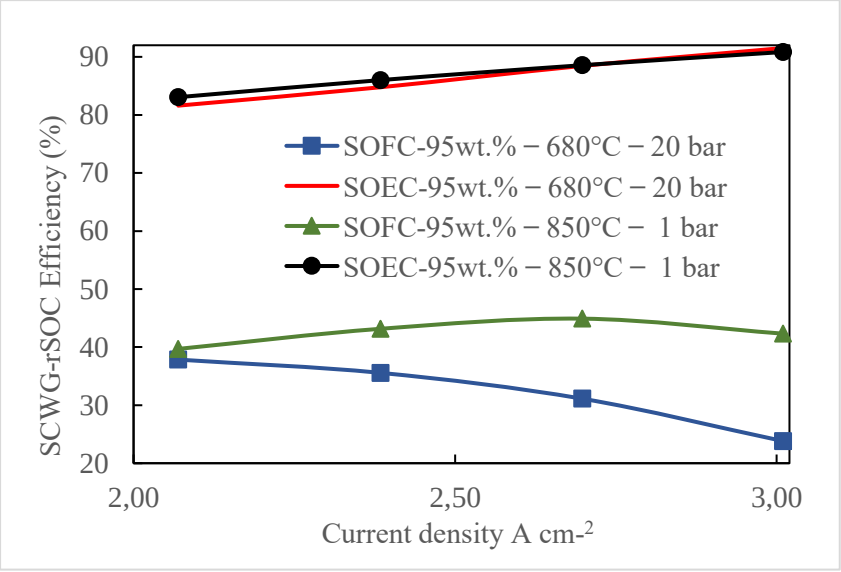

Figure 4.10. (continue).

Figure 4.10A illustrates the influence of the operating pressure and temperature of the rSOC on the SCWG–rSOC system in EL mode at 95 wt.% biomass moisture content.

At rSOC temperature of 680°C, the rSOC was exothermic; therefore, the cooling airflow was relatively small. In this situation, increasing the rSOC

pressure improved the system efficiency, from 87% at 1 bar, to 90% at 20 bar. At higher pressures, there was a significant increase in the temperature of fuel and air in the compressors. This greatly reduced the external heat demand for preheating. Further, higher pressure increased the rSOC voltage (due to increase in the Nernst voltage), making the stack more exothermic. This heat was used to preheat the air and fuel, further decreasing the external heat requirement. The stack power and air compressor power also increased at higher pressure, but the decrease in external heat requirement was more significant, increasing the overall system efficiency at higher pressures. The efficiency slightly increases after 13 bar, then stabilizes at 20 bar, obtaining the highest efficiency of 90%. Therefore, the calculation was made at 20 bar in the subsequent results. The system could also work optimally at pressures between 13 and 14 bar to reduce engineering limitations for practical application in future research

At rSOC temperature of 750°C, the rSOC was endothermic. The air flow required to provide this heat was also high. Therefore, the air compression power increased sharply as the pressure was increased. The stack power also increased at higher pressure, due to the increased Nernst voltage. Due to the high temperature and endothermic nature of the stack, a large amount of external heat was required to preheat the air and fuel. This heat demand decreased at higher pressures, just as mentioned before, but the increase in stack power and air compressor power were much more significant in this case, due to the higher air flow rate. Therefore, the system efficiency greatly decreased with increased pressure, from 88% at 1 bar to 81% at 20 bar.

At rSOC temperature of 850°C, the rSOC is more endothermic than at 750°C, and therefore the airflow required to heat the stack is much higher. Therefore, the decrease in efficiency with pressure is much sharper at 850°C due to the greater influence of air compressor power. Similarly, at 550°C, the rSOC is more exothermic than at 680°C and the cooling airflow is higher than at 680°C. Therefore, the improvement in efficiency with increased pressure is lower at 550°C, due to the greater influence of air compressor power.

In all these cases, higher pressure increases the exothermic methanation in the stack. However, because the biomass has 95% moisture, the amount of methanation is small, and these changes are not very significant compared to the other changes in BoP power and heat demand.

Notably, the thermal efficiency of biofuel production by SCWG–rSOC achieved with this approach overcomes the previously determined production efficiency limit of 45% for thermochemical biomass gasification plus steam electrolysis and of 30% for solar–electrochemical hydrogen [73], [237].

4.6.2 Effect of current density on the efficiency of the SCWG–rSOC system in EL mode

Figure 4.10B shows the variation of system energy efficiency with rSOC current density, for different biomass moisture contents. At each level of moisture, the flow rates of biomass had significant variations. This was because the dry biomass flow was held constant at 0.56 g/s, while the water flow rate (as part of the wet biomass) was changed as needed, from 2.24 g/s at 80 wt.% to 10.64 g/s at 95 wt.%. Because of this, if the rSOC active area would be held constant, then the current densities would vary too far away from the optimum efficiency values. Therefore, a different rSOC area had to be considered for each moisture level, to avoid excessively low or high current densities, thus maximising efficiencies. At 95 wt.%, this area was 2.624 m^2, and at 80 wt.%, it was 0.525 m^2.

At a 95 wt.% moisture content, the optimal current density was 3.4 A cm^{-2}, at which value the system reached a maximum energy efficiency of 91%. When the SOEC was operated at a lower moisture content, i.e., 80 wt.%, the maximum energy efficiency decreased to 86%, achieved at 2.9 A cm^{-2}. To electrochemically reduce H_2O at 95 wt.% moisture content, the rSOC required a higher current density and heat than at a lower moisture content owing to the larger flow rate. Maximum system efficiency was reached at a cell voltage (1.32 V) slightly greater than the thermoneutral voltage (approx. 1.26 V). The increased current density makes the rSOC system exothermic, which favours the highest system efficiency due to the use of this generated heat to meet the air and fuel preheating demand.

At a higher moisture content, the concentration of syngas produced in the SCWG was 5% of the gaseous mixture, which contained H_2, CH_4, CO, and CO_2, promoting the exothermic methanation reaction to some extent. However, at a lower moisture content, i.e., 80 wt.%, the mixture processed by the rSOC contained a larger proportion of syngas, which constituted approximately 20% of the gaseous mixture. This increased methanation, leading to additional heat generation, making the stack highly exothermic. This additional generated heat

provided for the heat requirements of the system. However, the power required to compress more air to remove the heat under exothermic operation had a greater negative effect on the system efficiency. Therefore, the peak efficiency at 80 wt.% moisture content was lower than at 95 wt.%.

The airflow rate and air inlet temperature (oxygen electrode) can be changed to extract or provide heat to the stack. The heat from the rSOC air electrode exhaust provided the heat for air and fuel preheating, as well as for the SCWG. The heat available from the stack was 4.7 kW at 95 wt.% moisture, and 1.5 kW at 80 wt.%. The power supplied to the compressor at 95 wt.% was 19% of the total power input, whereas it was 37% at 80 wt.%. The turbines recovered a significant amount of waste heat in the form of electricity, to the tune of 7.4 kW and 2.6 kW, at 95 wt.% and 80 wt.%, respectively. At the thermoneutral voltage, the least power was required to drive the compressor, but the external heat required by the system BoP to preheat the air and fuel was high, which reduced the efficiency. On the other hand, at the optimum voltage (slightly above thermoneutral voltage), the compressor power was higher, but the external heat requirements were very low, thus maximising the efficiency.

Any increase in the current density from the optimal value made the rSOC highly exothermic, causing it to generate excess heat that was removed by the airstream. This in turn increased the power required to drive the air compressor, and consequently reduced the system efficiency. However, at a current density lower than optimum, the rSOC exhibited endothermic behaviour. The airstream supplemented the heat demand of the system by increasing the inlet air flow rate and inlet temperature. Thus, the external heat provided the heat requirements of the electrolyser through the airflow, and the air compressor consumed more power, reducing the system efficiency.

4.6.3 The efficiency of the SCWG–rSOC system

Figure 4.10C shows the system efficiencies of the SCWG–rSOC system at 95 wt.% biomass moisture content as a function of the current density *j* of the rSOC, in both modes. The system efficiency in FC mode was higher at lower current densities, whereas the system efficiency in EL mode was higher at higher current densities. The rSOC can operate at different current densities in both modes [238].

The operation of the reversible system with an active area of 3.375 m^2 in a similar current density range (2–3 $A \cdot cm^{-2}$) in both modes. The rSOC in FC mode,

operating at high current densities saw an increment in the generated heat, reducing the efficiency. In EL mode, within the range under consideration, the efficiency increases with current density due to operation moving closer to thermoneutral point. The FC mode efficiency was around 40–45% whereas the EL mode efficiency was around 80–90%. The efficiency of biomass gasification and reversible solid–oxide cell stack reaches 50%–60% for power generation, 72%–76% for power storage mode is presented in the findings of [239].

4.6.4 Exergy destruction in the SCWG–rSOC system

Figure 4.11A illustrates the contribution of each process unit to the total exergy destruction of the SCWG–rSOC system in EL mode, for different biomass moisture contents at the highest system efficiencies from Figure 4.10B. The total exergy destruction increased with the biomass moisture content because of the increased exergy available. The most significant contributions to exergy destruction were from the rSOC, turbines, and preheating for rSOC reactants. The SCWG, preheating for SCWG reactants, and SEP exhibited lower exergy destruction rates. The exergy destruction due to chemical reactions was the largest component of exergy destruction in the rSOC–EL mode, increasing from 0.22 kW at 80 wt.% to 0.35 kW at 95 wt.%. A high biomass moisture content facilitated more chemical and electrochemical reactions in the rSOC owing to the higher water content, which led to a greater exergy destruction. The exergy destruction in preheating of rSOC reactants was caused by the significant temperature differences between the streams in the heat exchangers, considering that air and biomass entered the system at ambient pressure and temperature, and the hot streams had a temperature as high as 680°C. Exploring more efficient energy recovery pathways could therefore represent a promising topic for future studies. The exergy destruction of the SEP and SCWG reduced with moisture is remarkable. High water content determines gasification [205], [206].

Figure 4.11B describes the exergy destruction in each process unit of the SCWG–rSOC system in reversible operation at various operating conditions. At 680°C and 20 bar, the exergy efficiencies were 49% and 73% in the FC and EL mode, respectively. Variations in the operating pressure and temperature of the rSOC influenced the heat and power required by the system. The air and fuel preheating in the rSOC exhibited higher exergy destruction because of high temperature differences in the heat exchanger units. At a lower temperature and high pressure, the pressurised air and fuel required less process heat for preheating. Thus, the exergy destruction in heat exchangers was reduced.

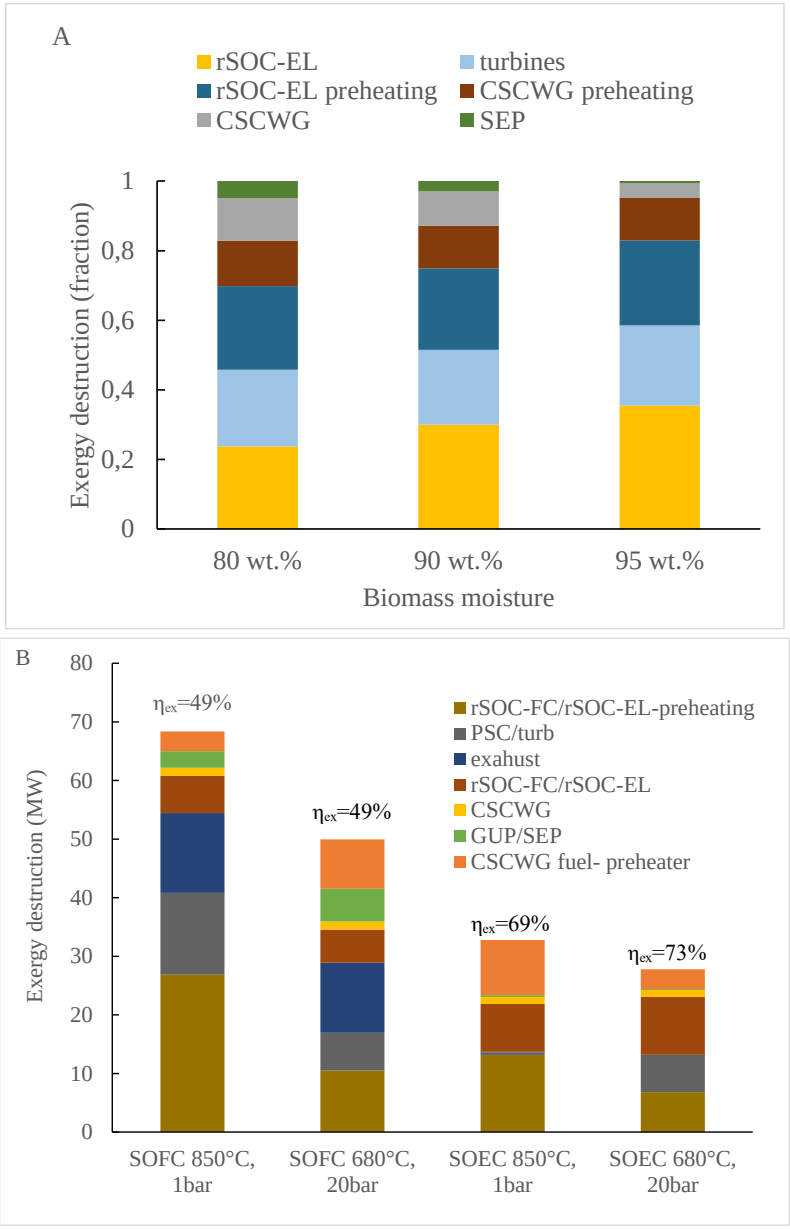

Figure 4.11. Contribution of process unit exergy destruction to the total exergy destruction. A) rSOC operation in EL mode as a function of biomass moisture content at 20 bar, 680°C, j = 2.9, 3.1 and 3.4 A cm^{-2} at 80, 90 and 95 wt.% moisture contents. B) FC and EL mode operation, biomass moisture content = 95 wt.%, 20 bar, 680°C, FC j = 1.5 A cm^{-2}, EL j = 3.4 A cm^{-2} and 1 bar, 850°C, FC j = 1.5 A cm^{-2}, EL j = 3.4 A cm^{-2} .

The exergy destruction in SEP is almost negligible due to the small fraction of separated water, unlike in GUP. Table 6 reports the key data describing the system performance.

4.7 Conclusions and Future Outlook

This study investigated a process design for a combined SCWG-rSOC system, which can attain high efficiencies in energy conversion and has a high capacity for hydrogen production. By doing so, three needs have been met effectively: sustainable sanitation, biofuel and power generation from waste, and renewable energy storage. As a standalone unit, SCWG using high moisture biomass produces syngas with high steam and CO_2 content. This system overcomes this limitation by converting the steam and CO_2 into more syngas. The integration of SCWG and rSOC technology represents a new approach that – together with improvements in materials, residence time, and stable catalysts at a competitive price – will help commercialise SCWG-rSOC technology.

The SCWG–rSOC system exhibited high performance at a biomass moisture content of 95 wt.%. At rSOC operating conditions of 680 °C and 20 bar, syngas production with the system in EL mode achieved energy and exergy efficiencies of 89% and 73%, respectively. The use of an rSOC (in EL mode) increased the yield of syngas by approximately thirteen times compared to that produced exclusively by the SCWG. The SCWG syngas production exergy efficiency reported in the literature at biomass moisture > 90 wt.% is around 20%. The total exergy destruction of the SCWG-EL mode is comprised of the following parts: exergy destruction in the electrolyser, heat exchange process, and turbines. The exergy destruction of gas/liquid separator is negligible. SOEC operation at high pressure and lower temperature result in lower total exergy destruction. Higher feedstock moisture increases the exergy destruction, but the utilisable exergy increases. The system efficiency reached a maximum of 91 % at a current density of 3.4 A cm^{-2}.

The high-quality syngas produced in EL mode was stored in a tank and then used in FC mode along with freshly produced syngas from the SCWG. This increased the power output in the FC mode by a factor of twelve, compared to the use of syngas produced solely by the SCWG. The system in FC mode achieved energy and exergy efficiencies of only 42% and 49%, respectively.

However, the proposed SCWG–rSOC energy storage system is currently subject to limitations that may prevent its use for large-scale power generation. First, in the rSOC field, a new system configuration for the SCWG–rSOC must be identified to reduce the mentioned exergy destruction and losses. Second, since the presence of CH_4 has a significant influence on the thermal behaviour of the rSOC, it is necessary to gain a better understanding of the chemical and electrochemical behaviour of CH_4 under fuel utilisation to improve the SCWG–rSOC performance.

The proposed technology has been shown to efficiently generate fuel or power. Manure, sewage, industrial waste, agriculture waste, or algae, can be used to feed the proposed system. As the increasing global population requires high quality water and air to ensure the health of all living species, increased efforts to develop sustainable methods for energy generation and sanitation provision are urgently required over the next decade(s); the proposed SCWG–rSOC system is a step in this direction.

5

Conclusion and Recommendation

The contributions of this study are as follows:

- A wastewater gasifier–SOFC system is a thermodynamically attractive method for highly efficient power generation from wastewater treatment.
- The parametric analysis of the SCWG–SOFC system shows that process streams have a high potential for integration with other processes at specific operational parameters, such as biomass moisture, SCWG operating temperature, and SOFC fuel utilisation.
- An SCWG–rSOC is a potential method for high–capacity and highly efficient H_2 production in an SCWG–rSOC–electrolysis mode. High–power generation in the SCWG–rSOC–fuel cell mode is also possible. This finding may contribute to reducing the operating costs of SCWG for H_2 production.

This dissertation provides three alternatives for wastewater treatment concepts that operate with sewage, a dry biomass flow rate of 0.56 kg s–1, and an MC of 75 to 95 wt.%. The technical attractiveness of a gasifier depends on achieving almost 100% CCE with no tar or char generation. The gasifier–SOC system must achieve minimum losses and exergy destruction, reaching high efficiencies. Table 5.1 shows the key parameters, characteristics, and operating conditions of the proposed wastewater treatment system.

1) A dry–gasifier–SOFC system concept: The system reached the highest efficiency of 65.3% with a biomass MC of 75 wt.%. The power production was approximately 6.4 kW. This system ensured almost complete conversion of the biomass into a gaseous product with no tar or char production using an indirectly heated two–stage gasifier. The influence of the high MC of biomass on system efficiency is low. The high efficiency achieved in this configuration depends on the high recovery of process heat. This configuration requires numerous heat exchangers, increasing its complexity and exergy destruction.
2) SCWG–SOFC system: A combination of operating conditions with biomass moisture content > 90 wt.% and temperature ≥ 500°C ensures almost complete conversion of wet biomass into a gas product in the SCWG. The system reached an efficiency within the range of approximately 50–60% under these conditions. The generated power is approximately 8 kW. The performance of the system can be improved by the heat integration of the process streams.

3) The SCWG–rSOC system: Ensuring complete conversion of biomass into a gaseous product at an extremely high MC of > 90 wt.% and temperature ≥ 500°C, the SCWG –rSOC–EL mode generates thirteen times more syngas than in the SCWG in an SCWG–SOFC system with an efficiency of > 90%. The SCWG–rSOC–FC mode produced 12 times more power than the SCWG–SOFC system, approximately 99 kW, with efficiency within the range of approximately 40–55%. This configuration requires reversible operation of the SOC for high–capacity power production, increasing complexity. This system is more promising than previous concepts because its high fuel and power production capacity is expected to reduce the operating costs.

Table 5.1. Key parameters, characteristics, and operating conditions of the proposed wastewater treatment system.

Concept	SOC Temp. °C	SOC Press. bar	Gasif. Temp. °C	Gasif. Press. bar	CGE	Biomass moist. wt.%	SOFC Uf	Power kW	Elec. LHV Ef.%	Syngas and elect. LHV Ef.%
Dry–Gasifier–SOFC			1100	Atm.	100	75	0.84	6.7	65.3	
	900	1.013	950	Atm.	100	85	0.84	6.4	63	
						90	0.84	6.1	60	
SCWG–SOFC	850	1.013	600	250	48	85	0.95	3.6	40	
					100	85	0.95	7.6	60	
					100	95	0.95	7.8	14	
SCWG–rSOC–FC	680	20	500	250	100	95	0.85	98	50	
SCWG–rSOC–EL	680	20	500	250	100	95	0.95	Syngas 121.6 Power 10.2		77

The following findings are drawn regarding these contributions:

Chapter 2 presents a conceptual design of a wastewater dry sludge - gasifier integrated with a SOFC, and the results are presented in Table 5.1. The system achieves high performance by increasing the yield of H_2 production in the gasifier and replacing external energy in the gasifier and dryer for process heat and electricity. This is achieved by integrating several process units, including an indirectly heated two–stage gasifier (PZR and PG stages), resulting in negligible tar production [102] and a simpler gas cleaning process. High H_2 yield was achieved by steam gasification during the plasma gasifier (PG) stage, which was appropriate for SOFC applications. Depleted gas from the cathode added to the PG partially oxidised the pyrolysis products, releasing heat. A two–stage SOFC generated power from clean syngas, and its intercooler provided heat to the pyrolysis reactor (PZR). Thus, the PG used less electrical energy to create plasma flames. The provision of heat from the SOFC to the PZR lowered the plasma torch power from 2.7 kW presented in the work of Liu et al. [69] to 0.27 kW in the present study (same biomass input flow rate). Water vapour released in the PZR reactor provided the steam required for reforming the PZR products in the PG. The electrical efficiency of the combined system was high at low steam to biomass ratio (SBR) values. The PZR is a critical component that defines syngas yield and electrical efficiency. The proposed gasifier increased the H_2 concentration from 40 vol.% to 60 vol.% presented in previous work for plasma gasification [69].

Removing a substantial amount of water from sewage with the superheated steam dryer unit contributes to the highest gasifier performance. The superheated steam dryer reused the heat released from the condensation of the pressurised water vapour. The MST operated the steam compressor. The system achieved its highest electrical efficiency of 66.5% with an initial biomass MC of 60 wt.% and 60% efficienty at 92 wt.% biomass moisture, more power to drive the compressor was required with higher moisture.

The operating conditions, such as temperature and fuel utilisation, of the SOFC determine power generation and heat production. The heat is used for fuel and air preheating. The variation in fuel utilisation influences fuel combustion in the PSC. The airflow rate for the SOFC cooling requirements increased with fuel utilisation. Thus, an optimal SOFC inlet temperature and fuel utilisation were obtained. The plant produced power and sufficient heat for air and fuel

preheating. The SOFC derived 85% of the power production, and the MST produced 15%. High exergy destruction was generated in the gasifier, SOFC, PSC, air, and fuel preheating owing to heat transfer in the heat exchangers. The significant temperature difference between streams caused considerable exergy destruction.

Thus far, no study on highly efficient, > 50%, power generation from biomass with MC higher than 75 wt.% has been reported. The highest system energy efficiency, 61%, that has been reported in the literature is a biomass MC of 50 wt.%, and the tar is catalytically cracked [75]. The previously reported gasifier – SOFC efficiency from the work of Ming Liu et al. [69] [70]. is < 10%, with a biomass MC higher than 75%.

Chapter 3 discussed power generation using SCWG combined with SOFCs. The primary design parameters of the combined system that affected efficiency were the SCWG catalyst, residence time, SCWG operating temperature, feedstock concentration, CCE, and SOFC fuel utilisation. The parametric analysis results indicated that the formation of H_2 predominates over CH_4 at high temperatures and MCs > 90 wt.%. High production of H_2 in the gasifier reduced the heat requirements of the SOFC for an endothermic CH_4 internal reforming reaction. Thus, the SOFC generated sufficient heat for air and fuel preheating.

The feedstock concentration and temperature significantly influenced CCE. Almost complete gasification was achieved only with a dry biomass concentration lower than 5 wt.%, temperature higher than 500°C, and long residence time [166]. These operating conditions required high heat requirements to heat the aqueous feedstock to supercritical water conditions and represented a challenge in the field of engineering and construction materials. In addition, a low yield of H_2 is not economically competitive. For industrial applications, the H_2 yield of SCWG of sewage sludge was obtained only with a biomass concentration higher than 15 wt.% [161]. The combination of high moisture and high temperature reduces the efficiency of the system. This study obtained a system efficiency of 14% at 95 wt.%, 600°C, and Uf 0.85. The system was not self–sustainable at operating temperatures higher than 650°C and 95 wt.% biomass moisture. However, despite its low efficiency, achieving complete biomass conversion at a moisture of 95 wt.% was advantageous. A gaseous product rich

in H_2O under SCW conditions was valuable. This process can be integrated into a bottoming cycle to recover the thermomechanical energy of the product gas.

Because of operation at a temperature lower than 500°C and dry–biomass concentration higher than 10 wt.%, expected in a real gasifier, complete conversion could not easily be achieved. This implies a demanding gas–cleaning unit and reduced efficiency. The net electrical efficiency varied from 29% to 40% at Uf 0.65–0.95 of the SCWG–SOFC at CCE of 48% according to available experiments, dry biomass content 15 wt.%, 600°C, and 25 MPa. Contrarily, assuming complete conversion, the efficiency reached 44% to 65%. The highest net electrical and exergy efficiencies of the SCWG–SOFC were 72% and 59%, respectively, at 80 wt.% moisture, Uf 0.95 (though achieving such a high fuel utilization might need significant research efforts and radically new cell designs). A lower MC resulted in excess thermomechanical exergy available in the system for use in bottoming cycles. This could be a route to improve the efficiency of the system.

The net electrical efficiency of the system was maximised at a high Uf and low biomass MC. A high Uf generated additional power and heat in the SOFC, and the generated heat efficiently preheated the air and fuel inlet streams. A high Uf reduced the mass fuel rate fed to the PSC and thus the mass flow rate of exhaust gases that preheated the feedstock entering SCWG, leading to low exergy destruction because of the reduction in the temperature difference between streams.

The energy and exergy efficiencies of the combined system significantly depended on the highest heat recovery from the product gas generated in SCWG. However, it also accounts for the highest exergy destruction because the fuel and air preheaters recovered the process heat using heat exchangers. Employing suitable catalysts and increasing the residence time and material quality were potential routes to improve the performance of SCWG. However, combining operational parameters such as the biomass MC, SCWG operating temperature, and SOFC fuel utilisation generated a process stream with high thermochemical energy appropriate for integration with other processes.

Chapter 4 the SCWG–rSOC system is a new concept that reduces operating costs by significantly increasing system capacity for H_2 and power production. The system operates intermittently in EL and FC modes. According to the parametric analysis in Section 3, the SCWG feed with feedstock at high moisture > 95wt.%

reaches almost complete biomass conversion into syngas, preventing the costly gas cleaning process and producing syngas with high steam and CO_2 content. The gas cleaning unit previously separated salts at T > 374°C and pressure > 221 bar. The SCWG–rSOC–EL mode recovered the thermochemical energy of syngas. It converted steam and CO_2 in syngas by storing renewable electric power in syngas and holding it in a tank. The syngas yield increased approximately thirteen times compared with that produced exclusively by SCWG. The system reached an energy efficiency of 91% and an exergy efficiency of 73%. The exergy efficiency of SCWG syngas production reported in the literature for biomass moisture > 90 wt.% is approximately 20% [2]. The SCWG–rSOC–EL system is more efficient because the heat of water evaporation is recovered in the electrolyser, it is one of the more importance factors. On the contrary, in the concepts presented in Table 4.1, the heat of evaporation is lost in the liquid-gas flash separator. In addition, the biomass SCWG–rSOC–EL mode overcomes the determined production of H_2 with 30% efficiency for solar–electrochemical H_2 [237] and dry gasification plus steam electrolysis with 45% efficiency [73].

Owing to the reversible characteristics of the electrochemical process, the SCWG–rSOC–FC mode converted the stored syngas along with the freshly produced syngas from the SCWG into power. The system increased power production by a factor of twelve times compared with the use of syngas made solely by SCWG. The system achieved energy and exergy efficiencies of only 42% and 49%, respectively.

Rsoc EL operation

The efficiency of the SCWG–rSOC–EL mode system depended on the external power and heat supplied to the system and the efficient utilisation of the process heat. The generated process heat almost satisfied the heat required by fuel and air preheaters. The variation in operating conditions determined the efficiency of the SCWG–rSOC–EL mode. The system reached the highest efficiency of 91% at high operation pressure between 13 and 20 bar, a temperature of 680°C, 95 wt.% biomass MC, and a current density of 3.4 A cm^{-2}. The pressurisation of fuel and air increased their temperatures, significantly reducing the external heat demand for preheating, and reduced heat transfer exergy destruction. The rSOC–EL stack power and air compressor increased at high pressures. However, a decrease in the external heat requirements was significant. By gradually increasing the temperature from 680°C to 750°C and

then 850°C, the stack became endothermic, and the efficiency decreased because a considerable amount of external heat was required to preheat air and fuel. The air compressor power was increased because the airflow required to provide heat was also high. The stack power also increased at high temperatures.

The system reached its maximum efficiency at a cell voltage (1.32 V) slightly higher than the thermoneutral voltage (approximately 1.26 V). The increased current density rendered the rSOC system exothermic, favouring the highest system efficiency owing to the use of generated heat to meet the air and fuel preheating demands. At high moisture 95 wt.%, the CH_4 concentration on the syngas was low but somewhat promoted the exothermic methanation reaction. At a lower MC of 80 wt.%, the fraction of CH_4 on syngas was high, promoting an increased methanation reaction, leading to additional heat generation, rendering the stack highly exothermic. The additional heat generated satisfied the heat requirements of the system. However, the power required to compress air to remove heat under exothermic operation had a more significant adverse effect on the system efficiency, resulting in lower efficiency than that at 95 wt.%.

Any increase in the current density from the optimal value rendered the rSOC highly exothermic. In contrast, reducing the current from the optimal value rendered the rSOC endothermic. In both cases, the power of the air compressor was increased to remove excess heat or provide external heat through the airflow. The most significant contributions to exergy destruction were from the rSOC, turbines, and preheating of the rSOC reactants. The exergy destruction in the preheated rSOC reactants was caused by the considerable temperature differences between the streams in the heat exchangers. The exergy destruction in SEP was almost negligible owing to the small fraction of separated water. The HE recovered most of the sensible heat from the gasification product gas. Process integration rendered heat recovery feasible, and a simple system configuration reduced exergy destruction. Some energy was recovered as electricity using turbines, although they exhibited high exergy destruction. The exhaust gas emitted into the environment was at ambient temperature; therefore, exergy loss was negligible.

Rsoc FC operation

The SCWG–rSOC FC mode produced twelve times more power when the rSOC used mixed syngas (stored gas + SCWG fresh syngas) than when it used only SCWG fresh syngas. This was because of the higher flow rate of the mixed

syngas. At a 95 wt.% biomass moisture, rSOC of 1 bar, and T of 850°C, the power generated by the rSOC fed by fresh syngas was 7.2 kW. Mixed syngas increased to 86.25 kW.

High–pressure operation increased the temperatures of air and fuel, reducing the external demand for heat for preheating. However, the compressor power requirements were significantly high and the efficiency was reduced. The effect of CH_4 reactions on the SOFC anode was greater at a biomass moisture of 80 wt.% than at 95 wt.% because of the higher CH_4 concentration on the generated syngas. A high temperature of 850°C promoted the endothermic reformation of CH_4, reducing heat generation. High pressure and a low temperature of 680°C promoted methanation reaction, increasing the heat generation of the stack. The maximum efficiency was 66% at a pressure of 1 bar, temperature of 850°C, and Uf of 0.95, whereas at 95 wt.%, the efficiency decreased to 56%. The system efficiency increased monotonically with increasing current density. The stack consumed a significant portion of the fuel. Therefore, the stack power output increased, whereas the PSC burns less fuel. Lower fuel combustion in the PSC led to minor combustion losses and lower exhaust gas temperatures. Consequently, a lower exhaust gas temperature led to a lower fuel temperature at the HE outlet. The lower exhaust gas temperatures also led to efficient heat transfer with the incoming air and fuel owing to the minor temperature differences in the heat exchangers.

RECOMMENDATIONS

The dry–gasifier–SOFC and SCWG–rSOC integrated concepts for wastewater treatment achieved high energy and exergy efficiencies for power and syngas production. The wastewater dry–gasifier–SOFC system is a relatively new and unstudied concept. The configuration presented in this study is only one of many other possible system configurations. A new dry–gasifier–SOFC configuration using a high–temperature gas–cleaning unit can reduce exergy destruction by heat transfer and reduce the number of heat exchangers. Indirectly heated two–stage gasifiers require further investigation at the modelling and experimental levels to demonstrate the complete conversion of biomass into gas. However, the proposed system is complex. New heat recovery methods that simplify this process are desirable. The PZR zone of the two–stage gasifier requires further investigation in terms of variations in operating conditions, gasifying agents, and feedstock composition.

Although both concepts achieve high energy efficiency, heat recovery needs to be improved using new techniques because of the significant temperature difference between streams in fuel and air preheating using process heat is the primary source of exergy destruction in both systems. The system requires a heat exchanger network design for energy saving using pinch technology and the application of advancements in computational heat pipe arrangements.

The combustion of the residual combustible gas from the SOFC anode produces highly concentrated CO_2. It can be used for multiple applications, such as fast–growing biomass or the electrochemical conversion of CO_2 into syngas powered by renewable electrical energy. The highest efficiency is reached at the highest increase in SOC fuel utilisation in the rSOC–FC mode. Contrarily, lower fuel utilisation can extend the lifetime of the stack with no degradation of the anode. The trade–off between high system efficiency at high fuel utilisation and stack lifetime requires further analysis.

The SCWG–rSOC system requires the complete separation of contaminants from the SCWG gas product in a gas–cleaning unit under supercritical conditions to prevent the blowing of downstream equipment. Further investigation is necessary to understand the elemental behaviour of wastewater in supercritical water to effectively quantify the operating parameters for SCW reactors and reduce the number of solid residues to be further processed [240] in the rSOC.

The exergy efficiency of the SCWG–rSOC–EL mode, 69%, is significantly higher than that of the SCWG–rSOC–FC mode, 49%. The PSC, air and fuel preheating, and gas upgrading units are the processes with the highest exergy destruction. The high complexity of the system operating in the FC mode increases the exergy destruction and reduces the exergy efficiency. New methods for creating a simpler configuration will improve the efficiency of the SCWG–rSOFC–FC system.

This study demonstrated conceptually and thermodynamically that the efficient production of sustainable energy and the provision of sanitation services can be achieved simultaneously. Sewage gasification–solid oxide technologies show great potential as an efficient alternative method for power generation and efficient wastewater treatment. The social implementation of new hybrid energy–sanitation methods will contribute to effective worldwide energy distribution,

mitigate climate change, and enable an equitable service infrastructure that provides a clean environment to ensure the well–being of all creatures on Earth.

Appendix A

The ohmic overpotential occurs due to the electrolyte resistance to the ionic current O^{-2}. The resistance include the solid electrolyte and the electrodes. In this work as assumed the electrode resistance are negligible. The Ohmic losses depend on the cell design, electrolyte thickness and material. They depend on the ionic and electronic conductivity σ_{el} [$\Omega^{-1}m^{-1}$] of the electrolyte [24]:

$$\eta_{ohm} = j \cdot \frac{\delta_{el}}{\sigma_{el}} \quad [A1]$$

Where δ_{el} is the electrolyte layer thickness, $r_{ohm,el}$ is the specific ohmic resistance of the electrolyte layer [Ωcm^2] and $r_{ohmic,const}$ is the resistance of interconnectors and wires [Ωcm^2], which is assumed to be constant. On the other hand, the electrolyte conductivity σ_{el} strongly depends on temperature and can be calculated as [241]:

$$\sigma_{el} = \sigma_{0,el} T^{-1} \cdot exp\left(-\frac{E_{el}}{R \cdot T}\right) \quad [A2]$$

where $\sigma_{0,el}$ [$\Omega^{-1}m^{-1}$] is an empirical pre–exponential factor, and E_{el} [J/mol] is the activation energy.

Concentration/Diffusion overpotential. During cell operation, the reactant and product are transported by diffusion through the porous media from the bulk of material to the TPB or vice versa. The geometrical effects and molecular interactions generate diffusion losses that result in lower reactant and product partial pressure at the TPB. Assuming the system contain binary components, the concentration losses according to [215] result:

$$\eta_{conc,fuel} = \frac{R \cdot T}{2 \cdot F} \cdot ln\left(\frac{p_{H_2O,tpb} \cdot p_{H_2,bulk}}{p_{H_2O,bulk} \cdot p_{H_2,tpb}}\right) \quad [A3]$$

$$\eta_{conc,oxygen} = \frac{R \cdot T}{4 \cdot F} \cdot ln\frac{p_{O_2,bulk}}{p_{O_2,tpb}} \quad [A4]$$

where $p_{i,bulk}$ and $p_{i,tpb}$ are respectively the bulk and TPB gas concentration as a function of the partial pressure of the species i in a binary mixture i and j. According to Fick's model, the gas concentration is given by [215]:

$$p_{i,tpb} = p_{i,bulk} - \frac{R \cdot T \cdot \delta_{an,cat}}{n_i \cdot F \cdot D_{eff,i}} \quad [A5]$$

considering that Knudsen diffusion and molecular diffusion compete with one another, the effective diffusion coefficient $D_{eff,i}$ [m^2/s] is determined by [215]:

$$D_{eff,i} = \frac{\varepsilon}{\tau} \cdot \left(\frac{1}{D_{ij}} + \frac{1}{D_{ik}}\right) \quad [A6]$$

where the path for the diffusion of the gas molecules within the pores has a tortuosity τ and average pore diameter ε. The pure Knudsen diffusion comprises the effect of the porous medium and is estimated by [215]:

$$D_{ik} = \frac{d_p}{3}\sqrt{\frac{8RT}{\pi M_i}} \quad [A7]$$

where M_i is the molecular weights of gas species i, and d_p is the mean pore size of the porous media. The binary diffusivity coefficient D_{ij} is given by [215]:

$$D_{ij} = \frac{1.43 \cdot 10^{-7} \cdot T^{1.75}}{p \cdot \sqrt{2/\left(M_i^{-1} + M_j^{-1}\right)}\left(V_{d,i}^{1/3} + V_{d,j}^{1/3}\right)^2} \quad [A8]$$

where V_d is the atomic diffusion volumes of species i and j.

Activation losses. The charge–transfer resistance depends on the TPB area and operating conditions such as gas composition and temperature. The inverted Butler–Volmer [223] Eqs. 26 and 29 compute the charge–transfer activation overpotentials ($\eta_{act,a}$ $\eta_{act,c}$). In the present work is assumed that only the oxidation

of H_2 takes place in the TPB, and the charge–transfer reaction at the TPB region is the limiting step in the anode and cathode. The limiting step reaction of electrochemical oxidation of H_2 is giving by Eq. 25, [221].

$$H_{(Ni)} + OH^{-}_{(YSZ)} \leftrightarrow (Ni) + H_2O_{(YSZ)} + e^{-}_{Ni} \quad \text{[A9]}$$

$$\eta^{a}_{act} = \frac{RT}{F}\left[sinh^{-1}\left(\frac{i}{2i_{0,anode}}\right)\right] \quad \text{[A10]}$$

where i_0 is the exchange current density:

$$i_0 = i^{*}_{H_2}\frac{\left(p_{H_2}/p^{*}_{H_2}\right)^{1/4}\left(p_{H_2O}\right)^{3/4}}{1+\left(p_{H_2}/p^{*}_{H_2}\right)^{1/2}} \quad \text{[A11]}$$

The balance between adsorption and desorption of hydrogen on the Ni determines the parameter $p^{*}_{H_2}$. According to [221] there are not yet established values for the forward and reverse rates of hydrogen adsorption and desorption on Ni, and they are a function of different variables such as the particular crystal face and surface defects. In the work of [221] the dissociative adsorption rate is written in terms of a sticking probability γ_0. Table 1 shows the parameters.

$$p^{*}_{H_2} = \frac{A_{des}\Gamma^2\sqrt{2\pi RTM_{H_2}}}{\gamma_0}exp\left(\frac{E_{des}}{RT}\right) \quad \text{[A12]}$$

$i^{*}_{H_2}$ depends on parameters associated with the charge–transfer reactions. However, parameters like the specific three–phase boundary length and the elementary charge–transfer rates are not directly known. Thus, here we take $i^{*}_{H_2}$ as a fitting value.

Eq. 29 describes the electrochemical reduction of oxygen incorporated at the electrode–electrolyte interface [223]:

$$\eta_{act}^{c} = \frac{RT}{F}\left[sinh^{-1}\left(\frac{i}{2i_{0,cathode}}\right)\right] \quad \text{[A13]}$$

The charge transfer and incorporation at the TPB [223]:

$$O_{ad_{(c)}} + V_{\ddot{O}_{(el)}} + 2e_{(c)}^{-} \leftrightarrow O_{O_{(el)}}^{\times} + (c) \quad \text{[A14]}$$

$O_{ad_{(c)}}$ is adsorbed atomic oxygen on the cathode surface and (c) is an unoccupied cathode surface site, $V_{\ddot{O}_{(el)}}$ is the oxide–ion vacancy and $O_{O_{(el)}}^{\times}$ is an oxide anion . i_0 is the exchange current density:

$$i_0 = i_{O_2}^{*}\frac{\left(p_{O_2}/p_{O_2}^{*}\right)^{1/4}}{1+\left(p_{O_2}/p_{O_2}^{*}\right)^{1/2}} \quad \text{[A15]}$$

$i_{O_2}^{*}$ is a fitting parameter, see Table 1 for parameters A_{O_2}, E_{O_2}

$$p_{O_2}^{*} = A_{O_2}\exp\left(-\frac{E_{O_2}}{RT}\right) \quad \text{[A16]}$$

References

[1] J. Chen, J. Liang, Z. Xu, J. E, Assessment of supercritical water gasification process for combustible gas production from thermodynamic, environmental and techno–economic perspectives: A review, Energy Convers. Manag. (2020). https://doi.org/10.1016/j.enconman.2020.113497.

[2] Z. Chen, X. Zhang, W. Han, L. Gao, S. Li, Exergy analysis on the process with integrated supercritical water gasification of coal and syngas separation, Appl. Therm. Eng. (2018). https://doi.org/10.1016/j.applthermaleng.2017.09.083.

[3] UNEP, Water Quality: Policy Brief, Unwater. (2011).

[4] World Water Assessment Programme (United Nations), Wastewater : the untapped resource : the United Nations world water development report 2017, n.d.

[5] A.U.N.S.B. Ki–moon, U. Ef, E. Anthony, New commitments in water and sanitation will transform children ' s lives, (2014). https://www.unicef.org/mena/press–releases/new–commitments–in–water–and–sanitation.

[6] UNHCR/Riccardo Gangale, Climate change and disaster displacement, (n.d.). https://www.unhcr.org/climate–change–and–disasters.html.

[7] United Nations Department of Economic and Social Affrairs, Global Population Growth and Sustainable Development, 2021. www.unpopulation.org.

[8] P. Semaha, Z. Lei, T. Yuan, Z. Zhang, K. Shimizu, Transition of biological wastewater treatment from flocculent activated sludge to granular sludge systems towards circular economy, Bioresour. Technol. Reports. 21 (2023). https://doi.org/10.1016/j.biteb.2022.101294.

[9] R. Du, C. Li, Q. Liu, J. Fan, Y. Peng, A review of enhanced municipal wastewater treatment through energy savings and carbon recovery to reduce discharge and CO2 footprint, Bioresour. Technol. 364 (2022) 128135. https://doi.org/https://doi.org/10.1016/j.biortech.2022.128135.

[10] R. Mei, T. Narihiro, M.K. Nobu, K. Kuroda, W.T. Liu, Evaluating digestion efficiency in full–scale anaerobic digesters by identifying active

microbial populations through the lens of microbial activity, Sci. Rep. 6 (2016). https://doi.org/10.1038/srep34090.

[11] F. Safari, I. Dincer, Development and analysis of a novel biomass–based integrated system for multigeneration with hydrogen production, Int. J. Hydrogen Energy. 44 (2019) 3511–3526. https://doi.org/10.1016/j.ijhydene.2018.12.101.

[12] M.U. Bin Khawer, S.R. Naqvi, I. Ali, M. Arshad, D. Juchelková, M.W. Anjum, M. Naqvi, Anaerobic digestion of sewage sludge for biogas & biohydrogen production: State–of–the–art trends and prospects, Fuel. 329 (2022) 125416. https://doi.org/https://doi.org/10.1016/j.fuel.2022.125416.

[13] A.H. Alaedini, H.K. Tourani, M. Saidi, A review of waste–to–hydrogen conversion technologies for solid oxide fuel cell (SOFC) applications: Aspect of gasification process and catalyst development, J. Environ. Manage. 329 (2023). https://doi.org/10.1016/j.jenvman.2022.117077.

[14] F.L.F. Bittencourt, M.F. Martins, Thermochemically–driven treatment units for fecal matter sanitation: A review addressed to the underdeveloped world, J. Environ. Chem. Eng. 10 (2022). https://doi.org/10.1016/j.jece.2022.108732.

[15] Z.H. Tabriz, L. Khani, M. Mohammadpourfard, G.G. Akkurt, Biomass driven polygeneration systems: A review of recent progress and future prospects, Process Saf. Environ. Prot. 169 (2023) 363–397. https://doi.org/10.1016/j.psep.2022.11.029.

[16] P. Tan, C. Zhang, J. Xia, Q.Y. Fang, G. Chen, Estimation of higher heating value of coal based on proximate analysis using support vector regression, Fuel Process. Technol. (2015). https://doi.org/10.1016/j.fuproc.2015.06.013.

[17] J.A. Libra, K.S. Ro, C. Kammann, A. Funke, N.D. Berge, Y. Neubauer, M.M. Titirici, C. Fühner, O. Bens, J. Kern, K.H. Emmerich, Hydrothermal carbonization of biomass residuals: A comparative review of the chemistry, processes and applications of wet and dry pyrolysis, Biofuels. (2011). https://doi.org/10.4155/bfs.10.81.

[18] A.M. Ali, M.A. Abu Hassan, R.R.K. Ibrahim, A.A. Jalil, N.H. Mat Nayan, B.I. Abdulkarim, A.H. Sabeen, Analysis of Solid residue and Flue Gas

from Thermal Plasma Treatment of Petroleum Sludge, J. Environ. Chem. Eng. (2019). https://doi.org/10.1016/j.jece.2019.103207.

[19] A. Mulchandani, P. Westerhoff, Recovery opportunities for metals and energy from sewage sludges, Bioresour. Technol. (2016). https://doi.org/10.1016/j.biortech.2016.03.075.

[20] M. Ajorloo, M. Ghodrat, J. Scott, V. Strezov, Recent advances in thermodynamic analysis of biomass gasification: A review on numerical modelling and simulation, J. Energy Inst. 102 (2022) 395–419. https://doi.org/10.1016/J.JOEI.2022.05.003.

[21] S. Du, J. Wang, Y. Yu, Q. Zhou, Coarse–grained CFD–DEM simulation of coal and biomass co–gasification process in a fluidized bed reactor: Effects of particle size distribution and operating pressure, Renew. Energy. 202 (2023) 483–498. https://doi.org/10.1016/J.RENENE.2022.11.073.

[22] D. Hong, Y. Wang, X. Zhai, A ReaxFF study of the effect of pressure on the contribution of char–CO2 gasification to char conversion during pressurized oxy–fuel combustion, Fuel. 329 (2022) 125439. https://doi.org/10.1016/J.FUEL.2022.125439.

[23] C. Netzer, N. Guo, I.S. Ertesvåg, T. Løvås, Feedstock flexible numerical analysis of sewage sludge gasification, Fuel. 338 (2023) 127297. https://doi.org/10.1016/J.FUEL.2022.127297.

[24] E. Shayan, V. Zare, I. Mirzaee, Hydrogen production from biomass gasification; a theoretical comparison of using different gasification agents, Energy Convers. Manag. 159 (2018) 30–41. https://doi.org/10.1016/j.enconman.2017.12.096.

[25] M. Cortazar, L. Santamaria, G. Lopez, J. Alvarez, L. Zhang, R. Wang, X. Bi, M. Olazar, A comprehensive review of primary strategies for tar removal in biomass gasification, Energy Convers. Manag. 276 (2023). https://doi.org/10.1016/j.enconman.2022.116496.

[26] V.S. Sikarwar, M. Zhao, P. Clough, J. Yao, X. Zhong, M.Z. Memon, N. Shah, E.J. Anthony, P.S. Fennell, An overview of advances in biomass gasification, Energy Environ. Sci. 9 (2016) 2939–2977. https://doi.org/10.1039/c6ee00935b.

[27] A. Gómez–Barea, P. Ollero, B. Leckner, Optimization of char and tar conversion in fluidized bed biomass gasifiers, Fuel. 103 (2013) 42–52. https://doi.org/10.1016/j.fuel.2011.04.042.

[28] C. Wang, L. Zhu, M. Zhang, Z. Han, X. Jia, D. Bai, W. Duo, X. Bi, A. Abudula, G. Guan, G. Xu, A two–stage circulated fluidized bed process to minimize tar generation of biomass gasification for fuel gas production, Appl. Energy. 323 (2022) 119639. https://doi.org/10.1016/J.APENERGY.2022.119639.

[29] M. Materazzi, P. Lettieri, L. Mazzei, R. Taylor, C. Chapman, Tar evolution in a two stage fluid bed–plasma gasification process for waste valorization, Fuel Process. Technol. 128 (2014) 146–157. https://doi.org/10.1016/J.FUPROC.2014.06.028.

[30] N. Gil–Lalaguna, J.L. Sánchez, M.B. Murillo, E. Rodríguez, G. Gea, Air–steam gasification of sewage sludge in a fluidized bed. Influence of some operating conditions, Chem. Eng. J. (2014). https://doi.org/10.1016/j.cej.2014.03.055.

[31] L. Cao, I.K.M. Yu, X. Xiong, D.C.W. Tsang, S. Zhang, J.H. Clark, C. Hu, Y.H. Ng, J. Shang, Y.S. Ok, Biorenewable hydrogen production through biomass gasification: A review and future prospects, Environ. Res. 186 (2020) 109547. https://doi.org/10.1016/J.ENVRES.2020.109547.

[32] Z.R. Xu, W. Zhu, S.H. Htar, Partial oxidative gasification of municipal sludge in subcritical and supercritical water, Environ. Technol. (United Kingdom). 33 (2012) 1217–1223. https://doi.org/10.1080/09593330.2011.618933.

[33] C. Rodriguez Correa, A. Kruse, Supercritical water gasification of biomass for hydrogen production – Review, J. Supercrit. Fluids. 133 (2018) 573–590. https://doi.org/10.1016/j.supflu.2017.09.019.

[34] N. Akiya, P.E. Savage, Roles of water for chemical reactions in high–temperature water, Chem. Rev. 102 (2002) 2725–2750. https://doi.org/10.1021/cr000668w.

[35] C. Rodriguez Correa, A. Kruse, Supercritical water gasification of biomass for hydrogen production – Review, J. Supercrit. Fluids. (2018). https://doi.org/10.1016/j.supflu.2017.09.019.

[36] A. Kruse, N. Dahmen, Water – A magic solvent for biomass conversion, J. Supercrit. Fluids. 96 (2015) 36–45. https://doi.org/10.1016/j.supflu.2014.09.038.

[37] A. Kruse, T. Henningsen, A. Smag, J. Pfeiffer, Biomass gasification in supercritical water: Influence of the dry matter content and the formation of phenols, Ind. Eng. Chem. Res. 42 (2003) 3711–3717. https://doi.org/10.1021/ie0209430.

[38] S.D. Manjare, K. Dhingra, Supercritical fluids in separation and purification: A review, Mater. Sci. Energy Technol. (2019). https://doi.org/10.1016/j.mset.2019.04.005.

[39] L.J. Guo, H. Jin, Z.W. Ge, Y.J. Lu, C.Q. Cao, Industrialization prospects for hydrogen production by coal gasification in supercritical water and novel thermodynamic cycle power generation system with no pollution emission, Sci. China Technol. Sci. 58 (2015) 1989–2002. https://doi.org/10.1007/s11431–015–5967–0.

[40] D. Castello, L. Fiori, Supercritical water gasification of biomass: Thermodynamic constraints, Bioresour. Technol. 102 (2011) 7574–7582. https://doi.org/10.1016/j.biortech.2011.05.017.

[41] L. Wang, J. Chen, J. Cui, G. Wang, H. Jin, L. Guo, Experimental study on treatment of mixed ion exchange resins by supercritical water gasification, J. Clean. Prod. 385 (2023) 135755. https://doi.org/https://doi.org/10.1016/j.jclepro.2022.135755.

[42] Z. Ge, H. Jin, L. Guo, Hydrogen production by catalytic gasification of coal in supercritical water with alkaline catalysts: Explore the way to complete gasification of coal, Int. J. Hydrogen Energy. 39 (2014) 19583–19592. https://doi.org/10.1016/j.ijhydene.2014.09.119.

[43] W. Cao, C. Cao, L. Guo, H. Jin, M. Dargusch, D. Bernhardt, X. Yao, Hydrogen production from supercritical water gasification of chicken manure, Int. J. Hydrogen Energy. (2016). https://doi.org/10.1016/j.ijhydene.2016.09.031.

[44] J. Chen, Y. Fan, X. Zhao, J. E, W. Xu, F. Zhang, G. Liao, E. Leng, S. Liu, Experimental investigation on gasification characteristic of food waste using supercritical water for combustible gas production: Exploring the way to complete gasification, Fuel. 263 (2020).

https://doi.org/10.1016/j.fuel.2019.116735.

[45] J. Chen, Q. Wang, Z. Xu, J. E, E. Leng, F. Zhang, G. Liao, Process in supercritical water gasification of coal: A review of fundamentals, mechanisms, catalysts and element transformation, Energy Convers. Manag. 237 (2021). https://doi.org/10.1016/j.enconman.2021.114122.

[46] R. Migliaccio, P. Brachi, F. Montagnaro, S. Papa, A. Tavano, P. Montesarchio, G. Ruoppolo, M. Urciuolo, Sewage Sludge Gasification in a Fluidized Bed: Experimental Investigation and Modeling, Ind. Eng. Chem. Res. 60 (2021) 5034–5047. https://doi.org/10.1021/acs.iecr.1c00084.

[47] M. Schmid, M. Beirow, D. Schweitzer, G. Waizmann, R. Spörl, G. Scheffknecht, Product gas composition for steam–oxygen fluidized bed gasification of dried sewage sludge, straw pellets and wood pellets and the influence of limestone as bed material, Biomass and Bioenergy. 117 (2018) 71–77. https://doi.org/10.1016/J.BIOMBIOE.2018.07.011.

[48] M. Schmid, S. Hafner, S. Biollaz, J. Schneebeli, G. Waizmann, G. Scheffknecht, Steam–oxygen gasification of sewage sludge: Reduction of tar, H2S and COS with limestone as bed additive, Biomass and Bioenergy. 150 (2021) 106100. https://doi.org/https://doi.org/10.1016/j.biombioe.2021.106100.

[49] T.Y. Mun, J.S. Kim, Air gasification of dried sewage sludge in a two–stage gasifier. Part 2: Calcined dolomite as a bed material and effect of moisture content of dried sewage sludge for the hydrogen production and tar removal, in: Int. J. Hydrogen Energy, 2013. https://doi.org/10.1016/j.ijhydene.2013.02.073.

[50] Y.K. Choi, T.Y. Mun, M.H. Cho, J.S. Kim, Gasification of dried sewage sludge in a newly developed three–stage gasifier: Effect of each reactor temperature on the producer gas composition and impurity removal, Energy. (2016). https://doi.org/10.1016/j.energy.2016.07.166.

[51] Y.K. Choi, J.H. Ko, J.S. Kim, Gasification of dried sewage sludge using an innovative three–stage gasifier: Clean and H2–rich gas production using condensers as the only secondary tar removal apparatus, Fuel. 216 (2018) 810–817. https://doi.org/10.1016/j.fuel.2017.12.068.

[52] A. Amrullah, Y. Matsumura, Supercritical water gasification of sewage

sludge in continuous reactor, Bioresour. Technol. (2018). https://doi.org/10.1016/j.biortech.2017.10.002.

[53] L. Guo, H. Jin, Boiling coal in water: Hydrogen production and power generation system with zero net CO2 emission based on coal and supercritical water gasification, in: Int. J. Hydrogen Energy, 2013: pp. 12953–12967. https://doi.org/10.1016/j.ijhydene.2013.04.089.

[54] C. Graves, S.D. Ebbesen, S.H. Jensen, S.B. Simonsen, M.B. Mogensen, Eliminating degradation in solid oxide electrochemical cells by reversible operation, Nat. Mater. 14 (2015) 239–244. https://doi.org/10.1038/nmat4165.

[55] B.J.M. Sarruf, J.E. Hong, R. Steinberger–Wilckens, P.E.V. de Miranda, Ceria–Co–Cu–based SOFC anode for direct utilisation of methane or ethanol as fuels, Int. J. Hydrogen Energy. (2019). https://doi.org/10.1016/j.ijhydene.2019.04.075.

[56] X. Lv, M. Chen, Z. Xie, L. Qian, L. Zhang, G. Zheng, Electrochemical conversion of C1 molecules to sustainable fuels in solid oxide electrolysis cells, Chinese J. Catal. (2022). https://doi.org/10.1016/S1872–2067(21)63838–X.

[57] A. Husain, M.U. Shariq, I. Khan, S.P. Ansari, M.M.A. Khan, A. Khan, 5 – Solid oxide fuel cell technology for sustainable development, in: A. Khan, A. Pizzi, M. Jawaid, N. Azum, A. Asiri, I. Isa (Eds.), Adv. Technol. Convers. Waste Into Fuels Chem., Woodhead Publishing, 2021: pp. 93–109. https://doi.org/https://doi.org/10.1016/B978–0–323–90150–5.00015–7.

[58] S. Huang, C. Yang, H. Chen, N. Zhou, D. Tucker, Coupling impacts of SOFC operating temperature and fuel utilization on system net efficiency in natural gas hybrid SOFC/GT system, Case Stud. Therm. Eng. 31 (2022). https://doi.org/10.1016/j.csite.2022.101868.

[59] A. Nakajo, F. Mueller, J. Brouwer, J. Van Herle, D. Favrat, Progressive activation of degradation processes in solid oxide fuel cells stacks: Part I: Lifetime extension by optimisation of the operating conditions, J. Power Sources. 216 (2012) 449–463. https://doi.org/10.1016/j.jpowsour.2012.05.078.

[60] Qidogn Xu, Zengjin Guo, Lingchao Xia, Qijiao He, Zheng Li, Idris

Temitope Bello, Keqing Zheng, Meng Ni, A comprehensive review of solid oxide fuel cells operating on various promising alternative fuels _ Enhanced Reader, (n.d.).

[61] X. Long, P. Boldrin, Y. Zhang, N. Brandon, N. Paterson, M. Millan, Towards integrated gasification and fuel cell operation with carbon capture: Impact of fuel gas on anode materials, Fuel. 318 (2022) 123561. https://doi.org/10.1016/J.FUEL.2022.123561.

[62] A.N. Tabish, H.C. Patel, A. Mani, J. Schoonman, P. V. Aravind, Effect of H2S and HCl contaminants on nickel and ceria pattern anode solid oxide fuel cells, Electrochim. Acta. 423 (2022) 140592. https://doi.org/10.1016/J.ELECTACTA.2022.140592.

[63] A. Cavalli, M. Kunze, P. V Aravind, Cross–influence of toluene as tar model compound and HCl on Solid Oxide Fuel Cell anodes in Integrated Biomass Gasifier SOFC Systems, Appl. Energy. 231 (2018) 1–11. https://doi.org/https://doi.org/10.1016/j.apenergy.2018.09.060.

[64] L. Fan, A. Mokhov, S.A. Saadabadi, N. Brandon, P.V. Aravind, Methane steam reforming reaction in solid oxide fuel cells: Influence of electrochemical reaction and anode thickness, J. Power Sources. (2021). https://doi.org/10.1016/j.jpowsour.2021.230276.

[65] L. Fryda, K.D. Panopoulos, J. Karl, E. Kakaras, Exergetic analysis of solid oxide fuel cell and biomass gasification integration with heat pipes, Energy. 33 (2008) 292–299. https://doi.org/10.1016/J.ENERGY.2007.07.006.

[66] T. Seitarides, C. Athanasiou, A. Zabaniotou, Modular biomass gasification–based solid oxide fuel cells (SOFC) for sustainable development, Renew. Sustain. Energy Rev. 12 (2008) 1251–1276. https://doi.org/10.1016/j.rser.2007.01.020.

[67] P.V. Aravind, A. Cavalli, H.C. Patel, M. Recalde, A. Saadabadi, A.N. Tabish, G. Botta, A. Thallam Tattai, A. Teodoru, Y. Hajimolana, P. Chundru, T. Woudstra, Opportunities and Challenges in Using SOFCs in Waste to Energy Systems, ECS Trans. (2017). https://doi.org/10.1149/07801.0209ecst.

[68] R.Ø. Gadsbøll, A. Vivar Garcia, J. Ahrenfeldt, U.B. Henriksen, Solid oxide fuel cell stack coupled with an oxygen–blown TwoStage gasifier

using minimal gas cleaning, Renew. Energy. (2019). https://doi.org/10.1016/j.renene.2019.03.038.

[69] M. Liu, T. Woudstra, E.J.O. Promes, S.Y.G. Restrepo, P. V. Aravind, System development and self–sustainability analysis for upgrading human waste to power, Energy. 68 (2014) 377–384. https://doi.org/10.1016/j.energy.2014.03.005.

[70] A. Mountouris, E. Voutsas, D. Tassios, Plasma gasification of sewage sludge: Process development and energy optimization, Energy Convers. Manag. 49 (2008) 2264–2271. https://doi.org/10.1016/j.enconman.2008.01.025.

[71] W. Wan, An innovative system by integrating the gasification unit with the supercritical water unit to produce clean syngas for solid oxide fuel cell (SOFC): System performance assessment, Int. J. Hydrogen Energy. 41 (2016) 22698–22710. https://doi.org/10.1016/j.ijhydene.2016.09.146.

[72] L.R. Clausen, Energy efficient thermochemical conversion of very wet biomass to biofuels by integration of steam drying, steam electrolysis and gasification, Energy. (2017). https://doi.org/10.1016/j.energy.2017.02.132.

[73] H.Æ. Sigurjonsson, L.R. Clausen, Solution for the future smart energy system: A polygeneration plant based on reversible solid oxide cells and biomass gasification producing either electrofuel or power, Appl. Energy. (2018). https://doi.org/10.1016/j.apenergy.2018.02.124.

[74] S. Qu, D. Guan, Z. Ma, X. Yi, A study on the optimal path of methane emissions reductions in a municipal solid waste landfill treatment based on the IPCC–SD model, J. Clean. Prod. 222 (2019) 252–266. https://doi.org/10.1016/J.JCLEPRO.2019.03.059.

[75] S. Herrmann, M. Jimenez Arreola, M. Gaderer, H. Spliethoff, Thermodynamic Evaluation of Integrated Heat–Pipe Reformer SOFC System, ECS Trans. . 68 (2015) 277–282. https://doi.org/10.1149/06801.0277ecst.

[76] E. Tilley, C. Lüthi, A. Morel, C. Zurbrügg, R. Schertenleib, Compendium of Sanitation Systems and Technologies, Development. (2014) 180. https://doi.org/SAN–12.

[77] Stockholm Environment Institute, Wastewater Management and Sustainability: from Waste Disposal to Resource Recovery, Stock. Environ. Inst. (2017).

[78] F. Rijsberman, A.P. Zwane, Sanitation & Water, in: Copenhagen Consens., 2012.

[79] Stockholm Environment Institute, Sustainable Sanitation and Agenda 2030, Sustain. Sanit. Agenda 2030. (2017).

[80] Bill & Melinda Gates Foundation, Water , Sanitation & Hygiene : Reinvent the Toilet Challenge, Bill Melinda Gates Found. (2013) 1–2.

[81] T. Onabanjo, K. Patchigolla, S.T. Wagland, B. Fidalgo, A. Kolios, E. McAdam, A. Parker, L. Williams, S. Tyrrel, E. Cartmell, Energy recovery from human faeces via gasification: A thermodynamic equilibrium modelling approach, Energy Convers. Manag. 118 (2016) 364–376. https://doi.org/10.1016/j.enconman.2016.04.005.

[82] P. Manara, A. Zabaniotou, Towards sewage sludge based biofuels via thermochemical conversion – A review, Renew. Sustain. Energy Rev. 16 (2012) 2566–2582. https://doi.org/10.1016/j.rser.2012.01.074.

[83] E. Danso–Boateng, R.G. Holdich, G. Shama, A.D. Wheatley, M. Sohail, S.J. Martin, Kinetics of faecal biomass hydrothermal carbonisation for hydrochar production, Appl. Energy. 111 (2013) 351–357. https://doi.org/10.1016/j.apenergy.2013.04.090.

[84] K. Cho, D. Kwon, M.R. Hoffmann, Electrochemical treatment of human waste coupled with molecular hydrogen production, RSC Adv. 4 (2014) 4596. https://doi.org/10.1039/c3ra46699j.

[85] K.S. Ro, K.B. Cantrell, P.G. Hunt, High–temperature pyrolysis of blended animal manures for producing renewable energy and value–added biochar, Ind. Eng. Chem. Res. 49 (2010) 10125–10131. https://doi.org/10.1021/ie101155m.

[86] F. Fabry, C. Rehmet, V. Rohani, L. Fulcheri, Waste gasification by thermal plasma: A review, Waste and Biomass Valorization. 4 (2013) 421–439. https://doi.org/10.1007/s12649–013–9201–7.

[87] E.E.R.C. of the Netherlands, Benefits of Allothermal Biomass Gasification for Co–Firing, in: 2nd Work. Cofiring Biomass with Coal,

Copenhagen, Denmark, 2012.

[88] P.G. Rutberg, A.N. Bratsev, V.A. Kuznetsov, V.E. Popov, A.A. Ufimtsev, S. V. Shtengel', On efficiency of plasma gasification of wood residues, Biomass and Bioenergy. 35 (2011) 495–504. https://doi.org/10.1016/j.biombioe.2010.09.010.

[89] K.D. Panopoulos, L. Fryda, J. Karl, S. Poulou, E. Kakaras, High temperature solid oxide fuel cell integrated with novel allothermal biomass gasification. Part II: Exergy analysis, J. Power Sources. 159 (2006) 586–594. https://doi.org/10.1016/j.jpowsour.2005.11.040.

[90] C. Bang–Møller, M. Rokni, Thermodynamic performance study of biomass gasification, solid oxide fuel cell and micro gas turbine hybrid systems, Energy Convers. Manag. 51 (2010) 2330–2339. https://doi.org/10.1016/j.enconman.2010.04.006.

[91] R. Toonssen, P. V. Aravind, G. Smit, N. Woudstra, A.H.M. Verkooijen, System study on hydrothermal gasification combined with a hybrid solid oxide fuel cell gas turbine, Fuel Cells. (2010). https://doi.org/10.1002/fuce.200900188.

[92] E. Facchinetti, M. Gassner, M. D'Amelio, F. Marechal, D. Favrat, Process integration and optimization of a solid oxide fuel cell – Gas turbine hybrid cycle fueled with hydrothermally gasified waste biomass, Energy. (2012). https://doi.org/10.1016/j.energy.2012.02.059.

[93] S. Santhanam, C. Schilt, B. Turker, T. Woudstra, P. V. Aravind, Thermodynamic modeling and evaluation of high efficiency heat pipe integrated biomass Gasifier–Solid Oxide Fuel Cells–Gas Turbine systems, Energy. 109 (2016) 751–764. https://doi.org/10.1016/j.energy.2016.04.117.

[94] J. Sadhukhan, Y. Zhao, N. Shah, N.P. Brandon, Performance analysis of integrated biomass gasification fuel cell (BGFC) and biomass gasification combined cycle (BGCC) systems, Chem. Eng. Sci. 65 (2010) 1942–1954. https://doi.org/10.1016/j.ces.2009.11.022.

[95] A.V. Bridgwater, The technical and economic feasibility of biomass gasification for power generation, Fuel. 74 (1995) 631–653. https://doi.org/10.1016/0016–2361(95)00001–L.

[96] Z. Rao, Y. Zhao, C. Huang, C. Duan, J. He, Recent developments in drying and dewatering for low rank coals, Prog. Energy Combust. Sci. 46 (2015) 1–11. https://doi.org/10.1016/j.pecs.2014.09.001.

[97] M. Aziz, Y. Kansha, A. Tsutsumi, Self–heat recuperative fluidized bed drying of brown coal, Chem. Eng. Process. Process Intensif. 50 (2011) 944–951. https://doi.org/10.1016/j.cep.2011.07.005.

[98] Y. Liu, Y. Kansha, M. Ishizuka, Q. Fu, A. Tsutsumi, Experimental and simulation investigations on self–heat recuperative fluidized bed dryer for biomass drying with superheated steam, Fuel Process. Technol. 136 (2015) 79–86. https://doi.org/10.1016/j.fuproc.2014.10.005.

[99] S. Heidenreich, P.U. Foscolo, New concepts in biomass gasification, Prog. Energy Combust. Sci. 46 (2015) 72–95. https://doi.org/10.1016/j.pecs.2014.06.002.

[100] C.Z. Li, Importance of volatile–char interactions during the pyrolysis and gasification of low–rank fuels – A review, Fuel. 112 (2013) 609–623. https://doi.org/10.1016/j.fuel.2013.01.031.

[101] Y.K. Choi, M.H. Cho, J.S. Kim, Steam/oxygen gasification of dried sewage sludge in a two–stage gasifier: Effects of the steam to fuel ratio and ash of the activated carbon on the production of hydrogen and tar removal, Energy. 91 (2015) 160–167. https://doi.org/10.1016/j.energy.2015.08.027.

[102] M. Materazzi, P. Lettieri, R. Taylor, C. Chapman, Performance analysis of RDF gasification in a two stage fluidized bed–plasma process, Waste Manag. 47 (2016) 256–266. https://doi.org/10.1016/j.wasman.2015.06.016.

[103] H. Huang, L. Tang, Treatment of organic waste using thermal plasma pyrolysis technology, Energy Convers. Manag. 48 (2007) 1331–1337. https://doi.org/10.1016/j.enconman.2006.08.013.

[104] J. Rezaiyan, N.P. Cheremisinoff, Gasification technologies: a primer for engineers and scientists, 2005. https://doi.org/10.3233/NRE–2011–0649.

[105] E. Gomez, D.A. Rani, C.R. Cheeseman, D. Deegan, M. Wise, A.R. Boccaccini, Thermal plasma technology for the treatment of wastes: A critical review, J. Hazard. Mater. 161 (2009) 614–626.

https://doi.org/10.1016/j.jhazmat.2008.04.017.

[106] M. Materazzi, P. Lettieri, L. Mazzei, R. Taylor, C. Chapman, Reforming of tars and organic sulphur compounds in a plasma–assisted process for waste gasification, Fuel Process. Technol. 137 (2015) 259–268. https://doi.org/10.1016/j.fuproc.2015.03.007.

[107] S.J. Yoon, Y.M. Yun, M.W. Seo, Y.K. Kim, H.W. Ra, J.G. Lee, Hydrogen and syngas production from glycerol through microwave plasma gasification, Int. J. Hydrogen Energy. 38 (2013) 14559–14567. https://doi.org/10.1016/j.ijhydene.2013.09.001.

[108] J. Balgaranova, Plasma chemical gasification of sewage sludge, Waste Manag. Res. 21 (2003) 38–41. https://doi.org/10.1177/0734242X0302100105.

[109] G.S.J. Sturm, A.N. Munoz, P. V. Aravind, G.D. Stefanidis, Microwave–Driven Plasma Gasification for Biomass Waste Treatment at Miniature Scale, IEEE Trans. Plasma Sci. 44 (2016) 670–678. https://doi.org/10.1109/TPS.2016.2533363.

[110] S. McIntosh, R.J. Gorte, Direct hydrocarbon solid oxide fuel cells, Chem. Rev. 104 (2004) 4845–4865. https://doi.org/10.1021/cr020725g.

[111] D. Lee, J. Myung, J. Tan, S.H. Hyun, J.T.S. Irvine, J. Kim, J. Moon, Direct methane solid oxide fuel cells based on catalytic partial oxidation enabling complete coking tolerance of Ni–based anodes, J. Power Sources. (2017). https://doi.org/10.1016/j.jpowsour.2017.02.003.

[112] J. Kupecki, K. Motylinski, J. Milewski, Dynamic analysis of direct internal reforming in a SOFC stack with electrolyte–supported cells using a quasi–1D model, Appl. Energy. (2017). https://doi.org/10.1016/j.apenergy.2017.07.122.

[113] V. Eveloy, Numerical analysis of an internal methane reforming solid oxide fuel cell with fuel recycling, Appl. Energy. 93 (2012) 107–115. https://doi.org/10.1016/j.apenergy.2010.10.045.

[114] S. Kang, K.–Y. Ahn, Dynamic modeling of solid oxide fuel cell and engine hybrid system for distributed power generation, Appl. Energy. 195 (2017) 1086–1099. https://doi.org/10.1016/j.apenergy.2017.03.077.

[115] M. Santarelli, L. Briesemeister, M. Gandiglio, S. Herrmann, P.

Kuczynski, J. Kupecki, A. Lanzini, F. Llovell, D. Papurello, H. Spliethoff, B. Swiatkowski, J. Torres–Sanglas, L.F. Vega, Carbon recovery and re–utilization (CRR) from the exhaust of a solid oxide fuel cell (SOFC): Analysis through a proof–of–concept, J. CO2 Util. 18 (2017) 206–221. https://doi.org/10.1016/j.jcou.2017.01.014.

[116] ASIMPTOTE, Cycle–Tempo, The Netherlands, 2015.

[117] T. Araki, T. Ohba, S. Takezawa, K. Onda, Y. Sakaki, Cycle analysis of planar SOFC power generation with serial connection of low and high temperature SOFCs, J. Power Sources. 158 (2006) 52–59. https://doi.org/10.1016/j.jpowsour.2005.09.003.

[118] P. V Aravind, C. Schilt, B. Türker, T. Woudstra, Thermodynamic Model of a Very High Efficiency Power Plant based on a Biomass Gasifier, SOFCs, and a Gas Turbine, Int. J. Renew. Energy Dev. 1 (2012) 51–55. https://doi.org/10.14710/ijred.1.2.51–55.

[119] J. Kupecki, M. Skrzypkiewicz, M. Wierzbicki, M. Stepien, Experimental and numerical analysis of a serial connection of two SOFC stacks in a micro–CHP system fed by biogas, Int. J. Hydrogen Energy. 42 (2017) 3487–3497. https://doi.org/10.1016/j.ijhydene.2016.07.222.

[120] M.R. Mahishi, D.Y. Goswami, Thermodynamic optimization of biomass gasifier for hydrogen production, Int. J. Hydrogen Energy. 32 (2007) 3831–3840. https://doi.org/10.1016/j.ijhydene.2007.05.018.

[121] C.O. Colpan, A.S. Fung, F. Hamdullahpur, Modeling of an integrated two–stage biomass gasifier and solid oxide fuel cell system, Biomass and Bioenergy. 42 (2012) 132–142. https://doi.org/10.1016/j.biombioe.2012.03.002.

[122] U. Henriksen, J. Ahrenfeldt, T.K. Jensen, B. Gøbel, J.D. Bentzen, C. Hindsgaul, L.H. Sørensen, The design, construction and operation of a 75 kW two–stage gasifier, Energy. 31 (2006) 1542–1553. https://doi.org/10.1016/j.energy.2005.05.031.

[123] P. Baële, S. Béchu, A. Bés, J. Pelletier, A. Lacoste, An open–ended coaxial plasma source with extended operating parameters: Plasma impedance, coupling and energy efficiency, Plasma Sources Sci. Technol. 23 (2014). https://doi.org/10.1088/0963–0252/23/6/064006.

[124] A. Molino, S. Chianese, D. Musmarra, Biomass gasification technology: The state of the art overview, J. Energy Chem. 25 (2016) 10–25. https://doi.org/10.1016/j.jechem.2015.11.005.

[125] J. Li, Y. Yin, X. Zhang, J. Liu, R. Yan, Hydrogen–rich gas production by steam gasification of palm oil wastes over supported tri–metallic catalyst, Int. J. Hydrogen Energy. 34 (2009) 9108–9115. https://doi.org/10.1016/j.ijhydene.2009.09.030.

[126] T. Song, J. Wu, L. Shen, J. Xiao, Experimental investigation on hydrogen production from biomass gasification in interconnected fluidized beds, Biomass and Bioenergy. 36 (2012) 258–267. https://doi.org/10.1016/j.biombioe.2011.10.021.

[127] M. Åhman, Assessing the future competitiveness of alternative powertrains, Int. J. Veh. Des. 33 (2003) 309–331. https://doi.org/10.1504/IJVD.2003.003582.

[128] J.M. Encinar, J.F. González, J. González, Fixed–bed pyrolysis of Cynara cardunculus L. Product yields and compositions, Fuel Process. Technol. 68 (2000) 209–222. https://doi.org/10.1016/S0378–3820(00)00125–9.

[129] M.A.A. Mohammed, A. Salmiaton, W.A.K.G. Wan Azlina, M.S. Mohammad Amran, A. Fakhru'L–Razi, Air gasification of empty fruit bunch for hydrogen–rich gas production in a fluidized–bed reactor, Energy Convers. Manag. 52 (2011) 1555–1561. https://doi.org/10.1016/j.enconman.2010.10.023.

[130] Y. Jiang, A. V. Virkar, Fuel Composition and Diluent Effect on Gas Transport and Performance of Anode–Supported SOFCs, J. Electrochem. Soc. 150 (2003) A942. https://doi.org/10.1149/1.1579480.

[131] P. Mottaghizadeh, S. Santhanam, M.P. Heddrich, K.A. Friedrich, F. Rinaldi, Process modeling of a reversible solid oxide cell (r–SOC) energy storage system utilizing commercially available SOC reactor, Energy Convers. Manag. 142 (2017) 477–493. https://doi.org/10.1016/j.enconman.2017.03.010.

[132] G.J. Offer, J. Mermelstein, E. Brightman, N.P. Brandon, Thermodynamics and kinetics of the interaction of carbon and sulfur with solid oxide fuel cell anodes, J. Am. Ceram. Soc. 92 (2009) 763–780. https://doi.org/10.1111/j.1551–2916.2009.02980.x.

[133] P. V. Aravind, Studies on High Efficiency Energy Systems based on Biomass Gasifiers and Solid Oxide Fuel Cells with Ni/GDC Anode, Delft University of Technology, 2007.

[134] A. Thallam Thattai, V. Oldenbroek, L. Schoenmakers, T. Woudstra, P.V. Aravind, Towards retrofitting integrated gasification combined cycle (IGCC) power plants with solid oxide fuel cells (SOFC) and CO2 capture – A thermodynamic case study, Appl. Therm. Eng. 114 (2017) 170–185. https://doi.org/10.1016/j.applthermaleng.2016.11.167.

[135] G. Qiu, H. Liu, S. Riffat, Expanders for micro–CHP systems with organic Rankine cycle, Appl. Therm. Eng. 31 (2011) 3301–3307. https://doi.org/10.1016/j.applthermaleng.2011.06.008.

[136] H. Wang, R.B. Peterson, T. Herron, Experimental performance of a compliant scroll expander for an organic Rankine cycle, Proc. Inst. Mech. Eng. Part A J. Power Energy. 223 (2009) 863–872. https://doi.org/10.1243/09576509JPE741.

[137] European Commission, 2030 Energy Strategy, Eur. Comm. (n.d.).

[138] E. and H. (UNU–I. University, United Nations, Institute for Water, Valuing Human Waste as an Energy Resource, A Res. Br. Assess. Glob. Wealth Waste. (2015).

[139] N. Boukis, E. Hauer, S. Herbig, J. Sauer, F. Vogel, Catalytic gasification of digestate sludge in supercritical water on the pilot plant scale, Biomass Convers. Biorefinery. 7 (2017) 415–424. https://doi.org/10.1007/s13399–017–0238–x.

[140] Y. Oka, S.I. Koshizuka, CONCEPT AND DESIGN OF A SUPERCRITICAL–PRESSURE, DIRECT–CYCLE LIGHT–WATER REACTOR, Nucl. Technol. 103 (1993) 295–302.

[141] P. Basu, V. Mettanant, Biomass Gasification in Supercritical Water — A Review, Int. J. Chem. React. Eng. (2009). https://doi.org/10.2202/1542–6580.1919.

[142] Y. Oka, S. Koshizuka, Supercritical–pressure, once–through cycle light water cooled reactor concept, J. Nucl. Sci. Technol. (2001). https://doi.org/10.1080/18811248.2001.9715139.

[143] A. Kruse, Supercritical water gasification, Biofuels, Bioprod. Biorefining.

2 (2008) 415–437. https://doi.org/10.1002/bbb.93.

[144] O. Yakaboylu, J. Harinck, K.G. Smit, W. De Jong, Testing the constrained equilibrium method for the modeling of supercritical water gasification of biomass, Fuel Process. Technol. (2015). https://doi.org/10.1016/j.fuproc.2015.05.009.

[145] C. He, C.L. Chen, A. Giannis, Y. Yang, J.Y. Wang, Hydrothermal gasification of sewage sludge and model compounds for renewable hydrogen production: A review, Renew. Sustain. Energy Rev. 39 (2014) 1127–1142. https://doi.org/10.1016/j.rser.2014.07.141.

[146] Y. Guo, S.Z. Wang, D.H. Xu, Y.M. Gong, H.H. Ma, X.Y. Tang, Review of catalytic supercritical water gasification for hydrogen production from biomass, Renew. Sustain. Energy Rev. 14 (2010) 334–343. https://doi.org/10.1016/j.rser.2009.08.012.

[147] W. Feng, H.J. Van Der Kooi, J. De Swaan Arons, Biomass conversions in subcritical and supercritical water: Driving force, phase equilibria, and thermodynamic analysis, Chem. Eng. Process. Process Intensif. (2004). https://doi.org/10.1016/j.cep.2004.01.004.

[148] K. Tekin, S. Karagöz, S. Bektaş, A review of hydrothermal biomass processing, Renew. Sustain. Energy Rev. (2014). https://doi.org/10.1016/j.rser.2014.07.216.

[149] A.A. Peterson, F. Vogel, R.P. Lachance, M. Fröling, M.J. Antal, J.W. Tester, Thermochemical biofuel production in hydrothermal media: A review of sub– and supercritical water technologies, Energy Environ. Sci. (2008). https://doi.org/10.1039/b810100k.

[150] S.S. Toor, L. Rosendahl, A. Rudolf, Hydrothermal liquefaction of biomass: A review of subcritical water technologies, Energy. (2011). https://doi.org/10.1016/j.energy.2011.03.013.

[151] O. Yakaboylu, J. Harinck, K.G. Smit, W. de Jong, Supercritical water gasification of biomass: A literature and technology overview, Energies. (2015). https://doi.org/10.3390/en8020859.

[152] O. Yakaboylu, G. Yapar, M. Recalde, J. Harinck, K.G. Smit, E. Martelli, W. De Jong, Supercritical water gasification of biomass: An integrated kinetic model for the prediction of product compounds, Ind. Eng. Chem.

Res. (2015). https://doi.org/10.1021/acs.iecr.5b02019.

[153] W.M. H., Catalytic hydrothermal gasification of biomass for the production of synthetic gas, ETH Zurich, 2007.

[154] A. Kruse, M. Faquir, Hydrothermal biomass gasification – Effects of salts, backmixing, and their interaction, Chem. Eng. Technol. (2007). https://doi.org/10.1002/ceat.200600409.

[155] A. Kruse, E. Dinjus, Influence of salts during hydrothermal biomass gasification: The role of the catalysed water–gas shift reaction, Zeitschrift Fur Phys. Chemie. (2005). https://doi.org/10.1524/zpch.219.3.341.59177.

[156] D.S. Gökkaya, M. Saglam, M. Yuksel, L. Ballice, Hydrothermal gasification of xylose: Effects of reaction temperature, pressure, and K2CO3 as a catalyst on product distribution, Biomass and Bioenergy. 91 (2016) 26–36. https://doi.org/10.1016/j.biombioe.2016.04.013.

[157] Z.R. Xu, W. Zhu, M. Li, Influence of moisture content on the direct gasification of dewatered sludge via supercritical water, Int. J. Hydrogen Energy. 37 (2012) 6527–6535. https://doi.org/10.1016/j.ijhydene.2012.01.086.

[158] L.J. Guo, Y.J. Lu, X.M. Zhang, C.M. Ji, Y. Guan, A.X. Pei, Hydrogen production by biomass gasification in supercritical water: A systematic experimental and analytical study, Catal. Today. 129 (2007) 275–286. https://doi.org/10.1016/j.cattod.2007.05.027.

[159] O. Yakaboylu, Supercritical Water Gasification of Wet Biomass and Experiments, Delft University of Technology, 2016.

[160] O. Yakaboylu, I. Albrecht, J. Harinck, K.G. Smit, G.A. Tsalidis, M. Di Marcello, K. Anastasakis, W. de Jong, Supercritical water gasification of biomass in fluidized bed: First results and experiences obtained from TU Delft/Gensos semi–pilot scale setup, Biomass and Bioenergy. (2018). https://doi.org/10.1016/j.biombioe.2016.12.007.

[161] M.S.H.K. Tushar, A. Dutta, C. Xu, Simulation and kinetic modeling of supercritical water gasification of biomass, Int. J. Hydrogen Energy. (2015). https://doi.org/10.1016/j.ijhydene.2015.02.033.

[162] I. Behnia, Z. Yuan, P. Charpentier, C. (Charles) Xu, Production of methane and hydrogen via supercritical water gasification of renewable

glucose at a relatively low temperature: Effects of metal catalysts and supports, Fuel Process. Technol. 143 (2016) 27–34. https://doi.org/10.1016/j.fuproc.2015.11.006.

[163] Y. Chen, L. Guo, W. Cao, H. Jin, S. Guo, X. Zhang, Hydrogen production by sewage sludge gasification in supercritical water with a fluidized bed reactor, in: Int. J. Hydrogen Energy, 2013: pp. 12991–12999. https://doi.org/10.1016/j.ijhydene.2013.03.165.

[164] L. Zhang, P. Champagne, C. Xu, Screening of supported transition metal catalysts for hydrogen production from glucose via catalytic supercritical water gasification, Int. J. Hydrogen Energy. 36 (2011) 9591–9601. https://doi.org/10.1016/j.ijhydene.2011.05.077.

[165] L. Zhang, P. Champagne, C. Charles Xu, Supercritical water gasification of an aqueous by–product from biomass hydrothermal liquefaction with novel Ru modified Ni catalysts, Bioresour. Technol. 102 (2011) 8279–8287. https://doi.org/10.1016/j.biortech.2011.06.051.

[166] Y.J. Lu, H. Jin, L.J. Guo, X.M. Zhang, C.Q. Cao, X. Guo, Hydrogen production by biomass gasification in supercritical water with a fluidized bed reactor, Int. J. Hydrogen Energy. 33 (2008) 6066–6075. https://doi.org/10.1016/j.ijhydene.2008.07.082.

[167] J. Hanna, W.Y. Lee, Y. Shi, A.F. Ghoniem, Fundamentals of electro– and thermochemistry in the anode of solid–oxide fuel cells with hydrocarbon and syngas fuels, Prog. Energy Combust. Sci. (2014). https://doi.org/10.1016/j.pecs.2013.10.001.

[168] Ibram Ganesh, Chapter 4: The Electrochemical Conversion of Carbon Dioxide to Carbon Monoxide Over Nanomaterial Based Cathodic Systems: Measures to Take to Apply This Laboratory Process Industrially, in: Sneha Mohan Bhgyaraj, O.S. Oluwafemi, N. Kalarikkal, S. Thomas (Eds.), Appl. Nanomater., 2018: pp. 83–131.

[169] M. Recalde, T. Woudstra, P. V. Aravind, Renewed sanitation technology: A highly efficient faecal–sludge gasification–solid oxide fuel cell power plant, Appl. Energy. (2018). https://doi.org/10.1016/j.apenergy.2018.03.175.

[170] R. O'Hayre, S.–W. Cha, W. Colella, F.B. Prinz, Chapter 2: Fuel Cell Thermodynamics, in: Fuel Cell Fundam., John Wiley & Sons, Inc.,

Hoboken, New Jersey, 2016. https://doi.org/10.1002/9781119191766.ch2.

[171] M.J. Moran, Fundamentals of Engineering Thermodynamics, Seven Ed, Don Fowley, United States of America, 2011.

[172] Aspen Plus, Getting Started Modeling Processes with Solids Aspen Plus, Toll Free. (2012). https://doi.org/10.1016/S1164–0235(02)00075–4.

[173] T. Tanim, D.J. Bayless, J.P. Trembly, Modeling of a 5 kW e tubular solid oxide fuel cell based system operating on desulfurized JP–8 fuel for auxiliary and mobile power applications, J. Power Sources. 221 (2013) 387–396. https://doi.org/10.1016/j.jpowsour.2012.08.024.

[174] W. Zhang, E. Croiset, P.L. Douglas, M.W. Fowler, E. Entchev, Simulation of a tubular solid oxide fuel cell stack using AspenPlus™ unit operation models, Energy Convers. Manag. 46 (2005) 181–196. https://doi.org/10.1016/j.enconman.2004.03.002.

[175] T. Tanim, D.J. Bayless, J.P. Trembly, Modeling a 5 kWeplanar solid oxide fuel cell based system operating on JP–8 fuel and a comparison with tubular cell based system for auxiliary and mobile power applications, J. Power Sources. 245 (2014) 986–997. https://doi.org/10.1016/j.jpowsour.2013.07.008.

[176] E. Kozeschnik, A numerical model for evaluation of unconstrained and compositionally constrained thermodynamic equilibria, Calphad Comput. Coupling Phase Diagrams Thermochem. (2000). https://doi.org/10.1016/S0364–5916(01)00003–7.

[177] O. Yakaboylu, J. Harinck, K.G. Smit, W. De Jong, Supercritical water gasification of biomass: A detailed process modeling analysis for a microalgae gasification process, Ind. Eng. Chem. Res. (2015). https://doi.org/10.1021/acs.iecr.5b00942.

[178] Y. Chen, M. Wang, V. Liso, S. Samsatli, N.J. Samsatli, R. Jing, J. Chen, N. Li, Y. Zhao, Parametric analysis and optimization for exergoeconomic performance of a combined system based on solid oxide fuel cell–gas turbine and supercritical carbon dioxide Brayton cycle, Energy Convers. Manag. (2019). https://doi.org/10.1016/j.enconman.2019.02.036.

[179] M. İlbaş, B. Kümük, Modeling and analysis of a model solid oxide fuel

cell running on low calorific value coal gases, Int. J. Hydrogen Energy. (2019). https://doi.org/10.1016/j.ijhydene.2019.01.286.

[180] Z. Yan, P. Zhao, J. Wang, Y. Dai, Thermodynamic analysis of an SOFC–GT–ORC integrated power system with liquefied natural gas as heat sink, Int. J. Hydrogen Energy. (2013). https://doi.org/10.1016/j.ijhydene.2012.12.101.

[181] L. Fiori, M. Valbusa, D. Castello, Supercritical water gasification of biomass for H2 production: Process design, Bioresour. Technol. (2012). https://doi.org/10.1016/j.biortech.2012.06.116.

[182] M. Recalde, G. Botta, A. Fernandes, T. Woudstra, P.V. Aravind, Modelling of a novel catalytic supercritical water gasification power plant combined with reversible solid oxide cell, in: ECS Trans., 2017. https://doi.org/10.1149/07801.2997ecst.

[183] IEA, World Energy Outlook 2018 – Scenarios, 2018.

[184] BP, BP Energy outlook 2017, BP Stat. Rev. World Energy. (2017) 52. https://doi.org/10.1017/CBO9781107415324.004.

[185] International Energy Agency, Renewables 2020, Int. Energy Agency. (2020).

[186] UNICEF, The Impact of Poor Sanitation on Nutrition, 2014.

[187] U.M. Damo, M.L. Ferrari, A. Turan, A.F. Massardo, Solid oxide fuel cell hybrid system: A detailed review of an environmentally clean and efficient source of energy, Energy. (2019). https://doi.org/10.1016/j.energy.2018.11.091.

[188] sunfire, (n.d.). https://www.sunfire.de/en/hydrogen.

[189] L.R. Clausen, G. Butera, S.H. Jensen, High efficiency SNG production from biomass and electricity by integrating gasification with pressurized solid oxide electrolysis cells, Energy. (2019). https://doi.org/10.1016/j.energy.2019.02.039.

[190] R. Anghilante, C. Müller, M. Schmid, D. Colomar, F. Ortloff, R. Spörl, A. Brisse, F. Graf, Innovative power–to–gas plant concepts for upgrading of gasification bio–syngas through steam electrolysis and catalytic methanation, Energy Convers. Manag. (2019).

https://doi.org/10.1016/j.enconman.2018.12.101.

[191] S. Ali, K. Sørensen, M.P. Nielsen, Modeling a novel combined solid oxide electrolysis cell (SOEC) – Biomass gasification renewable methanol production system, Renew. Energy. (2020). https://doi.org/10.1016/j.renene.2019.12.108.

[192] Y.P. Xu, Z.H. Lin, T.X. Ma, C. She, S.M. Xing, L.Y. Qi, S.G. Farkoush, J. Pan, Optimization of a biomass–driven Rankine cycle integrated with multi–effect desalination, and solid oxide electrolyzer for power, hydrogen, and freshwater production, Desalination. (2022). https://doi.org/10.1016/j.desal.2021.115486.

[193] A. Habibollahzade, E. Gholamian, A. Behzadi, Multi–objective optimization and comparative performance analysis of hybrid biomass–based solid oxide fuel cell/solid oxide electrolyzer cell/gas turbine using different gasification agents, Appl. Energy. (2019). https://doi.org/10.1016/j.apenergy.2018.10.075.

[194] B. Erlach, B. Harder, G. Tsatsaronis, Combined hydrothermal carbonization and gasification of biomass with carbon capture, Energy. (2012). https://doi.org/10.1016/j.energy.2012.01.057.

[195] S. van Wyk, A.G.J. van der Ham, S.R.A. Kersten, Potential of supercritical water desalination (SCWD) as zero liquid discharge (ZLD) technology, Desalination. (2020). https://doi.org/10.1016/j.desal.2020.114593.

[196] M. Hodes, P.A. Marrone, G.T. Hong, K.A. Smith, J.W. Tester, Salt precipitation and scale control in supercritical water oxidation – Part A: Fundamentals and research, J. Supercrit. Fluids. (2004). https://doi.org/10.1016/S0896–8446(03)00093–7.

[197] M.T. Timko, A.F. Ghoniem, W.H. Green, Upgrading and desulfurization of heavy oils by supercritical water, J. Supercrit. Fluids. 96 (2015) 114–123. https://doi.org/10.1016/j.supflu.2014.09.015.

[198] M.J. Antal, S.G. Allen, D. Schulman, X. Xu, R.J. Divilio, Biomass Gasification in Supercritical Water †, Ind. Eng. Chem. Res. 39 (2000) 4040–4053. https://doi.org/10.1021/ie0003436.

[199] P. Basu, V. Mettanant, Biomass Gasification in Supercritical Water — A

Review, Int. J. Chem. React. Eng. 7 (2009). https://doi.org/10.2202/1542–6580.1919.

[200] C.S. Lee, A. V. Conradie, E. Lester, Review of supercritical water gasification with lignocellulosic real biomass as the feedstocks: Process parameters, biomass composition, catalyst development, reactor design and its challenges, Chem. Eng. J. (2021). https://doi.org/10.1016/j.cej.2021.128837.

[201] A.B.A. Ibrahim, H. Akilli, Supercritical water gasification of wastewater sludge for hydrogen production, Int. J. Hydrogen Energy. (2019). https://doi.org/10.1016/j.ijhydene.2019.02.184.

[202] A. Onigbajumo, A. Taghipour, G. Will, T. Chu Van, S. Couperthwaite, T. Steinberg, T. Rainey, Effects of process–thermal configuration on energy, exergy, and thermo–economic performance of solar driven supercritical water gasification, Energy Convers. Manag. (2022). https://doi.org/10.1016/j.enconman.2021.115002.

[203] J. Louw, C.E. Schwarz, J.H. Knoetze, A.J. Burger, Thermodynamic modelling of supercritical water gasification: Investigating the effect of biomass composition to aid in the selection of appropriate feedstock material, Bioresour. Technol. (2014). https://doi.org/10.1016/j.biortech.2014.09.129.

[204] A. Rahbari, M.B. Venkataraman, J. Pye, Energy and exergy analysis of concentrated solar supercritical water gasification of algal biomass, Appl. Energy. (2018). https://doi.org/10.1016/j.apenergy.2018.07.002.

[205] J.A. Okolie, R. Rana, S. Nanda, A.K. Dalai, J.A. Kozinski, Supercritical water gasification of biomass: A state–of–the–art review of process parameters, reaction mechanisms and catalysis, Sustain. Energy Fuels. (2019). https://doi.org/10.1039/c8se00565f.

[206] A. Kruse, Supercritical water gasification, Biofuels, Bioprod. Biorefining. (2008). https://doi.org/10.1002/bbb.93.

[207] A. Darmawan, M.W. Ajiwibowo, F. Anggoro Cahyo, M. Aziz, K. Tokimatsu, Co–production of hydrogen and power from palm mill wastes, in: Energy Procedia, 2019. https://doi.org/10.1016/j.egypro.2019.01.437.

[208] S. Guo, F. Meng, P. Peng, J. Xu, H. Jin, Y. Chen, L. Guo, Thermodynamic

analysis of the superiority of the direct mass transfer design in the supercritical water gasification system, Energy. (2022). https://doi.org/10.1016/j.energy.2021.122722.

[209] M. Recalde, T. Woudstra, P.V. Aravind, Gasifier, Solid Oxide Fuel Cell Integrated Systems for Energy Production From Wet Biomass, Front. Energy Res. 7 (2019). https://doi.org/10.3389/fenrg.2019.00129.

[210] Z. Chen, L. Gao, X. Zhang, W. Han, S. Li, High–efficiency power generation system with integrated supercritical water gasification of coal, Energy. (2018). https://doi.org/10.1016/j.energy.2018.06.140.

[211] M. Samavati, M. Santarelli, A. Martin, V. Nemanova, Thermodynamic and economy analysis of solid oxide electrolyser system for syngas production, Energy. (2017). https://doi.org/10.1016/j.energy.2017.01.067.

[212] O. Yakaboylu, J. Harinck, K.G. Gerton Smit, W. de Jong, Supercritical water gasification of manure: A thermodynamic equilibrium modeling approach, Biomass and Bioenergy. (2013). https://doi.org/10.1016/j.biombioe.2013.07.011.

[213] Y. Du, Y. Qin, G. Zhang, Y. Yin, K. Jiao, Q. Du, Modelling of effect of pressure on co–electrolysis of water and carbon dioxide in solid oxide electrolysis cell, Int. J. Hydrogen Energy. (2019). https://doi.org/10.1016/j.ijhydene.2018.12.078.

[214] M. Lo Faro, W. Oliveira da Silva, W. Valenzuela Barrientos, G.G.A. Saglietti, S.C. Zignani, E.A. Ticianelli, V. Antonucci, A.S. Aricò, The role of CuSn alloy in the co–electrolysis of CO2 and H2O through an intermediate temperature solid oxide electrolyser, J. Energy Storage. (2020). https://doi.org/10.1016/j.est.2019.100820.

[215] M. Hauck, S. Herrmann, H. Spliethoff, Simulation of a reversible SOFC with Aspen Plus, Int. J. Hydrogen Energy. 42 (2017) 10329–10340. https://doi.org/10.1016/j.ijhydene.2017.01.189.

[216] TNO, ECN Phyllis classification, Phyllis2. (2020).

[217] S. Biswas, A.P. Kulkarni, D. Fini, S. Singh Rathore, A. Seeber, S. Giddey, S. Bhattacharya, Catalyst–induced enhancement of direct methane synthesis in solid oxide electrolyser, Electrochim. Acta. 391 (2021).

https://doi.org/10.1016/j.electacta.2021.138934.

[218] C.H. Wendel, P. Kazempoor, R.J. Braun, A thermodynamic approach for selecting operating conditions in the design of reversible solid oxide cell energy systems, J. Power Sources. 301 (2016) 93–104. https://doi.org/10.1016/j.jpowsour.2015.09.093.

[219] V.S. Bagotsky, Fundamentals of Electrochemistry: Second Ed., 2005. https://doi.org/10.1002/047174199X.

[220] M. Lang, C. Bohn, M. Henke, G. Schiller, C. Willich, F. Hauler, Understanding the Current–Voltage Behavior of High Temperature Solid Oxide Fuel Cell Stacks, J. Electrochem. Soc. (2017). https://doi.org/10.1149/2.1541713jes.

[221] H. Zhu, R.J. Kee, V.M. Janardhanan, O. Deutschmann, D.G. Goodwin, Modeling Elementary Heterogeneous Chemistry and Electrochemistry in Solid–Oxide Fuel Cells, J. Electrochem. Soc. 152 (2005) A2427. https://doi.org/10.1149/1.2116607.

[222] S. Wang, X. Hao, W. Zhan, Research on a low temperature reversible solid oxide cell, Int. J. Hydrogen Energy. 42 (2017) 29881–29887. https://doi.org/10.1016/j.ijhydene.2017.09.181.

[223] L. Bernadet, J. Laurencin, G. Roux, D. Montinaro, F. Mauvy, M. Reytier, Effects of Pressure on High Temperature Steam and Carbon Dioxide Co–electrolysis, Electrochim. Acta. 253 (2017) 114–127. https://doi.org/10.1016/j.electacta.2017.09.037.

[224] P. Kazempoor, R.J. Braun, Model validation and performance analysis of regenerative solid oxide cells for energy storage applications: Reversible operation, in: Int. J. Hydrogen Energy, 2014: pp. 5955–5971. https://doi.org/10.1016/j.ijhydene.2014.01.186.

[225] M.J. Moran, Engineering thermodynamics: Fundamentals, in: I. John Wiley & Sons (Ed.), CRC Handb. Therm. Eng. Second Ed., Matthew Deans, United States of America, 2017. https://doi.org/10.4324/9781315119717.

[226] A. Nurdiawati, I.N. Zaini, A.R. Irhamna, D. Sasongko, M. Aziz, Novel configuration of supercritical water gasification and chemical looping for highly–efficient hydrogen production from microalgae, Renew. Sustain.

Energy Rev. (2019). https://doi.org/10.1016/j.rser.2019.05.054.

[227] G. Botta, H. Patel, F. Sebastiani, P. V Aravind, Thermodynamic and Exergy Analysis of Reversible Solid Oxide Cell Systems, ECS Trans. 68 (2015) 3265–3277. https://doi.org/10.1017/CBO9781107415324.004.

[228] A. Fernandes, J. Brabandt, O. Posdziech, A. Saadabadi, M. Recalde, L. Fan, E.O.E.O. Promes, M. Liu, T. Woudstra, P.V.P.V. Aravind, Design, construction, and testing of a gasifier–specific solid oxide fuel cell system, Energies. 11 (2018). https://doi.org/10.3390/en11081985.

[229] G. Parks, R. Boyd, J. Cornish, R. Remick, Hydrogen Station Compression, Storage, and Dispensing Technical Status and Costs: Systems Integration, 2014.

[230] M.M. Whiston, W.O. Collinge, M.M. Bilec, L.A. Schaefer, Exergy and economic comparison between kW–scale hybrid and stand–alone solid oxide fuel cell systems, J. Power Sources. (2017). https://doi.org/10.1016/j.jpowsour.2017.03.113.

[231] A.N. Tabish, H.C. Patel, J. Schoonman, P. V. Aravind, A detailed look into hydrogen electrochemical oxidation on ceria anodes, Electrochim. Acta. (2018). https://doi.org/10.1016/j.electacta.2018.05.058.

[232] J. Banner, A. Akter, R. Wang, J. Pietras, S. Sulekar, O.A. Marina, S. Gopalan, Rare earth Nickelate electrodes containing heavily doped ceria for reversible solid oxide fuel cells, J. Power Sources. (2021). https://doi.org/10.1016/j.jpowsour.2021.230248.

[233] E. Ioannidou, M. Chavani, S.G. Neophytides, D.K. Niakolas, Effect of the PH2O/PCO2 and PH2 on the intrinsic electro–catalytic interactions and the CO production pathway on Ni/GDC during solid oxide H2O/CO2 co–electrolysis, J. Catal. (2021). https://doi.org/10.1016/j.jcat.2021.09.024.

[234] L. Wang, M. Rao, S. Diethelm, T.E. Lin, H. Zhang, A. Hagen, F. Maréchal, J. Van herle, Power–to–methane via co–electrolysis of H2O and CO2: The effects of pressurized operation and internal methanation, Appl. Energy. (2019). https://doi.org/10.1016/j.apenergy.2019.05.098.

[235] A.A. AlZahrani, I. Dincer, Modeling and performance optimization of a solid oxide electrolysis system for hydrogen production, Appl. Energy. (2018). https://doi.org/10.1016/j.apenergy.2018.04.124.

[236] D. Oryshchyn, N.F. Harun, D. Tucker, K.M. Bryden, L. Shadle, Fuel utilization effects on system efficiency in solid oxide fuel cell gas turbine hybrid systems, Appl. Energy. (2018). https://doi.org/10.1016/j.apenergy.2018.07.004.

[237] L. Mastropasqua, I. Pecenati, A. Giostri, S. Campanari, Solar hydrogen production: Techno–economic analysis of a parabolic dish–supported high–temperature electrolysis system, Appl. Energy. (2020). https://doi.org/10.1016/j.apenergy.2019.114392.

[238] E.P. Reznicek, R.J. Braun, Reversible solid oxide cell systems for integration with natural gas pipeline and carbon capture infrastructure for grid energy management, Appl. Energy. (2020). https://doi.org/10.1016/j.apenergy.2019.114118.

[239] L. Wang, Y. Zhang, C. Li, M. Pérez–Fortes, T.E. Lin, F. Maréchal, J. Van herle, Y. Yang, Triple–mode grid–balancing plants via biomass gasification and reversible solid–oxide cell stack: Concept and thermodynamic performance, Appl. Energy. (2020). https://doi.org/10.1016/j.apenergy.2020.115987.

[240] E.M. Moghaddam, A. Goel, M. Siedlecki, K. Michalska, O. Yakaboylu, W. de Jong, Supercritical water gasification of wet biomass residues from farming and food production practices: lab–scale experiments and comparison of different modelling approaches, Sustain. Energy Fuels. 5 (2021) 1521–1537. https://doi.org/10.1039/d0se01635g.

[241] V. Menon, V.M. Janardhanan, O. Deutschmann, A mathematical model to analyze solid oxide electrolyzer cells (SOECs) for hydrogen production, Chem. Eng. Sci. (2014). https://doi.org/10.1016/j.ces.2013.10.025.

Nomenclature

A	area of the stack
d_p	particle diameter (nm)
E	cell voltage (V)
E_r	reversible potential (V)
e_f	specific flow exergy per unit of mol (kJ mol^{-1})
Ex	exergy (kW)
$\overline{ex}_i^{ch}$	chemical exergy (kJ mol^{-1})
$\dot{E}_d$	exergy destruction rate (kW)
F	Faraday constant (C mol^{-1})
ΔG	change in specific molar Gibbs free energy ($Jmol^{-1}$)
ΔH	change in specific molar enthalpy ($Jmol^{-1}$)
h	specific enthalpy (kJ kg^{-1})
I	current (A)
j	current density (Acm^{-2})
$\dot{m}$	mass flow rate (kg s^{-1})
M	molecular weight
n	number of moles
$\dot{n}$	mole flow rate (mol s^{-1})
P	pressure (Pa), power (kW),
p	partial pressure
Q	heat (kW)
R	gas constant ($Jmol^{-1}K^{-1}$)
ΔS	change in specific molar entropy (kJ mol K^{-1})
S	specific entropy (kJ K kg^{-1})
T	temperature (K)
U_f	fuel utilisation ratio
V	voltage (V)
x	mass fraction
y	mole fraction
$\dot{W}$	rate of work (kW)

Greek letters

Δ	thickness (μm)
β	surface ratio

η	efficiency, cell resistant ($\Omega\ m^2$)
τ	tortuosity
ε	porosity
μ	chemical potential ($Jmol^{-1}$)
Γ	surface site density ($mol\ cm^2$)
δ	conductivity

Subscripts, superscript

act	activation
ch	chemical
conc	concentration
cv	control volumen
des	desorption
e	exit
f	thermochemical
ex	exergy
i	inlet, mixture components
j	number of component present in a mixture
0	properties at the reference environment
ohm	Ohmic
ox	oxidant
r	reversible
sys	system
TN	thermoneutral
an	anode
cat	cathode

Abbreviations

BOP	balance of the plant
CGE	cold gas efficiency
CE	carbon gasification efficiency
SCWG	supercritical water gasification
GT	gas turbine
GUP	gas upgrading unit
LHV	lower heating value ($kJmol^{-1}$)
HE	heat exchanger
HHV	high heating value ($kJmol^{-1}$)

PSC	post combustor
TPB	three–phase boundary
ASR	area–specific resistance
rSOC	reversible–solid oxide cell
SOFC	solid–oxide fuel cell
SOEC	solid–oxide electrolyser cell
SEP	gas/liquid separator
SCW	supercritical water

Acknowledgements

It is very gratifying to see small rivers flowing down the Andean mountains. And the water channels that surround the cities of the Netherlands. Therefore, I am very grateful to my promotors, prof. dr. Purushothaman Vellayani Aravind and Bendiks Jan Boersma for allowing me to be part of the TUDelft Solid Oxide Cell group, investigating the field of energy and water treatment. This opportunity became a test that has shown me that pursuing a goal makes life happy. My special thanks go out to P.V. Aravind, who patiently supervised my PhD project and the writing of this thesis. Participating in important international conferences and visiting Poland and Belgium with the Solid Oxide Cell group motivates the development of the program. The lakes and oceans form because the course of the rivers cannot do anything else.

The essential part of this research was to develop thermodynamic models. In this sense, I am grateful to Theo Woudstra and Alvaro Fernandez. It is noticeable that the will has more power than electricity, Albert Einstein.

I also thank Prof. Adrian Verkooijen for motivating me and inspiring scientific discussions that contributed to developing efficient thermodynamic systems. I like to thank Prof. Joop Shoutmann for introducing me to the exciting field of materials, an essential part of SOC development. I also thank Wiebren de Jong, who answered numerous questions and provided me with valuable scientific responses.

A project combining supercritical water gasification with solid oxide cells results from cooperation between Julia Botta and Alvaro Fernandez in the model simulation. I especially thank Amogh and Vikrant for their contribution to finishing this project. I want to thank John Harinck for helping me since I started researching supercritical water.

Experiments are an essential part of the investigation. I thank Michael, Jaap, Martijn and Bas and also I want to thank Raphael for developing experiments to analyse the electrochemical oxidation of methane in solid oxide fuel cells. We had interesting discussions during the SOFC meetings with my colleagues Ming Liu, Eva, Alvaro, Patel, Lyua Fan, Aditia, Tabish, Giulia, Alexandro, Ali, Lindern, Jelle, Rashi, Vikrant, Yashar and Ana. I also enjoyed their pleasant company. Thanks to the people that maintain my place at the TUDelft office clean. I like to thank Eveline for her management support and

Mascha Toppenberg for her leadership support in the graduate school program. The financial provision of SENESCYT Ecuador is greatly appreciated.

My special thanks to Giulia Botta, Alexandro Cavalli, Tabish, Ali, and Liyaun Fan; they make me feel why life is worth living. My thanks to my dear neighbours of Singelstraat, Anna van der Heijden and Els; their friendship made my life in Delft pleasant.

I want to thank my dear family and my friends. Your love empowers me to finalise this work.

About the author

She was born on 30 November 1970 in Riobamba, a city in the Andes of Ecuador. In 1998, she obtained her bachelor's degree in Mechanical Engineering from Chimborazo Polytechnic, Ecuador. She worked as a mechanical engineer at Petroleum facilites companies in Ecuador from 2000 to 2008. In May 2008, she got a scholarship to study at the Delft University of Technology, the Netherlands, where she got the MSc degree in Sustainable Process and Energy Technology with the thesis "Reaction kinetic simulation of supercritical water gasification of wet biomass" in 2011. She joined the solid oxide fuel cell group at Delft University of Technology under the supervision of Prof. dr. ir. P.V. Aravind and Prof. dr. ir. B.J. Boersma in 2014, with the thesis "*Wet biomass treatment sanitation–energy system concepts*".

List of Publications

Journal Publications

- Energy and exergy analysis of catalytic supercritical water gasification combined with reversible solid oxide cell. Recalde M., Amladi A., V. Venkataraman, Woudstra, T. & Aravind, P. V., Energy Conversion and Management (2022).
- Gasifier, solid oxide fuel cell integrated systems for energy production from wet biomass. Recalde, M., Woudstra, T. & Aravind, P. V., Frontiers of Energy (2019).
- Renewed sanitation technology: A highly efficient faecal–sludge gasification–solid oxide fuel cell power plant. Recalde, M., Woudstra, T. & Aravind, P. V., Applied Energy. 222, p. 515–529 (2018).
- Design, Construction, and Testing of a Gasifier–Specific Solid Oxide Fuel Cell System. Monteiro Fernandes, Á., Brabandt, J., Posdziech, O., Saadabadi, A., Recalde, M., Fan, L., Promes, E., Liu, M., Woudstra, T. & Purushothaman Vellayani, Energies. 11, 8, 17 p., 1985 (2018).
- Supercritical water gasification of biomass: An integrated kinetic model for the prediction of product compounds. Yakaboylu O., Yapar G., Recalde M., Harinck J., Smit K. G., Martelli E. & de Jong, W., Industrial and Engineering Chemistry Research. 54, 33, p. 8100–8112 13 p (2015).

Conference Proceedings

- Modelling of a novel catalytic supercritical water gasification power plant combined with reversible solid oxide cell. Recalde M., Botta, G., Monteiro Fernandes, A. B., Woudstra, T. & Purushothaman Vellayani, ECS Transactions; 78, 2997 (2017).
- Opportunities and challenges in using SOFCs in waste to energy systems. Purushothaman Vellayani, A., Cavalli, A., Patel, H., Recalde M., Saadabadi, A., Tabish, T., Botta, G., Thallam Thattai, A., Teodoru, A., Hajimolana, Y., Chundru, P. & Woudstra, T. ECS Transactions; 78, 209 (2017).
- Potential of Waste Biomass Gasification Hybrid Solid Oxide Fuel Cell, Turbine Integrated System. Recalde M., Purushothaman Vellayani, A., Woudstra, T. Proceedings of the 12th European SOFC & SOE Forum 2016. Luzern, Switzerland (2016).

- Thermodynamic performance of a high efficient power plant based on faecal biomass gasification, solid oxide fuel cell and micro steam turbine. Recalde M., Woudstra, T., Liu, M. & Aravind, P. V. ECS Transactions; 68, 241 (2016).
- An SOFC integrated sanitation system: Thermodynamics. Recalde M., Woudstra, T., Aravind, P.V. 8th Workshop in Fuel Cell Systems University of Birmingham. Bruges, Belgium (2015).